MASSIVELY PARALLEL MONTE CARLO METHODS FOR DISCRETE LINEAR AND NONLINEAR SYSTEMS

by

Stuart R. Slattery

A dissertation submitted in partial fulfillment of
the requirements for the degree of

Doctor of Philosophy

(Nuclear Engineering and Engineering Physics)

at the

UNIVERSITY OF WISCONSIN–MADISON

24 March 2013

© Copyright by Stuart R. Slattery 24 March 2013
All Rights Reserved

Acknowledgments

Great thanks are owed to my advisor and friend Paul Wilson for providing me years of guidance and the opportunity to develop this work. Without him, this work would have never been possible.

Tom Evans is responsible for presenting me with the seeds of this work and for that I thank him. His mentoring over the past few years has been invaluable.

Roger Pawlowski and other members of the Consortium for Advanced Simulation of Light Water Reactors and Trilinos teams as well as many staff members at Oak Ridge National Laboratory have provided tremendous resources for my professional and technical development and have greatly facilitated this work.

This work was performed under appointment to the Nuclear Regulatory Commission Fellowship program at the University of Wisconsin - Madison Department of Engineering Physics.

Contents

List of Figures

MASSIVELY PARALLEL MONTE CARLO METHODS FOR DISCRETE LINEAR AND NONLINEAR SYSTEMS

Stuart R. Slattery

Under the supervision of Professor Paul P.H. Wilson
At the University of Wisconsin-Madison

Paul P.H. Wilson

Chapter 1

Introduction

In many fields of engineering and physics, linear and nonlinear problems are a primary focus of study. Recent focus on multiple physics systems in the nuclear reactor modeling and simulation community adds a new level of complexity to common nonlinear systems as solution strategies change when they are coupled to other problems (U.S. Department of Energy, 2011). Furthermore, a desire for predictive simulations to enhance the safety and performance of nuclear systems creates a need for extremely high fidelity computations to be performed for these coupled systems as a means to capture effects not modeled by coarser methods.

In order to achieve this high fidelity, state-of-the-art computing must be leveraged in a way that is both efficient and considerate of hardware-related issues. As scientific computing moves towards exascale facilities with machines of $\mathsf{O}(1,000,000)$ cores already coming on-line, new algorithms to solve these complex problems must be developed to leverage this new hardware (Kogge and Dysart, 2011). Issues such as resiliency to node failure, limited growth of memory available per node, and scaling to large numbers of cores will be pertinent to robust algorithms aimed at this new hardware. Considering these issues, this dissertation develops a massively parallel Monte Carlo method for linear problems and a novel Monte Carlo method to advance solution techniques for nonlinear problems.

We discuss in this chapter motivation for advancing Monte Carlo solvers by providing multiphysics problems of interest in nuclear reactor analysis. Hardware-based motivations are also provided by considering the impact of forthcoming computing architectures. In addition, background on the current solver techniques for multiphysics problems and a brief comparison to the proposed methods is provided to further motivate this work.

1.1 Physics-Based Motivation

Predictive modeling and simulation capability requires the combination of high fidelity models, high performance computing hardware that can handle the intense computational loads required by these models, and modern algorithms for solving these problems that leverage this high performance hardware. For nuclear reactor analysis, this predictive capability can enable tighter design tolerances for improved thermal performance and efficiency, higher fuel burn-up and therefore reduction in generated waste, and high confidence in accident scenario models. The physics that dominate these types of analysis include neutronics, thermal hydraulics, computational fluid dynamics, and structural mechanics.

Although solution techniques in each of these individual categories has advanced over the last few decades and in fact leveraged modern algorithms and computer architectures, true predictive capability for engineered systems can only be achieved through a coupled, multiple physics analysis where the effects of feedback between physics are modeled. For example, consider the safety analysis of a departure from nucleate boiling scenario in the subchannel of a nuclear fuel assembly. When this event occurs, heat transfer is greatly reduced between the fuel and the coolant due to the vapor layer generated by boiling, causing the fuel center-line temperature to rapidly rise. To characterize this boiling phenomena and how it affects fuel failure we must consider a neutronics analysis in order to compute power generation in the fuel pins, fluid dynamics analysis to characterize coolant boiling, temperature, and density, solid material heat transfer to characterize fuel and cladding temperature and heat transfer with the coolant, and nuclear data processing to characterize how changing material temperatures and densities changes the cross sections needed for the neutronics calculation. As shown in Figure 1.1, many couplings are required among individual physics components in order to accurately model this situation with each

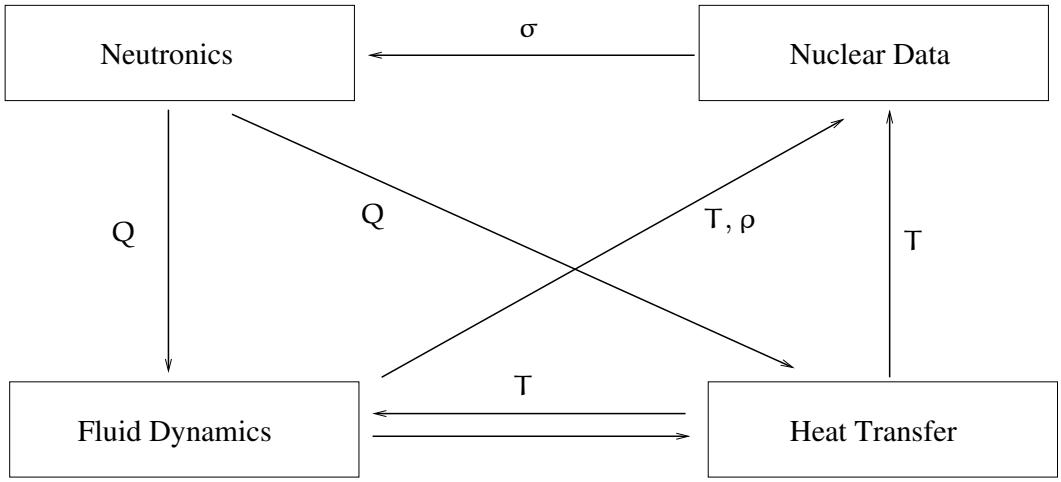

Figure 1.1: **Multiphysics dependency analysis of departure from nucleate boiling.** *A neutronics solution is required to compute power generation in the fuel pins, fluid dynamics is required to characterize boiling and fluid temperature and density, heat transfer is required to compute the fuel and cladding temperature, and the nuclear data modified with the temperature and density data. Strong coupling among the variables creates strong nonlinearities.*

physics generating and receiving many responses. Those variables that are very tightly coupled, such as the temperatures generated by the fluid dynamics and heat transfer components, will have strong nonlinearities in their behavior and would therefore benefit from fully consistent nonlinear solution schemes instead of fixed-point type iterations between physics[1]. Furthermore, the space and time scales over which these effects occur will also vary greatly.

The computational resources required to solve such problems are tremendous. Recent work in modeling coupled fluid flow and solid material heat and mass transfer in a reactor subsystem, similar to the same components of the departure from nucleate boiling example above, was performed as part of

[1]Fixed-point iterations between physics are commonly referred to as Picard iterations.

analysis of the Department of Energy's Consortium for Advanced Simulation of Light Water Reactors (CASL) modeling and simulation hub. CASL used the Drekar multiphysics code developed at Sandia National Laboratories (Pawlowski et al., 2012) for modeling goals in grid-to-rod-fretting analysis and will use a similar coupled physics structure for future departure from nucleate boiling analysis with comparison to experimental data. Using Drekar, multiphysics simulations have been performed with fully consistent methods for the solution of nonlinear systems using meshes of $\mathsf{O}(1 \times 10^9)$ elements leveraging $\mathsf{O}(100,000)$ cores on leadership class machines. Neutronics components to be implemented in CASL for multiphysics analysis, such as the Exnihilo radiation transport suite developed at Oak Ridge National Laboratory (Evans et al., 2010), compute trillions of unknowns for full core reactor analysis on $\mathsf{O}(1 \times 10^9)$ element meshes and $\mathsf{O}(100,000)$ cores as well. Given the large scale and complexity of these problems, if we aim to advance multiphysics solution techniques, then we are motivated to advance the solution of complex and general nonlinear problems exploiting leadership class levels of parallelism.

1.2 Hardware-Based Motivation

As leadership class machines move towards the exascale, new algorithms must be developed that leverage their strengths and adapt to their shortcomings. Basic research is required now to advance methods in time for these new machines to become operational. Organized work is already moving forward in this area with the Department of Energy's Advanced Scientific Computing Research office specifically allocating funding for the next several years to research resilient solver technologies for exascale facilities (U.S. Department of Energy, 2012). Based on the language in this call for proposals, we can identify key issues for which a set of robust, massively parallel Monte Carlo solvers could provide a solution. As machines begin to operate at hundreds

of petaflops peak performance and beyond, trends toward reduced energy consumption will require incredibly high levels of concurrency to achieve the desired computation rates. Furthermore, this drop in power consumption will mean increased pressure on memory as memory per node is expected to stagnate while cores per node is expected to increase. As the number of cores increases, their clock speed is expected to stagnate or even decrease to further reduce power consumption and manufacturing costs.

The end result of these hardware changes is that the larger numbers of low-powered processors will be prone to both soft failures such as bit errors in floating point operations and hard failures where the data owned by that processor cannot be recovered. Because these failures are predicted to be common, resilient solver technologies are required to overcome these events. With linear and nonlinear solvers based on Monte Carlo techniques, such issues are alleviated by statistical arguments. In the case of soft failures, isolated floating point errors in Monte Carlo simulation are absorbed within tally statistics while completely losing hardware during a hard failure is manifested as a high variance event where some portion of the Monte Carlo histories are lost. These stochastic methods are a paradigm shift from current deterministic solver techniques that will suffer greatly from the non-deterministic behavior expected from these exascale machines.

In addition to resiliency concerns, the memory restrictions on future hardware will hinder modern solvers that derive their robustness from using large amounts of memory. Stochastic methods that are formulated to use less memory than conventional methods will serve to alleviate some of this pressure. In addition, new parallel strategies that may be implemented with stochastic methods could offer a new avenue for leveraging the expected levels of high concurrency in exascale machines.

1.3 Research Outline

For some time, the particle transport community has been utilizing Monte Carlo methods for the solution of transport problems (Lewis, 1993). The partial differential equation (PDE) community has focused on various deterministic methods for solutions to linear problems (Saad, 2003; Kelley, 1995). In between these two areas are a not widely known group of Monte Carlo methods for solving sparse linear systems (Forsythe and Leibler, 1950; Hammersley and Handscomb, 1964; Halton, 1962, 1994). In recent years, these methods have been further developed for radiation transport problems in the form of Monte Carlo Synthetic-Acceleration (MCSA) (Evans and Mosher, 2009; Evans et al., 2012) but have yet to be applied to more general sparse linear systems commonly generated by the computational physics community. Compared to other methods in this regime, MCSA offers three attractive qualities; (1) the linear problem operator need not be symmetric or positive-definite, thereby reducing preconditioning complexity, (2) the stochastic nature of the solution method provides a natural solution to the issue of resiliency, and (3) is amenable to parallelization using modern methods developed by the transport community (Wagner et al., 2010). The development of MCSA as a general linear solver and the development of a parallel MCSA method will be new and unique features of this work, providing a framework with which other issues such as resiliency may be addressed in the future.

In addition to linear solver advancements, nonlinear solvers may also benefit from a general and parallel MCSA scheme. In the nuclear engineering community, nonlinear problems are often addressed by either linearizing the problem or building a segregated scheme and using traditionally iterative or direct methods to solve the resulting system (Pletcher et al., 1997). In the mathematics community, various Newton methods have been popular (Kelley, 1995). Recently, Jacobian-Free Newton-Krylov (JFNK) schemes

(Knoll and Keyes, 2004) have been utilized in multiple physics architectures and advanced single physics codes (Gaston et al., 2009). The benefits of JFNK schemes are that the Jacobian is never formed, simplifying the implementation, and a Krylov solver is leveraged (typically GMRES or Conjugate Gradient), providing excellent convergence properties for well-conditioned and well-scaled systems. However, there are two potential drawbacks to these methods for high fidelity predictive simulations: (1) the Jacobian is approximated by a first-order differencing method on the order of machine precision such that this error can grow beyond that of those in a fine-grained system (Kelley, 1995) and (2) for systems that are not symmetric positive-definite (which will be the case for most multiphysics systems and certainly for most preconditioned systems) the Krylov subspace generated by the GMRES solver may become prohibitively large (Knoll and McHugh, 1995). To address these issues, this thesis develops a new and novel method for nonlinear systems based on the MCSA method.

The Forward-Automated Newton-MCSA (FANM) method is developed as new nonlinear solution method. The key features of FANM are: full Jacobian generation using modern Forward Automated Differentiation (FAD) methods (Bartlett et al., 2006), and MCSA as the inner linear solver. This method has several attractive properties. First, the first-order approximation to the Jacobian used in JFNK type methods is eliminated by generating the Jacobian explicitly with the model equations through FAD. Second, the Jacobian need not be explicitly formed by the user but is instead automated through FAD; this eliminates the complexity of hand-coding derivatives and has also been demonstrated to be more efficient computationally than evaluating difference derivatives. Third, unlike GMRES, MCSA does not build a subspace during iterations. Although the Jacobian must be explicitly formed to use MCSA, for problems that take more than a few GMRES iterations to converge the size of the Krylov subspace will grow beyond that of the Jacobian. Finally, using MCSA for the linear solve provides its

benefits for preconditioning, potential resiliency, and parallelism.

This preliminary report outlines in Chapter 2 the conventional methods used in practice for solving linear problems to provide a mathematical basis upon which to build new algorithms that aim to solve some of the aforementioned issues. Parallel schemes for conventional methods are also provided for background and understanding of how current methods may or may not map to future hardware. In addition, some components of their parallel implementations may be applied to stochastic methods development. In Chapter 3, Monte Carlo algorithms for solving linear systems and new parallel strategies will be outlined in full with links made to past work and their potential for offering improvements to the multiphysics analysis community. From these stochastic methods, a new nonlinear method is developed in Chapter 8 and compared to conventional methods for solving nonlinear problems.

Chapter 2

Conventional Solution Methods for Linear Systems

The discretization of partial differential equations (*PDEs*) through common methods such as finite differences (LeVeque, 2007), finite volumes (LeVeque, 2002), and finite elements (Zienkiewicz et al., 2005) ultimately generates sets of coupled equations in the form of matrix problems. In many cases, these matrices are sparse, meaning that the vast majority of their constituent elements are zero. This sparsity is due to the fact that the influence of a particular grid element only expands as far as a few of its nearest neighbors depending on the order of discretization used and therefore coupling among variables in a particular discrete equation in the system leads to a few non-zero entries. Because of the natural occurrence of sparse matrices in common numerical methods many iterative techniques have been developed to solve such systems. We discuss here conventional stationary and projection methods for solving sparse systems to provide the necessary background for the remainder of this work. Details on the parallelization of conventional methods are discussed.[1]

2.1 Preliminaries

We seek solutions of the general linear problem in the following form:

$$\mathbf{A}\mathbf{x} = \mathbf{b}\,, \tag{2.1}$$

[1]The contents of this chapter, particularly those sections relating to projection methods and matrix analysis, are heavily based on Saad's text (Saad, 2003).

where $\mathbf{A} \in \mathbb{R}^{\mathsf{N}\times\mathsf{N}}$ is a matrix operator such that $\mathbf{A} : \mathbb{R}^{\mathsf{N}} \to \mathbb{R}^{\mathsf{N}}$, $\mathbf{x} \in \mathbb{R}^{\mathsf{N}}$ is the solution vector, and $\mathbf{b} \in \mathbb{R}^{\mathsf{N}}$ is the forcing term. The solutions to Eq (2.1) will be generated by inverting $\mathbf{A}$ either directly or indirectly:

$$\mathbf{x} = \mathbf{A}^{-1}\mathbf{b}\,. \tag{2.2}$$

In addition we can define the residual:

$$\mathbf{r} = \mathbf{b} - \mathbf{A}\mathbf{x}\,, \tag{2.3}$$

such that an exact solution $\mathbf{x}$ has been found when $\mathbf{r} = \mathbf{0}$. From the statement in Eq (2.2) we can already place a restriction on $\mathbf{A}$ by requiring that it be *nonsingular*, meaning that we can in fact compute $\mathbf{A}^{-1}$. In this work we will focus our efforts on approximately inverting the operator through various means.

In a discussion of methods for solving linear systems, several mathematical tools are useful in characterizing the qualities of the linear system. Among the most useful are the *Eigenvalues* of the matrix, $\sigma(\mathbf{A})$. We find these by solving the Eigenvalue problem:

$$\mathbf{A}\mathbf{x} = \lambda\mathbf{x},\ \lambda \in \sigma(\mathbf{A})\,. \tag{2.4}$$

By writing Eq (2.4) in a different form,

$$(\mathbf{A} - \lambda\mathbf{I})\mathbf{x} = 0\,, \tag{2.5}$$

and demanding that non-trivial solutions for $\mathbf{x}$ exist, it is then required that $|\mathbf{A} - \lambda\mathbf{I}| = 0$. Expanding this determinant yields a characteristic polynomial in terms of λ with roots that form the set of Eigenvalues, $\sigma(\mathbf{A})$. Each component of $\sigma(\mathbf{A})$ can then be used to solve Eq (2.5) for a particular permutation of $\mathbf{x}$. The set of all permutations form the *Eigenvectors* of $\mathbf{A}$. A quantity of particular interest that is computable from the eigenvalues of

a matrix $\mathbf{A}$ is the *spectral radius*, $\rho(\mathbf{A})$, defined by Saad (Saad, 2003) as:

$$\rho(\mathbf{A}) = \max_{\lambda \in \sigma(\mathbf{A})} |\lambda| \,. \tag{2.6}$$

In addition, for problems that have a large scale over which the independent variables may exist (e.g. a problem with events on timescales ranging from nanoseconds to hours), a good measure of this range is supplied by the *stiffness ratio*:

$$\mathsf{StiffnessRatio} = \frac{\max_{\lambda \in \sigma(\mathbf{A})} |\lambda|}{\min_{\lambda \in \sigma(\mathbf{A})} |\lambda|} \tag{2.7}$$

Those problems that have a wide range of scales in their independent variables, which will then be reflected in the operator, will then have a large stiffness ratio. We will define such problems with large stiffness ratios as *stiff*.

General to both matrices and vectors, *norms* are a mechanism for collapsing objects of many elements to a single value. Per LeVeque's text (LeVeque, 2007), the q-norm of a vector is defined as:

$$\|\mathbf{v}\|_q = \left[\sum_{i=1}^{N} |v_i|^q \right]^{1/q}, \ \mathbf{v} \in \mathbb{R}^N \,, \ q \in \mathbb{Z}^+ \tag{2.8}$$

where v_i is the i^{th} component of the vector. Depending on the value chosen for q, local or global qualities of the vector may be obtained. For example, $q = 2$ provides the root of a quadrature sum of all elements in the vector giving a global measure of the vector while $q = \infty$ gives the maximum value in the vector, a local quantity that does not give information regarding the other elements in the vector.

We can also compute the norm of a matrix by inferring from the norm of the vector on which it is operating. Per LeVeque, we search for a constant that is equivalent to $\|\mathbf{A}\|$:

$$\|\mathbf{A}\mathbf{x}\| \leqslant C\|\mathbf{x}\| \,, \tag{2.9}$$

where the minimum value of C that satisfies Eq (2.9) is equivalent to $\|\mathbf{A}\|$ and is valid $\forall \mathbf{x} \in \mathbb{R}^N$. The general definition in Eq (2.9) can be expanded in simple terms for common norms including the infinity norm:

$$\|\mathbf{A}\|_\infty = \max_{1 \leqslant i \leqslant N} \sum_{j=1}^{N} |a_{ij}| \,, \tag{2.10}$$

and the 2-norm:

$$\|\mathbf{A}\|_2 = \sqrt{\rho(\mathbf{A}^T\mathbf{A})} \,, \tag{2.11}$$

where ρ is the spectral radius as defined in Eq (2.6).

Knowing this, we can then define several useful properties of matrices including the *condition number*:

$$\kappa(\mathbf{A}) = \|\mathbf{A}\| \, \|\mathbf{A}^{-1}\| \,, \tag{2.12}$$

which gives as a metric on assessing how close to singular the system is. This is due to the fact $\|\mathbf{A}^{-1}\|$ is large near singularities (and undefined for a singular matrix) and thus a large condition number will be generated. We define such matrices as *ill-conditioned*.

2.2 Stationary Methods

Stationary methods for linear systems arise from splitting the operator in Eq (2.1):

$$\mathbf{A} = \mathbf{M} - \mathbf{N} \,, \tag{2.13}$$

where the choice of $\mathbf{M}$ and $\mathbf{N}$ will be dictated by the particular method chosen. Using this split definition of the operator we can then write:

$$\mathbf{M}\mathbf{x} - \mathbf{N}\mathbf{x} = \mathbf{b} \,. \tag{2.14}$$

By rearranging, we can generate a form more useful for analysis:

$$\mathbf{x} = \mathbf{H}\mathbf{x} + \mathbf{c}\,, \tag{2.15}$$

where $\mathbf{H} = \mathbf{M}^{-1}\mathbf{N}$ is defined as the *iteration matrix* and $\mathbf{c} = \mathbf{M}^{-1}\mathbf{b}$. With the solution vector on both the left and right hand sides, an iterative method can then be formed:

$$\mathbf{x}^{\mathsf{k}+1} = \mathbf{H}\mathbf{x}^{\mathsf{k}} + \mathbf{c}\,, \tag{2.16}$$

with $\mathsf{k} \in \mathbb{Z}^{+}$ defined as the *iteration index*. In general, we will define methods in the form of Eq (7.4) as *stationary methods*. Given this, we can then generate a few statements regarding the convergence of such stationary methods. Defining $\mathbf{e}^{\mathsf{k}} = \mathbf{u}^{\mathsf{k}} - \mathbf{u}$ as the solution error at the k^{th} iterate, we can subtract Eq (7.3) from Eq (7.4) to arrive at an error form of the linear problem:

$$\mathbf{e}^{\mathsf{k}+1} = \mathbf{H}\mathbf{e}^{\mathsf{k}}\,. \tag{2.17}$$

Our error after k iterations is then:

$$\mathbf{e}^{\mathsf{k}} = \mathbf{H}^{\mathsf{k}}\mathbf{e}^{0}\,. \tag{2.18}$$

In other words, successive application of the iteration matrix is the mechanism driving down the error in a stationary method. We can then place restrictions on the iteration matrix by using the tools developed in § (2.1). By assuming $\mathbf{H}$ is diagonalizable[2] (Saad, 2003), we then have:

$$\mathbf{e}^{\mathsf{k}} = \mathbf{R}\mathbf{\Lambda}^{\mathsf{k}}\mathbf{R}^{-1}\mathbf{e}^{0}\,, \tag{2.19}$$

where $\mathbf{\Lambda}$ contains the Eigenvalues of $\mathbf{H}$ on its diagonal and the columns of $\mathbf{R}$ contain the Eigenvectors of $\mathbf{H}$. Computing the 2-norm of the above form

[2]We may generalize this to non-diagonalizable matrices with the Jordan canonical form of $\mathbf{H}$.

then gives:

$$||\mathbf{e}^{\mathsf{k}}||_2 \leqslant ||\boldsymbol{\Lambda}^{\mathsf{k}}||_2 \; ||\mathbf{R}||_2 \; ||\mathbf{R}^{-1}||_2 \; ||\mathbf{e}^0||_2 \,, \tag{2.20}$$

which gives:

$$||\mathbf{e}^{\mathsf{k}}||_2 \leqslant \rho(\mathbf{H})^{\mathsf{k}} \kappa(\mathbf{R}) ||\mathbf{e}^0||_2 \,. \tag{2.21}$$

For iteration matrices where the Eigenvectors are orthogonal, $\kappa(\mathbf{R}) = 1$ and the error bound reduces to:

$$||\mathbf{e}^{\mathsf{k}}||_2 \leqslant \rho(\mathbf{H})^{\mathsf{k}} ||\mathbf{e}^0||_2 \,. \tag{2.22}$$

We can now restrict $\mathbf{H}$ by asserting that $\rho(\mathbf{H}) < 1$ for a stationary method to converge such that k applications of the iteration matrix will not cause the error to grow in Eq (7.10).

2.3 Projection Methods

Among the most common iterative methods used in scientific computing today for sparse systems are of a broad class known as *projection methods*. These methods not only provide access to more powerful means of reaching a solution, but also a powerful means of encapsulating the majority of common iterative methods including the stationary methods just discussed in a common mathematical framework. All projection methods are built around a core structure where the solution to Eq (2.1) is extracted from a *search subspace* $\mathcal{K}$ and bound by a *constraint subspace* $\mathcal{L}$ that will vary in definition depending on the iterative method selected. We build the approximate solution $\tilde{\mathbf{x}}$ by starting with an initial guess $\mathbf{x}_0$ and extracting a correction $\boldsymbol{\delta}$ from $\mathcal{K}$ such that:

$$\tilde{\mathbf{x}} = \mathbf{x}_0 + \boldsymbol{\delta}, \;\; \boldsymbol{\delta} \in \mathcal{K} \,. \tag{2.23}$$

We bound this correction by asserting that the new residual, $\tilde{\mathbf{r}}$, be orthogonal to $\mathcal{L}$:

$$\langle \tilde{\mathbf{r}}, \mathbf{w} \rangle = 0, \ \forall \mathbf{w} \in \mathcal{L} \ . \tag{2.24}$$

We can generate a more physical and geometric-based understanding of these constraints by writing the new residual as $\tilde{\mathbf{r}} = \mathbf{r}_0 - \mathbf{A}\boldsymbol{\delta}$ and again asserting the residual must be orthogonal to $\mathcal{L}$. If $\tilde{\mathbf{r}}$ is to be orthogonal to $\mathcal{L}$, then $\mathbf{A}\boldsymbol{\delta}$ must be the projection of $\mathbf{r}_0$ onto the subspace $\mathcal{L}$ that eliminates the components of the residual that exist in $\mathcal{L}$. This situation is geometrically presented in Figure 2.1.

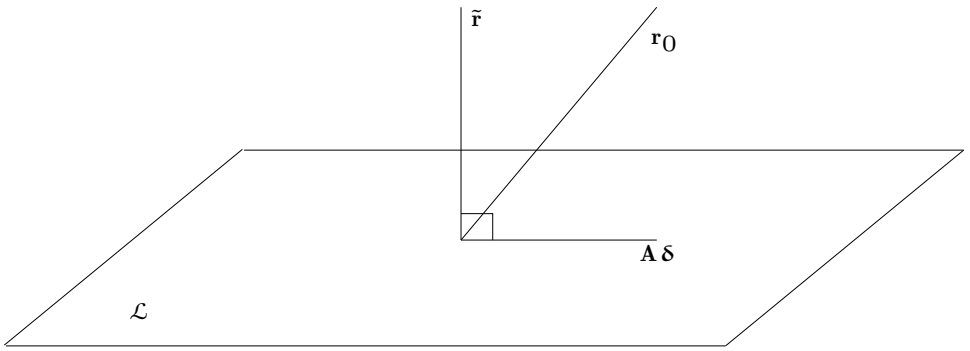

Figure 2.1: **Orthogonality constraint of the new residual with respect to $\mathcal{L}$.** *By projecting $\mathbf{r}_0$ onto the constraint subspace, we minimize the new residual by removing those components.*

From Figure 2.1 we then note that the following geometric condition must hold:

$$||\tilde{\mathbf{r}}||_2 \leqslant ||\mathbf{r}_0||_2, \ \forall \mathbf{r}_0 \in \mathbb{R}^{\mathsf{N}} \ , \tag{2.25}$$

meaning that the residual of the system will always be *minimized* with respect to the constraints.

Given this minimization condition for the residual, we can form the outline of an iterative projection method. Consider a matrix $\mathbf{V}$ to form a basis of $\mathcal{K}$ and a matrix $\mathbf{W}$ to form a basis of $\mathcal{L}$. As $\boldsymbol{\delta} \in \mathcal{K}$ by definition in

Eq (2.23), then $\boldsymbol{\delta}$ can instead be rewritten as:

$$\boldsymbol{\delta} = \mathbf{V}\mathbf{y}, \ \forall \mathbf{y} \in \mathbb{R}^{\mathsf{N}} : \tag{2.26}$$

where $\mathbf{V}$ *projects* $\mathbf{y}$ onto $\mathcal{K}$. From the orthogonality constraint in Eq (2.24) it then follows that:

$$\mathbf{y} = (\mathbf{W}^{\mathsf{T}}\mathbf{A}\mathbf{V})^{-1}\mathbf{W}^{\mathsf{T}}\mathbf{r}_0 \, , \tag{2.27}$$

where here the projection onto $\mathcal{K}$ is constrained by the projection onto $\mathcal{L}$. Knowing this, we can then outline the following iteration scheme for a projection method:

$$\mathbf{r}^{\mathsf{k}} = \mathbf{b} - \mathbf{A}\mathbf{x}^{\mathsf{k}} \, , \tag{2.28a}$$

$$\mathbf{y}^{\mathsf{k}} = (\mathbf{W}^{\mathsf{T}}\mathbf{A}\mathbf{V})^{-1}\mathbf{W}^{\mathsf{T}}\mathbf{r}^{\mathsf{k}} \, , \tag{2.28b}$$

$$\mathbf{x}^{\mathsf{k}+1} = \mathbf{x}^{\mathsf{k}} + \mathbf{V}\mathbf{y}^{\mathsf{k}} \, , \tag{2.28c}$$

where $\mathbf{V}$ and $\mathbf{W}$ are generated from the definitions of $\mathcal{K}$ and $\mathcal{L}$ and are updated prior to each iteration.

From an iteration standpoint, as we choose $\boldsymbol{\delta}$ from $\mathcal{K}$ and constrain it with $\mathcal{L}$, each iteration performs a projection that systematically annihilates the components of the residual that exists in $\mathcal{L}$. This then means that if our convergence criteria for an iterative method is bound to the residual of the system, then Eq (2.25) tells us that each projection step guarantees us that the norm of the new residual will never be worse than that of the previous step and will typically move us towards convergence. Depending on the qualities of the system in Eq (2.1), the selection of the subspaces $\mathcal{K}$ and $\mathcal{L}$ can serve to both guarantee convergence and optimize the rate at which the residual is decreased.

Krylov Subspace Methods

Among the most common projection techniques used in practice are a class of methods known as *Krylov subspace methods*. Here, the search subspace is defined as the *Krylov subspace*:

$$\mathcal{K}_m(\mathbf{A}, \mathbf{r}_0) = \mathrm{span}\{\mathbf{r}_0, \mathbf{A}\mathbf{r}_0, \mathbf{A}^2\mathbf{r}_0, \ldots, \mathbf{A}^{m-1}\mathbf{r}_0\}\,, \tag{2.29}$$

where m denotes the dimensionality of the subspace. In order to accommodate a more general structure for the operator in Eq (2.1), we often choose an *oblique* projection method where $\mathcal{K} \neq \mathcal{L}$. If we choose $\mathcal{L} = \mathbf{A}\mathcal{K}_m(\mathbf{A}, \mathbf{r}_0)$, then we are ultimately solving the normal system $\mathbf{A}^\mathsf{T}\mathbf{A}\mathbf{x} = \mathbf{A}^\mathsf{T}\mathbf{b}$ where $\mathbf{A}^\mathsf{T}\mathbf{A}$ will be symmetric positive definite if $\mathbf{A}$ is nonsingular, thereby expanding the range of operators over which these methods are valid. This choice of constraint subspace also then gives us the result via Eq (2.24) that the residual is minimized for all $\boldsymbol{\delta} \in \mathcal{K}$, forming the basis for the *generalized minimum residual method* (GMRES) (Saad and Schultz, 1986).

Choosing GMRES as our model Krylov method, we are first tasked with finding a projector onto the subspace. We seek an orthonormal basis for $\mathcal{K}_m(\mathbf{A}, \mathbf{r}_0)$ by an orthogonalization procedure that is commonly based on, but not limited to, the *Arnoldi* recurrence relation. The Arnoldi procedure will generate an orthonormal basis, $\mathbf{V}_m \in \mathbb{R}^{N \times m}$, via a variant of the Gram-Schmidt procedure that re-applies the operator for each consecutive vector, thus forming a basis that spans the subspace in Eq (2.29). Due to its equivalent dimensionality, m, to that of the subspace, we will refer to such recurrence relations as *long recurrence relations*. Those orthogonal projection procedures that have a dimensionality less than m will be referred to as *short recurrence relations*. Once $\mathbf{V}_m$ is found, per the constraint subspace definition it then follows that its basis is defined as $\mathbf{W}_m = \mathbf{A}\mathbf{V}_m$. Knowing the projections onto the search and constraint subspaces, the GMRES iteration may be formulated as follows:

Algorithm 2.1 GMRES Iteration

$\mathbf{r}_0 := \mathbf{b} - \mathbf{A}\mathbf{x}_0$
$\beta := \|\mathbf{r}_0\|_2$
$\mathbf{v}_1 := \mathbf{r}_0/\beta$ ▷ Create the orthonormal basis for the Krylov subspace
for $j = 1, 2, \cdots, m$ **do**
  $h_{ij} \leftarrow \langle w_j, v_j \rangle$
  $w_j \leftarrow w_j - h_{ij} v_i$
end for
$h_{j+1,j} \leftarrow \|w_j\|_2$
$v_{j+1} \leftarrow w_j / h_{j+1,j}$ ▷ Apply the orthogonality constraints
$\mathbf{y}_m \leftarrow \mathrm{argmin}_y \|\beta \mathbf{e}_1 - \mathbf{H}_m \mathbf{y}\|_2$
$\mathbf{x}_m \leftarrow \mathbf{x}_0 + \mathbf{V}_m \mathbf{y}_m$

We note here several properties of this formulation and how they may facilitate or hinder the solution of large-scale, sparse linear problems, also noting that these properties are common among many Krylov methods. First, from a memory perspective GMRES is efficient in that the operator $\mathbf{A}$ need not be explicitly stored. Rather, only the ability to compute the action of that operator on a vector of valid size is required. However, these savings in memory are balanced by the fact that the long recurrence relations used in the Arnoldi procedure require all vectors that span the Krylov space to be stored. If the size of these vectors becomes prohibitive, the Arnoldi procedure can be restarted at the cost of losing information in the orthogonalization process, creating the potential to generate new search directions that are not orthogonal to all previous search directions (and therefore less than optimal). From an implementation perspective, because the operator is not required to be formed, GMRES is significantly more flexible in its usage in that there are many instances where various processes serve to provide the action of that operator (e.g. radiation transport sweeps (Evans et al., 2010)) that normally may not be amenable to its full construction. In addition, the minimization problem is a straight-forward least-squares problem where $\mathbf{H}$ is an upper-Hessenberg matrix.

2.4 Parallel Projection Methods

Modern parallel implementations of projection methods on distributed memory architectures rely heavily on capabilities provided by general linear algebra frameworks. For methods like GMRES, this arises from the fact that Krylov methods require only a handful of operation types in their implementation that can be efficiently programmed on these architectures. Per Saad's text (Saad, 2003) and as noted in Algorithm 2.1, these operations are preconditioning, matrix-vector multiplications, vector updates, and inner products. For the last three items, linear algebra libraries such as PETSc (Gropp and Smith, 1993) and Trilinos (Heroux et al., 2005) provide efficient parallel implementations for these operations. Depending on the type of preconditioning used, efficient parallel implementations may also be available for those operations. Due to their prevalence in modern numerical methods, parallel formulations these operations have warranted intense study (Tuminaro et al., 1998). In all cases, a series of scatter/gather operations are required such that global communication operations must occur. Although the relative performance of such operations is bound to the implementation, asymptotically performance should be the same across all implementations.

We will look at the three primary parallel matrix/vector operations as preconditioning is not an immediate requirement for implementing the algorithms. We note here that variants are available that reduce the number of global communications required (consider Sosonkina et al. (1998) as an example of reducing global operation counts using a different orthogonalization procedure than Arnoldi), however, we will only consider the basic algorithms here as this handful of operations can be generalized to fit more complicated algorithms. In all of these cases, we assume a general matrix/vector formulation that is distributed in parallel such that both local and global knowledge of their decomposition is available on request. Furthermore, it is assumed that these objects are partitioned in such a way that the parallel

formulation of the operator and vectors in Eq (2.1) will be such that each parallel process contains only a subset of the global problem and that subset forms a local set of complete equations. The form of this partitioning is problem dependent and often has a geometric or graph-based aspect to its construction in order to optimize communication patterns. Libraries such as Zoltan (Devine et al., 2002), provide implementations of such algorithms.

Parallel Vector Update

Parallel vector update operations arise from the construction of the orthonormal basis and the application of the correction generated by the constraints to the solution vector. Vector update operations are embarrassingly parallel in that they require no communication operations to be successfully completed; all data operated on is local. These operations are globally of the form:

$$\mathbf{y}[\mathfrak{n}] \leftarrow \mathbf{y}[\mathfrak{n}] + \mathfrak{a} * \mathbf{x}[\mathfrak{n}],\ \forall \mathfrak{n} \in [1, \mathsf{N}_\mathfrak{g}]\,, \tag{2.30}$$

and locally of the form:

$$\mathbf{y}[\mathfrak{n}] \leftarrow \mathbf{y}[\mathfrak{n}] + \mathfrak{a} * \mathbf{x}[\mathfrak{n}],\ \forall \mathfrak{n} \in [1, \mathsf{N}_\mathfrak{l}]\,, \tag{2.31}$$

where $\mathbf{y}$ and $\mathbf{x}$ are vectors of global size $\mathsf{N}_\mathfrak{g}$, local size $\mathsf{N}_\mathfrak{l}$, and $\mathfrak{a} \in \mathbb{R}^{\mathsf{N}}$. In order to avoid communication, the vectors $\mathbf{y}$ and $\mathbf{x}$ must have the same parallel decomposition where each parallel process owns the same pieces of each vector.

Parallel Vector Product

Vector product operations are used in several instances during a Krylov iteration including vector norm computations and the orthogonalization procedure. By definition, the vector product is a global operation that effectively collapses a set of vectors to a single value. Therefore, we cannot

eliminate all global communications. Instead, vector product operations are formulated as *global reduction operations* that are efficiently supported by modern message passing libraries. For the dot product of two vectors $\mathbf{y}$ and $\mathbf{x}$, a single reduction is required such that:

$$\mathtt{d}_\mathtt{l} = \mathbf{y}_\mathtt{l} \cdot \mathbf{x}_\mathtt{l}, \;\; \mathtt{d}_\mathtt{g} = \sum_\mathtt{p} \mathtt{d}_\mathtt{l} \; , \tag{2.32}$$

where the $\mathtt{l}$ subscript denotes a local quantity, $\mathtt{d}_\mathtt{l}$ is the local vector dot product, and $\mathtt{d}_\mathtt{g}$ is the global dot product generated by summing the local dot products over all $\mathtt{p}$ processes. Parallel norm operations can be conducted with the same single reduction. Consider the infinity norm operation:

$$\|\mathbf{x}\|_{\infty,\mathtt{l}} = \max_\mathtt{n} \mathbf{y}[\mathtt{n}], \;\; \forall \mathtt{n} \in [1, \mathtt{N}_\mathtt{l}] \tag{2.33a}$$

$$\|\mathbf{x}\|_{\infty,\mathtt{g}} = \max_\mathtt{p} \|\mathbf{x}\|_{\infty,\mathtt{l}} \; . \tag{2.33b}$$

In this form, the local infinity norm is computed over the local piece of the vector. The reduction operation is then formed over all $\mathtt{p}$ processes such that the global max of the vector is computed and distributed to all processes.

Parallel Matrix-Vector Multiplications

We finally consider parallel matrix-vector multiplication operations using sparse matrices in a compressed storage format by considering Saad's outline as well as the more formal work of Tuminaro (Tuminaro et al., 1998). For these operations, more complex communication patterns will be required given that the entire global vector is required in order to compute a single element of the local product vector. Fortunately, the vast majority of the global vector components will be multiplied by zero due to the sparsity of the matrix and therefore much of the vector can be neglected. Instead we only require data from a handful of other processes that can be acquired

through asynchronous/synchronous communications. Consider the sparse matrix-vector multiply in Figure 2.2 that is partitioned on 3 processors. Each process owns a set of equations that correlate to the physical domain

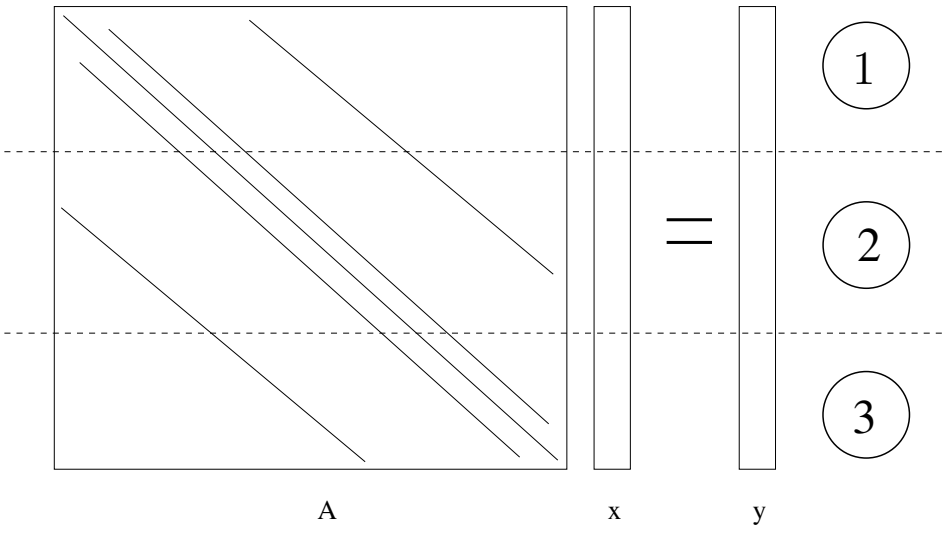

Figure 2.2: **Sparse matrix-vector multiply Ax = y operation partitioned on 3 processors.** *Each process owns a set of equations that correlates to its physical domain.*

of which it has ownership. We can break down the equations owned by each process in order to devise an efficient scheme for the multiplication. Consider the portion of the matrix-vector multiply problem owned by process 1 in Figure 2.2. As shown in Figure 2.3, the components of the matrix will be multiplied by pieces of the vector that are owned by all processors. For those pieces of the matrix that are owned by process 1 that act on the vector owned by process 1, we do these multiplications first as no communication is required. Next, process 1 gathers the components of the global vector owned by the other two processes that it requires to complete its part of the vector product. For this example, the components of matrix owned by process 1 that will operate on the global vector components owned by process 3 are

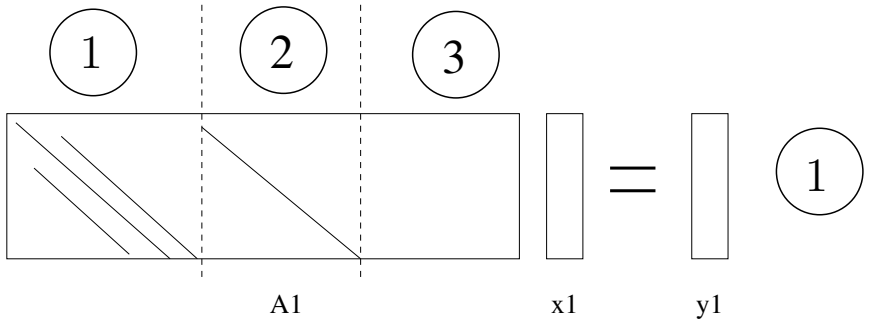

Figure 2.3: **Components of sparse matrix-vector multiply operation owned by process 1.** *The numbers above the matrix columns indicate the process that owns the piece of the global vector they are acting on. In order to compute its local components of the matrix-vector product, process 1 needs its matrix elements along with all elements of the global vector owned by processes 2 and 3. The piece of the matrix shown is* $\mathbf{A}_1$ *and it is acting locally on* $\mathbf{x}_1$ *to compute the local piece of the product,* $\mathbf{y}_1$.

zero, and therefore no vector elements are required to be scattered from process 3 to process 1. Those matrix elements owned by process 1 that will act on the piece of the vector owned by process 2 are not all non-zero, and therefore we must gather the entire process 2 vector components onto process 1 to complete the multiplication. Conversely, processes 2 and 3 must scatter their vector components that are required by other processes (such as process 1) in order to complete their pieces of the product. This then implies that these domain connections for proper gather and scatter combinations must be constructed a priori. These data structures are typically generated by a data partitioning library. Mathematically, if we are performing a global matrix-vector multiply of the form $\mathbf{Ax} = \mathbf{y}$, then for this example on process 1 we have a sequence of local matrix-vector multiplications:n $\mathbf{A}_1\mathbf{x}_1 + \mathbf{A}_1\mathbf{x}_2 = \mathbf{y}_1$, with the subscripts provided by notation in Figure 2.3. Here, some of the data is intrinsically local, and some must be gathered from other processes using the partitioning data structures.

Parallel Performance Implications for Krylov Methods

Knowing the parallel characteristics of the key operations we must perform in order to implement Krylov methods, we can make a few statements about parallel performance and implications for operation on machines of increasing size. Reconsider the matrix and vector operations required to implement Algorithm 2.1. For very large distributed machines, the global reduction operations required at several levels of Krylov algorithms stand to reduce scalability and performance. In the case of GMRES, these reductions include vector norm operations and the inner products required for basis orthogonalization. Furthermore, communication between adjacent domains in matrix-vector multiply operations may also cause a bottleneck as the number of domains used in a simulation grows and the number of processors participating in the gather/scatter sequence requires a large communication bandwidth. The end result is that global data must be collected and communicated. For scaling improvement, we seek a reduction in these types of operations. In addition, these issues become more prominent as the Krylov iterations progress, causing the Krylov subspace to grow and the total number of operations needed to orthogonalize that subspace to increase.

As an example of these performance implications in practice, in a 2001 work, Gropp and colleagues presented results on fluid dynamic simulations that heavily leveraged Krylov methods in their solution schemes (Gropp et al., 2001). In this follow-on to their 1997 Bell Prize-winning work, part of their analysis included identifying parallel scalability bottlenecks generated by solver implementations in a strong scaling exercise where the number of processors was increased with respect to a fixed global problem size. Gropp's observations show that for their particular hardware, a distributed memory machine similar to modern architectures, that global reduction operations

did not impede scalability, meaning that the global reduction operation occupied approximately the same percentage of compute time independent of the number of processors used. Rather, it was the gather/scatter operations required to communicate data to neighboring processors that reduced performance with an increasing percentage of compute time consumed by these operations as processor count was increased. Furthermore, it was noted that this reduction in scaling was a product of poor algorithmic strong scaling rather than hardware or implementation related issues as the algorithm requires more data to be scattered/gathered as the number of processors and therefore computational domains increased. In the case of a weak scaling exercise, we would instead expect this percentage to exhibit a more desirable behavior of remaining constant for gather/scatter operations as problem size would be scaled with the number of processors.

Chapter 3

Monte Carlo Solution Methods for Linear Systems

An alternative approach to approximate matrix inversion is to employ Monte Carlo methods that sample a distribution with an expectation value equivalent to that of the inverted operator. Such methods have been in existence for decades with the earliest reference noted here an enjoyable manuscript published in 1950 by Forsythe and Leibler (Forsythe and Leibler, 1950). In their outline, Forsythe and Liebler in fact credit the creation of this technique to J. Von Neumann and S.M. Ulam some years earlier than its publication. In 1952 Wasow provided a more formal explanation of Von Neumann and Ulam's method (Wasow, 1952) and Hammersley and Handscomb's 1964 monograph (Hammersley and Handscomb, 1964) and Spanier and Gelbard's 1969 book (Spanier and Gelbard, 1969) present additional detail on this topic using a collection of references from the 1950's and early 1960's.

3.1 Preliminaries

We begin our discussion of Monte Carlo methods using these texts by seeking a solution to Eq (2.1). For a given linear operator $\mathbf{A}$, we can use diagonal splitting in a similar manner as the stationary method in Eq (7.3) to define the following operator[1]:

$$\mathbf{H} = \mathbf{I} - \mathbf{A} \,, \tag{3.1}$$

[1]It should be noted that non-diagonal splittings have been recently explored in (Srinivasan, 2010) and have the potential to improve efficiency.

such that we are solving the system:

$$\mathbf{x} = \mathbf{H}\mathbf{x} + \mathbf{b}\,. \tag{3.2}$$

We can then form an alternative representation for $\mathbf{A}^{-1}$ by generating the *Neumann series*:

$$\mathbf{A}^{-1} = (\mathbf{I} - \mathbf{H})^{-1} = \sum_{k=0}^{\infty} \mathbf{H}^k\,, \tag{3.3}$$

which will converge if the spectral radius of $\mathbf{H}$ is less than 1. If we then apply this Neumann series to the right hand side of Eq (2.1) we acquire the solution to the linear problem:

$$\mathbf{A}^{-1}\mathbf{b} = \sum_{k=0}^{\infty} \mathbf{H}^k\mathbf{b} = \mathbf{x}\,. \tag{3.4}$$

An approximation of this summation by truncation will therefore lead to an approximation of the solution. If we expand the summation with a succession of matrix-vector multiply operations, we arrive at an alternative perspective of this summation by considering its i^{th} component:

$$\chi_i = \sum_{k=0}^{\infty} \sum_{i_1}^{N} \sum_{i_2}^{N} \cdots \sum_{i_k}^{N} h_{i,i_1} h_{i_1,i_2} \ldots h_{i_{k-1},i_k} b_{i_k}\,, \tag{3.5}$$

which can interpreted as a series of transitions between states,

$$\nu = i \to i_1 \to \cdots \to i_{k-1} \to i_k\,, \tag{3.6}$$

in $\mathbf{H}$ where ν is interpreted as a particular random walk sequence permutation. We can generate these sequences of transitions through Monte Carlo random walks by assigning them both a probability and weight. As a reinterpretation of the iteration matrix, we then form the *Neumann-Ulam*

decomposition of **H**:

$$\mathbf{H} = \mathbf{P} \circ \mathbf{W} \,, \tag{3.7}$$

where $\circ$ denotes the Hadamard product operation[2], **P** denotes the transition probability matrix, and **W** denotes the transition weight matrix. This decomposition, a generalization of Dimov's work (Dimov et al., 1998), is an extension of the original Neumann-Ulam scheme in that now a weight cutoff can be used to terminate a random walk sequence and therefore truncate the Neumann series it is approximating. The formulation of **P** and **W** will be dependent on whether we choose a direct or adjoint Monte Carlo sequence to estimate the state transitions in Eq (3.5).

3.2 Direct Method

In the context of matrix inversion, a direct method resembles an adjoint Monte Carlo method in the reactor physics community where the solution state is sampled and the source terms that contribute to it are assembled. To achieve this, we build the direct method Neumann-Ulam decomposition per Dimov's approach by first choosing a probability matrix that is a row scaling of **H** such that its components are:

$$\mathfrak{p}_{ij} = \frac{|\mathfrak{h}_{ij}|}{\sum_j |\mathfrak{h}_{ij}|} \,. \tag{3.8}$$

From this, we then see that the probability of transitioning from a state $\mathfrak{i}$ to a state $\mathfrak{j}$ is implicitly linked to the original operator **A** in that those terms with large values, and therefore those that make the greatest contribution to the numerical solution, will be sampled with a higher probability than smaller terms. In addition, the row scaling provides a normalization over the state to which we are transitioning such that $\sum_j \mathfrak{p}_{ij} = 1$, meaning that we sample the probabilities over the rows of the matrix. The components of

[2]The Hadamard product $\mathbf{A} = \mathbf{B} \circ \mathbf{C}$ is defined element-wise as $\mathfrak{a}_{ij} = \mathfrak{b}_{ij}\mathfrak{c}_{ij}$.

the weight matrix are then defined by Eq (3.7) as:

$$w_{ij} = \frac{h_{ij}}{p_{ij}} \, . \tag{3.9}$$

It should be noted here that if **A** is sparse, then **H**, **P**, and **W** must be sparse as well by definition. Additionally, we only compute **P** and **W** from the non-zero elements of **H** as those components that are zero will not participate in the random walk. Doing so prevents an infinite weight from being generated in Eq (3.9) and eliminates unnecessary computations.

Using these matrices, we can then form the expectation value of the direct solution. For a given random walk permutation ν with k events, we define the weight of that permutation to be:

$$W_m = w_{i,i_1} w_{i_1,i_2} \cdots w_{i_{m-1},i_m} \, , \tag{3.10}$$

such that the weight of each transition event contributes to the total. The contribution to the solution from a particular random walk permutation is then:

$$X_\nu(i_0 = i) = \sum_{m=0}^{k} W_m b_{i_m} \, , \tag{3.11}$$

where $X_\nu(i_0 = i)$ signifies that the solution state in which we are tallying defines state i. We can interpret this precisely as before in that during the random walk we collect the source in the states that are visited and apply them to the solution tally. We then define the probability that a particular random walk permutation of k events will occur:

$$P_\nu = p_{i,i_1} p_{i_1,i_2} \cdots p_{i_{k-1},i_k} \, . \tag{3.12}$$

Finally, we define the expectation value of X to be the collection of all

random walk permutations and their probabilities:

$$\mathsf{E}\{\mathsf{X}(\mathsf{i}_0 = \mathsf{i})\} = \sum_{\nu} \mathsf{P}_\nu \mathsf{X}_\nu \,, \tag{3.13}$$

which, if expanded, directly recovers the exact solution:

$$\begin{aligned}\mathsf{E}\{\mathsf{X}(\mathsf{i}_0 = \mathsf{i})\} &= \sum_{k=0}^{\infty} \sum_{i_1}^{N} \sum_{i_2}^{N} \cdots \sum_{i_k}^{N} p_{i,i_1} p_{i_1,i_2} \cdots p_{i_{k-1},i_k} w_{i,i_1} w_{i_1,i_2} \cdots w_{i_{k-1},i_k} b_{i_k} \\ &= x_i \,,\end{aligned} \tag{3.14}$$

therefore providing an unbiased Monte Carlo estimator.

In cases where we seek only approximate solutions, we need only to perform a minimal number of random walks in order to generate an approximation for $\mathbf{x}$. If we are only to approximate the solution, we also need conditions by which we may terminate a random walk. We do this by noticing that the factors added to Eq (3.10) will become diminishingly small due to their definition in Eq (3.9) and therefore their contributions to the solution estimate will become negligible. Using this, we choose terminate a random walk sequence with a *weight cutoff*, W_c, that is enforced when $W_m < W_c$ for a particular random walk permutation.

Direct Method: Evolution of a Solution

As a means of visually demonstrating the direct Monte Carlo method, consider a 2-dimensional thermal diffusion problem with sources on the left and right hand sides of the domain and a smaller uniform source as shown in Figure 3.1. For this problem, the number of histories used to compute the solution at each state in the domain was increased from 1 to 1000 in order to show its effects on the solution and the statistical nature of the method. Figure 3.2 gives these results. As the number of histories used per

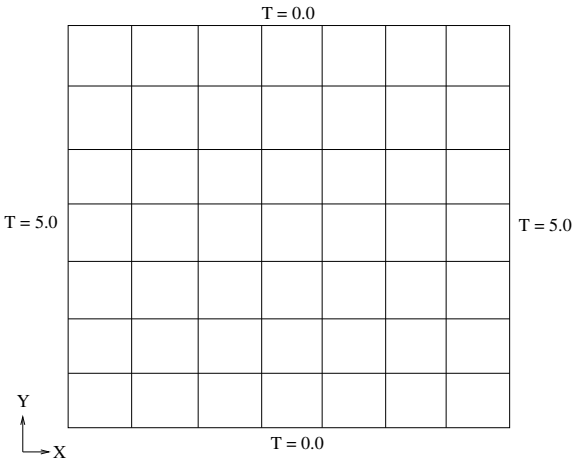

Figure 3.1: **Problem setup for 2D heat equation.** *Dirichlet conditions are set for the temperature on all 4 boundaries of the Cartesian grid. Background source of 1/5 the value of the boundary sources present.* 50×50 *grid.*

state is increased, the statistical variance of the solutions is decreased as more tallies are made. At 1000 histories per state, enough tallies have been made to generate a reasonable estimate for the structure of the solution.

Estimator Variance

We can compute the variance of the estimator through traditional methods by defining the variance, σ_i, for each component in the solution:

$$\sigma_i{}^2 = E\{X(i_0 = i) - (\mathbf{A}^{-1}\mathbf{b})_i\}^2 = E\{X(i_0 = i)^2\} - x_i^2 \,, \tag{3.15}$$

where the vector exponentials are computed element-wise. Inserting Eq (3.13) gives:

$$\sigma_i^2 = \Big(\sum_\nu P_\nu X_\nu^2 \Big)_i - x_i^2 \,, \tag{3.16}$$

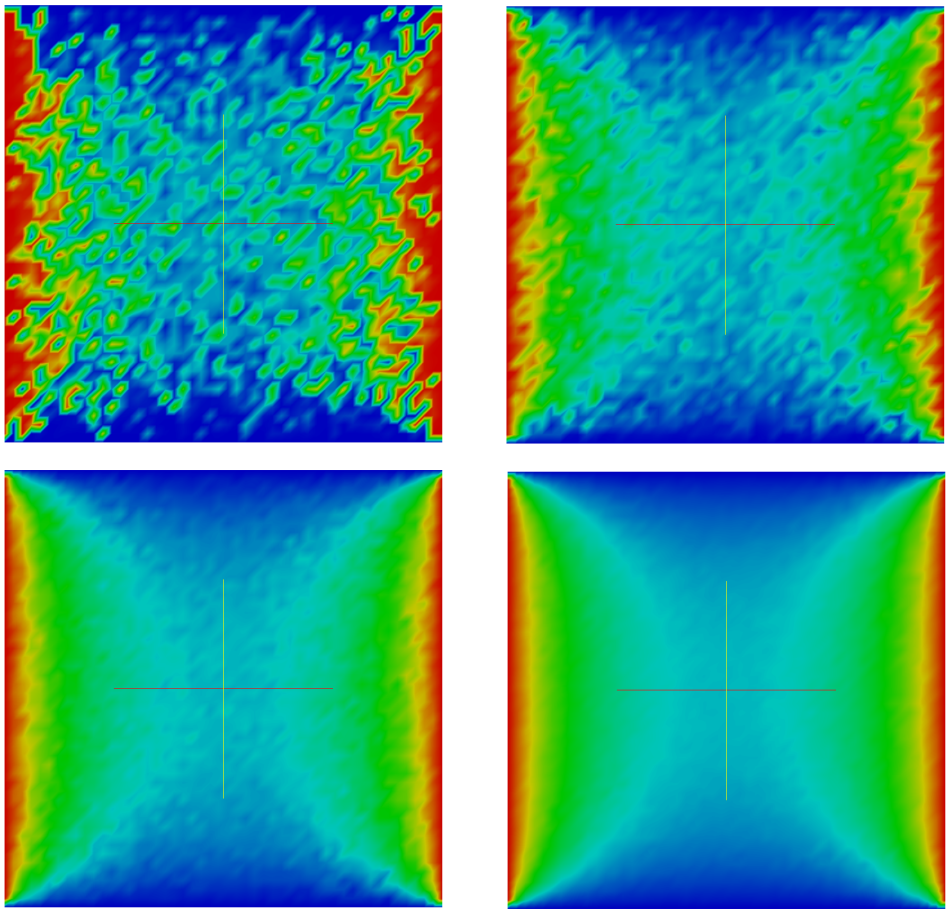

Figure 3.2: **Direct Monte Carlo solution to the heat equation with varying numbers of histories.** *Top left: 1 history per state. Top right: 10 histories per state. Bottom left: 100 histories per state. Bottom right: 1000 histories per state.*

and applying Eq (3.11):

$$\sigma_i^2 = \Big(\sum_{\nu} P_\nu \sum_{m=0}^{k} W_m^2 b_{i_m}^2 \Big)_i - x_i^2 \,. \tag{3.17}$$

Finally, expanding the transition probabilities yields the variance:

$$\sigma_i^2 = \sum_{k=0}^{\infty} \sum_{i_1}^{N} \sum_{i_2}^{N} \cdots \sum_{i_k}^{N} p_{i,i_1} p_{i_1,i_2} \cdots p_{i_{k-1},i_k} w_{i,i_1}^2 w_{i_1,i_2}^2 \cdots w_{i_{k-1},i_k}^2 b_{i_m} - \chi_i^2 \,. \tag{3.18}$$

Using this definition for the variance, we can arrive at a more natural reason for enforcing $\rho(\mathbf{H}) < 1$ for our Monte Carlo method to converge. Per the Hadamard product, we can concatenate the summation in Eq (3.18):

$$(\mathbf{P} \circ \mathbf{W} \circ \mathbf{W})^k = \sum_{k=0}^{\infty} \sum_{i_1}^{N} \sum_{i_2}^{N} \cdots \sum_{i_k}^{N} p_{i,i_1} p_{i_1,i_2} \cdots p_{i_{k-1},i_k} w_{i,i_1}^2 w_{i_1,i_2}^2 \cdots w_{i_{k-1},i_k}^2 . \tag{3.19}$$

If we assign $\mathbf{G} = \mathbf{P} \circ \mathbf{W} \circ \mathbf{W}$ as in Eq (3.7), we then have a new formulation for the variance:

$$\sigma_i^2 = \sum_{k=0}^{\infty} \sum_{i_1}^{N} \sum_{i_2}^{N} \cdots \sum_{i_k}^{N} g_{i,i_1} g_{i_1,i_2} \cdots g_{i_{k-1},i_k} b_{i_k}^2 - \chi_i^2 \,, \tag{3.20}$$

which contains the general Neumann series for $\mathbf{G}$,

$$\mathbf{T} = \sum_{k=0}^{\infty} \mathbf{G}^k \,, \tag{3.21}$$

where $\mathbf{T} = (\mathbf{I} - \mathbf{G})^{-1}$. We can then insert T back into the variance formulation for a more concise definition:

$$\sigma_i^2 = (\mathbf{T}\mathbf{b})_i - \chi_i^2 \,. \tag{3.22}$$

We can relate $\mathbf{G}$ to $\mathbf{H}$ by noting that $\mathbf{G}$ simply contains an additional Hadamard product with the weight matrix. The Hadamard product has the property that:

$$|\mathbf{H} \circ \mathbf{W}| \geqslant |\mathbf{H}| \, |\mathbf{W}| \,. \tag{3.23}$$

Using the norm property of the Hadamard product and Eq (3.7), we can define the norm of $\mathbf{W}$ as:

$$\frac{|\mathbf{H}|}{|\mathbf{P}|} \geqslant |\mathbf{W}| \,. \tag{3.24}$$

Choosing the infinity norm of the operator as defined in Eq (2.10), the row normalized probability matrix will yield a norm of 1 giving the following inequality for relating $\mathbf{G}$ and $\mathbf{H}$:

$$|\mathbf{G}| \geqslant |\mathbf{H}|^2 \tag{3.25}$$

Using these relations to analyze Eq (3.22), we see that if $\rho(\mathbf{G}) > 1$, then the sum in Eq (3.21) will not converge and an infinite variance will arise as the elements of $\mathbf{T}$ become infinite in Eq (3.22). We must restrict $\mathbf{G}$ to alleviate this and therefore restrict $\mathbf{H}$ due to Eq (3.25) with $\rho(\mathbf{H}) < 1$ so that our expectation values for the solution may have a finite variance.

3.3 Adjoint Method

An alternative formulation for Monte Carlo matrix inversion is the adjoint method. We begin by defining the linear system adjoint to Eq (2.1):

$$\mathbf{A}^{\mathsf{T}}\mathbf{y} = \mathbf{d} \,, \tag{3.26}$$

where $\mathbf{y}$ and $\mathbf{d}$ are the adjoint solution and source respectively and $\mathbf{A}^{\mathsf{T}}$ is the adjoint operator. We can split this equation to mirror Eq (3.2) by defining the following inner product equivalence (Spanier and Gelbard, 1969):

$$\langle \mathbf{A}^{\mathsf{T}}\mathbf{x}, \mathbf{y} \rangle = \langle \mathbf{x}, \mathbf{A}\mathbf{y} \rangle \,. \tag{3.27}$$

With this statement we can then define the split equation:

$$\mathbf{y} = \mathbf{H}^{\mathsf{T}}\mathbf{y} + \mathbf{d} \,. \tag{3.28}$$

As was required for convergence with the direct method using Eq (3.2), the spectral radius of $\mathbf{H}$ must remain less than 1 as $\mathbf{H}^{\mathsf{T}}$ contains the same eigenvalues and therefore has the same spectral radius. From this definition it follows that:

$$\langle \mathbf{x}, \mathbf{d} \rangle = \langle \mathbf{y}, \mathbf{b} \rangle \, . \tag{3.29}$$

Using these definitions, we can derive an estimator from the adjoint method that will also give the solution vector, $\mathbf{x}$. As with the direct method, we can acquire the adjoint solution by forming the Neumann series by writing Eq (3.28) as:

$$\mathbf{y} = (\mathbf{I} - \mathbf{H}^{\mathsf{T}})^{-1}\mathbf{d} \, , \tag{3.30}$$

which in turn yields the Neumann series using the adjoint operator:

$$\mathbf{y} = \sum_{k=0}^{\infty} (\mathbf{H}^{\mathsf{T}})^{k}\mathbf{d} \, . \tag{3.31}$$

We expand this summation to again yield a series of transitions that can be approximated by a Monte Carlo random walk sequence, this time forming the Neumann series in reverse order:

$$y_i = \sum_{k=0}^{\infty} \sum_{i_1}^{N} \sum_{i_2}^{N} \cdots \sum_{i_k}^{N} h_{i_k, i_{k-1}} \ldots h_{i_2, i_1} h_{i_1, i} d_{i_k} \, . \tag{3.32}$$

We can readily build an estimator for the adjoint solution from this series expansion, but we instead desire the direct solution. We achieve this by using Eq (3.29) as a constraint. Here we have 2 unknowns, $\mathbf{y}$ and $\mathbf{d}$, and therefore we require two constraints to close the system. We use Eq (3.29) as the first constraint and as a second constraint we select:

$$\mathbf{d} = \boldsymbol{\delta}_j \, , \tag{3.33}$$

where $\boldsymbol{\delta}_j$ is one of a set of vectors in which the j^{th} component is the Kronecker delta function $\delta_{i,j}$. If we apply Eq (3.33) to our first constraint Eq (3.29), we get the following convenient outcome:

$$\langle \mathbf{y}, \mathbf{b} \rangle = \langle \mathbf{x}, \boldsymbol{\delta}_j \rangle = x_j \,, \tag{3.34}$$

meaning that if we compute the inner product of the original source and the adjoint solution using a delta function source, we recover one component of the original solution.

In terms of particle transport, this adjoint method is equivalent to a traditional forward method. As a result of using the adjoint system, we modify our probabilities and weights using the *adjoint Neumann-Ulam decomposition* of $\mathbf{H}$:

$$\mathbf{H}^{\mathsf{T}} = \mathbf{P} \circ \mathbf{W} \,, \tag{3.35}$$

where now we are forming the decomposition with respect to the transpose of $\mathbf{H}$[3]. We then follow the same procedure as the direct method for forming the probability and weight matrices in the decomposition. Using the adjoint form, probabilities should instead be column-scaled:

$$p_{ij} = \frac{|h_{ji}|}{\sum_j |h_{ji}|} \,, \tag{3.36}$$

such that we expect to select a new state j from the current state in the random walk j by sampling column-wise. Per Eq (3.35), the transition weight is then defined as:

$$w_{ij} = \frac{h_{ji}}{p_{ij}} \,. \tag{3.37}$$

Using the decomposition we can then define an expectation value for the adjoint method. Given Eq (3.10) as the weight generated for a particular random walk permutation as in Eq (3.6) and our result from Eq (3.34)

[3]This is sometimes referred to as the adjoint form for real-valued matrices

generated by applying the adjoint constraints, the contribution to the solution in state $\mathtt{i}$ from a particular random walk permutation is then:

$$X_\nu = \sum_{m=0}^{k} W_m \delta_{i,i_m} \,, \tag{3.38}$$

where the Kronecker delta indicates that the tally contributes only in the current state and b_{i_0} will be the sampled source starting weight. Note here that the estimator in Eq (3.38) does not have a dependency on the source state as in Eq (3.38), providing a remedy for the situation in the direct method where we must start a random walk in each source state for every permutation such that we may compute a contribution for that state. In the adjoint method, we instead tally in all states and those of lesser importance will not be visited as frequently by the random walk. Finally, the expectation value using all permutations is:

$$E\{X\} = \sum_{\nu} P_\nu X_\nu \tag{3.39}$$

which, if expanded in the same way as the direct method, directly recovers the exact solution:

$$\begin{aligned} E\{X_j\} &= \sum_{k=0}^{\infty} \sum_{i_1}^{N} \sum_{i_2}^{N} \cdots \sum_{i_k}^{N} b_{i_0} h_{i_0,i_1} h_{i_1,i_2} \cdots h_{i_{k-1},i_k} \delta_{i_k,j} \\ &= x_j \,, \end{aligned} \tag{3.40}$$

therefore also providing an unbiased Monte Carlo estimate of the solution.

Like the direct method, we also desire a criteria for random walk termination for problems where only an approximate solution is necessary. For the adjoint method, we utilize a *relative weight cutoff*:

$$W_f = W_c b_{i_0} \,, \tag{3.41}$$

where W_c is defined as in the direct method. The adjoint random walk will then be terminated after m steps if $W_m < W_f$ as tally contributions become increasingly small.

Adjoint Method: Evolution of a Solution

As a means of visually demonstrating the adjoint Monte Carlo method, again considerthe a 2-dimensional thermal diffusion problem with sources on the left and right hand sides of the domain and a smaller uniform source as shown in Figure 3.1. For the adjoint method, the number of histories sampled from the source was increased from 10 to 10,000,000 in order to show its effects on the solution and the statistical nature of the method. Figure 3.3 gives these results. As the number of histories used per state is increased, the statistical variance of the solutions is decreased as more tallies are made. At 10,000,000 histories per state, enough tallies have been made to generate a reasonable estimate for the structure of the solution. The visual difference between Figures 3.2 and 3.3 is precisely that determined by their mathematics. As the adjoint solution evolves with the addition of histories, more histories emanate from the source with more penetrating the domain and making contributions to those tallies. As the direct method evolves, the solution simply comes into focus as histories are emanated from each state in the system and contribute only to the solution in that state regardless of their path.

3.4 Sequential Monte Carlo

The direct and adjoint Neumann-Ulam methods described are limited by a convergence rate of $1/\sqrt{N}$ by the Central Limit Theorem where N is the number of random walk permutations. In 1962, Halton presented a residual Monte Carlo method that moves towards exponential convergence rates (Halton, 1962) and further refined his work some years later (Halton,

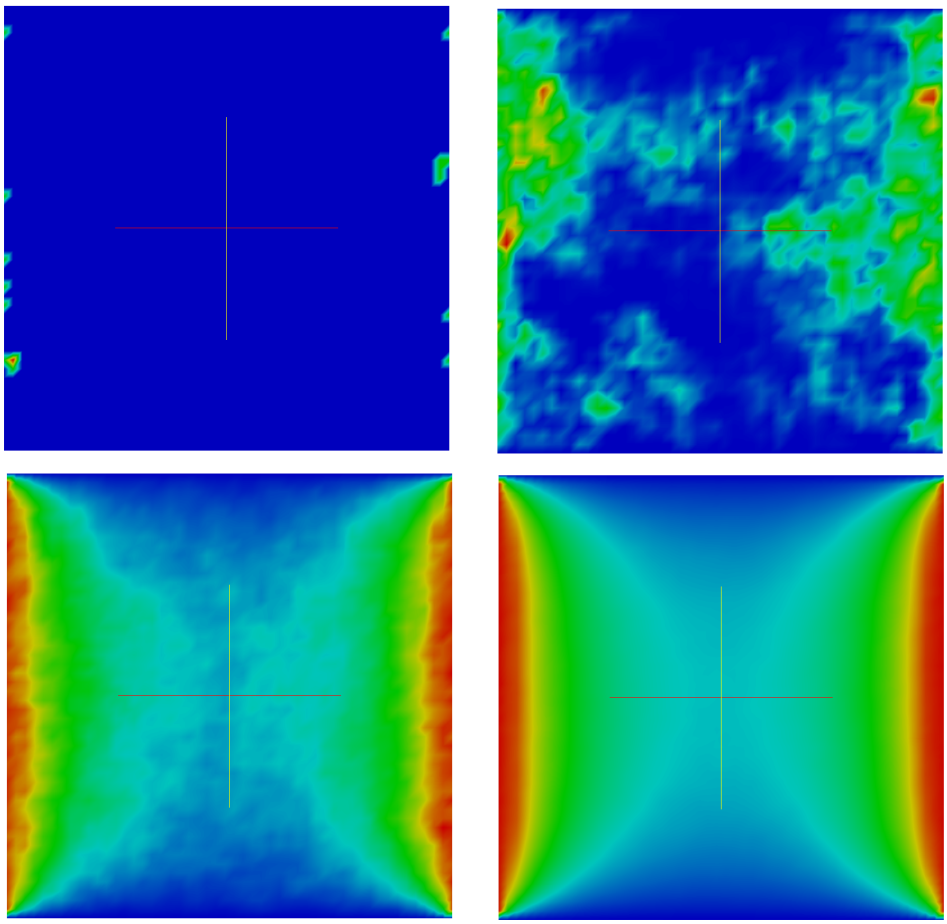

Figure 3.3: **Adjoint Monte Carlo solution to the heat equation with varying numbers of histories.** *Top left: 10 histories per state. Top right: 1,000 histories per state. Bottom left: 100,000 histories per state. Bottom right: 10,000,000 histories per state.*

1994). Applications of his work by the transport community have confirmed convergence rates on the order of of $\exp(-N)$ (Evans et al., 2003). In much the same way as projection methods, Halton's method, sequential Monte Carlo, utilizes the adjoint Monte Carlo solver as a means of directly reducing the residual vector. He proposed the following iterative scheme as a solution

to Eq (2.1)

$$\mathbf{r}^{\mathrm{k}} = \mathbf{b} - \mathbf{A}\mathbf{x}^{\mathrm{k}} \,, \tag{3.42a}$$

$$\mathbf{A}\boldsymbol{\delta}^{\mathrm{k}} = \mathbf{r}^{\mathrm{k}} \,, \tag{3.42b}$$

$$\mathbf{x}^{\mathrm{k+1}} = \mathbf{x}^{\mathrm{k}} + \boldsymbol{\delta}^{\mathrm{k}} \,, \tag{3.42c}$$

where the correction $\boldsymbol{\delta}$ is computed by the adjoint Monte Carlo method. The merits of Halton's approach are immediately visible in that we have now broken the binding of the convergence rate to the Central Limit Theorem. Here, the Monte Carlo solver is used to produce a correction from the residual, analogous to using the residual to extract a correction from the search subspace in a projection method. By doing this, the Monte Carlo error is bound in the correction used to update the solution and therefore does not explicitly manifest itself in the overall convergence of the solution. The downside of such a method is that if the solution guess is poor, then many iterations are required in order to reach exponential converge as the Monte Carlo error (and therefore the Central Limit Theorem) does dominate in this situation. Therefore, if a good initial guess is not available, Halton's method is still characterized by poor performance.

3.5 Monte Carlo Synthetic-Acceleration

Using the ideas of Halton, Evans and Mosher recently developed a Monte Carlo solution method that was not prohibited severely by the quality of the initial guess for the system (Evans and Mosher, 2009) and later applied it more rigorously as a solution mechanism for the radiation diffusion equation (Evans et al., 2012). With their new methods, they achieved identical numerical results as and marginally better performance than conventional Krylov solvers. Their approach was instead to use residual Monte Carlo as a synthetic acceleration for a stationary method. To derive this method, we

begin by splitting the operator in Eq (2.1)

$$\mathbf{x} = (\mathbf{I} - \mathbf{A})\mathbf{x} + \mathbf{b} \,. \tag{3.43}$$

With this we can then define the stationary method *Richardson's iteration* as:

$$\mathbf{x}^{k+1} = (\mathbf{I} - \mathbf{A})\mathbf{x}^{k} + \mathbf{b} \,, \tag{3.44}$$

which will converge if $\rho(\mathbf{I} - \mathbf{A}) < 1$. We then define the solution error at the k^{th} iterate relative to the true solution:

$$\delta\mathbf{x}^{k} = \mathbf{x} - \mathbf{x}^{k} \,. \tag{3.45}$$

Subtracting Eq (3.44) from Eq (3.43) we get:

$$\delta\mathbf{x}^{k+1} = (\mathbf{I} - \mathbf{A})\delta\mathbf{x}^{k} \,. \tag{3.46}$$

Subtracting from this $(\mathbf{I} - \mathbf{A})\delta\mathbf{x}^{k+1}$ yields:

$$\begin{aligned} \mathbf{A}\delta\mathbf{x}^{k+1} &= (\mathbf{I} - \mathbf{A})(\mathbf{x}^{k+1} - \mathbf{x}^{k}) \\ &= \mathbf{r}^{k+1} \,. \end{aligned} \tag{3.47}$$

Using this, we define the following scheme that will converge in one iteration if $\mathbf{A}$ is inverted exactly.

$$\mathbf{x}^{k+1} = (\mathbf{I} - \mathbf{A})\mathbf{x}^{k} + \mathbf{b} \,, \tag{3.48a}$$

$$\mathbf{A}\delta\mathbf{x}^{k+1} = \mathbf{r}^{k+1} \,, \tag{3.48b}$$

$$\mathbf{x} = \mathbf{x}^{k+1} + \delta\mathbf{x}^{k+1} \,. \tag{3.48c}$$

However, $\mathbf{A}$ is only approximately inverted by our numerical methods and therefore we instead pose an iterative scheme in which the Monte Carlo solvers are used to invert the operator. The *Fixed-Point Monte Carlo*

Synthetic-Acceleration (MCSA) method is defined as:

$$\mathbf{x}^{k+1/2} = \mathbf{x}^{k} + \mathbf{r}^{k} \,, \tag{3.49a}$$

$$\mathbf{r}^{k+1/2} = \mathbf{b} - \mathbf{A}\mathbf{x}^{k+1/2} \,, \tag{3.49b}$$

$$\mathbf{A}\delta\mathbf{x}^{k+1/2} = \mathbf{r}^{k+1/2} \,, \tag{3.49c}$$

$$\mathbf{x}^{k+1} = \mathbf{x}^{k+1/2} + \delta\mathbf{x}^{k+1/2} \,, \tag{3.49d}$$

where the adjoint Monte Carlo method is used to generate the solution correction from the residual. Using Monte Carlo in this way achieves the same effect as Halton's method, decoupling its convergence rate from the overall convergence rate of the method. Here, the approximate Monte Carlo solution is not driven to a particular convergence as it merely supplies a correction for the initial guess generated by Richardson's iteration. Rather, only a set number of histories are required using the adjoint method to generate the correction.

In addition to the Monte Carlo solver parameters dictating the number of histories and weight cutoff, the outer MCSA iterations also have the following stopping criteria:

$$||\mathbf{r}||_{\infty} < \epsilon \, ||\mathbf{b}||_{\infty} \,, \tag{3.50}$$

where ϵ is a user-defined parameter. We therefore have 3 parameters to tune in an MCSA implementation: the number of Monte Carlo histories computed in the adjoint solve during each MCSA iteration, the weight cutoff for those histories, and the total MCSA convergence tolerance as specified by ϵ.

Preconditioning MCSA

In most cases, at least a minimal amount of *preconditioning* of the linear system will be required in order to use the class of stochastic methods

described. Although these methods have no symmetry requirements for convergence, they do require that the spectral radius of the iteration matrix be less than one. To achieve this for diagonally dominant matrices, a Jacobi preconditioner, a form of left preconditioning, is used such that the preconditioning matrix $\mathbf{M}$ is:

$$\mathbf{M} = \mathtt{diag}(\mathbf{A}) \,, \tag{3.51}$$

such that its application means we are instead solving the following linear system:

$$\mathbf{M}^{-1}\mathbf{A}\mathbf{x} = \mathbf{M}^{-1}\mathbf{b} \,. \tag{3.52}$$

Next, we can apply MCSA to solve Eq (3.52):

$$\mathbf{x}^{\mathrm{k}+1/2} = \mathbf{x}^{\mathrm{k}} + \mathbf{M}^{-1}\mathbf{r}^{\mathrm{k}} \,, \tag{3.53a}$$

$$\mathbf{r}^{\mathrm{k}+1/2} = \mathbf{b} - \mathbf{A}\mathbf{x}^{\mathrm{k}+1/2} \,, \tag{3.53b}$$

$$\mathbf{M}^{-1}\mathbf{A}\delta\mathbf{x}^{\mathrm{k}+1/2} = \mathbf{M}^{-1}\mathbf{r}^{\mathrm{k}+1/2} \,, \tag{3.53c}$$

$$\mathbf{x}^{\mathrm{k}+1} = \mathbf{x}^{\mathrm{k}+1/2} + \delta\mathbf{x}^{\mathrm{k}+1/2} \,. \tag{3.53d}$$

Choosing Jacobi preconditioning with MCSA is advantageous for several reasons. First, $\rho(\mathbf{I}-\mathbf{M}^{-1}\mathbf{A}) < 1$ is true for all $\mathbf{A}$ that is diagonally dominant and is easy to formulate because the inversion of $\mathbf{M}$ is trivial. Second, because the adjoint Monte Carlo method used within MCSA to compute the correction operates on a linear problem with the preconditioned operator, then $\mathbf{H}$ in the adjoint solver will have a zero term in each of its diagonal elements, thereby eliminating all in-state transitions during the random walk sequence. Because of this, Jacobi preconditioning should always be performed, regardless of any other preconditioning that is applied to the system.

3.6 Monte Carlo Method Selection

The MCSA method defined in Eq. (3.49) uses the adjoint method to estimate the error in residual Monte Carlo solve instead of the direct method outlined in § 3.2. To demonstrate the effectiveness of the adjoint method over the direct method within the context of MCSA, we choose the 2D time-dependent Poisson equation as a simple model problem:

$$\frac{\partial \mathbf{u}}{\partial t} = \nabla^2 \mathbf{u} \,. \tag{3.54}$$

For all comparisons, a single time step is computed with backwards Euler time integration. The Laplacian is differenced on a square Cartesian grid with a second-order five-point stencil,

$$\nabla_5^2 = \frac{1}{\Delta^2}[u_{i-1,j} + u_{i+1,j} + u_{i,j-1} + u_{i,j+1} - 4u_{i,j}] \,, \tag{3.55}$$

and a fourth-order nine-point stencil,

$$\begin{aligned}\nabla_9^2 = \frac{1}{6\Delta^2}[&4u_{i-1,j} + 4u_{i+1,j} + 4u_{i,j-1} + 4u_{i,j+1} + u_{i-1,j-1} \\ &+ u_{i-1,j+1} + u_{i+1,j-1} + u_{i+1,j+1} - 20u_{i,j}] \,,\end{aligned} \tag{3.56}$$

both assuming a grid size of Δ in both the i and j directions. For a single time step solution, we then have the following sparse linear system to be solved with the MCSA method:

$$\mathbf{A}\mathbf{u}^{n+1} = \mathbf{u}^n \,. \tag{3.57}$$

Both the stencils will be used to vary the size and density of the sparse linear system in Eq. (3.57).

A timing and convergence study is used to demonstrate the effectiveness of the adjoint method as compared to the direct method. To assess both

the CPU time and number of iterations required to converge to a solution, a problem of constant Δ was used with varying values of grid size, fixing the spectral radius of the system at a constant value for each variation. Both the five-point and nine-point stencils were used with both the direct and adjoint solvers. For each case, $\mathsf{N} \times \mathsf{N}$ total random walk permutations were computed per MCSA iteration where $\mathsf{N} \times \mathsf{N}$ is the number of discrete grid points in the system. Solver parameters were set to a weight cutoff of 1×10^{-4} for the stochastic linear solver and a convergence tolerance of 1×10^{-8} for the MCSA iterative solver. Figure 3.4 gives the CPU time needed for each case to converge in seconds and Figure 3.5 gives the number of iterations needed for each case to converge to the specified tolerance as a function of the problem size. All computations presented in this section and § 3.7 were completed on a 3.0 GHz Intel Core 2 Quad Q9650 CPU machine with 16 GB 1067 MHz DDR3 memory.

We see clearly in Figure 3.4 that the using the adjoint solver with MCSA results in a speedup over the direct solver while the number of iterations required to converge is also reduced as shown in Figure 3.5. We expect this for several reasons. First, with an equivalent number of histories specified for both solvers per MCSA iteration and a system of size $\mathsf{N} \times \mathsf{N}$, the direct solver will compute a single random walk for each state in the system per iteration to acquire a solution in that state, regardless of the size of the residual in that state. This is necessary in the direct method to ensure a contribution from each state as the random walk sequence will only contribute to the starting state. For the adjoint method, a total of $\mathsf{N} \times \mathsf{N}$ random walk events will have their starting state determined by sampling the residual vector. Because the random walk sequence contributes to the state in which it currently resides, sampling the residual vector as the Monte Carlo source gives a higher density of random walk events in regions with a high residual, thus giving a more accurate correction in that region due to reduced statistical error. From an iteration perspective, Figure 3.5 shows that using the direct method

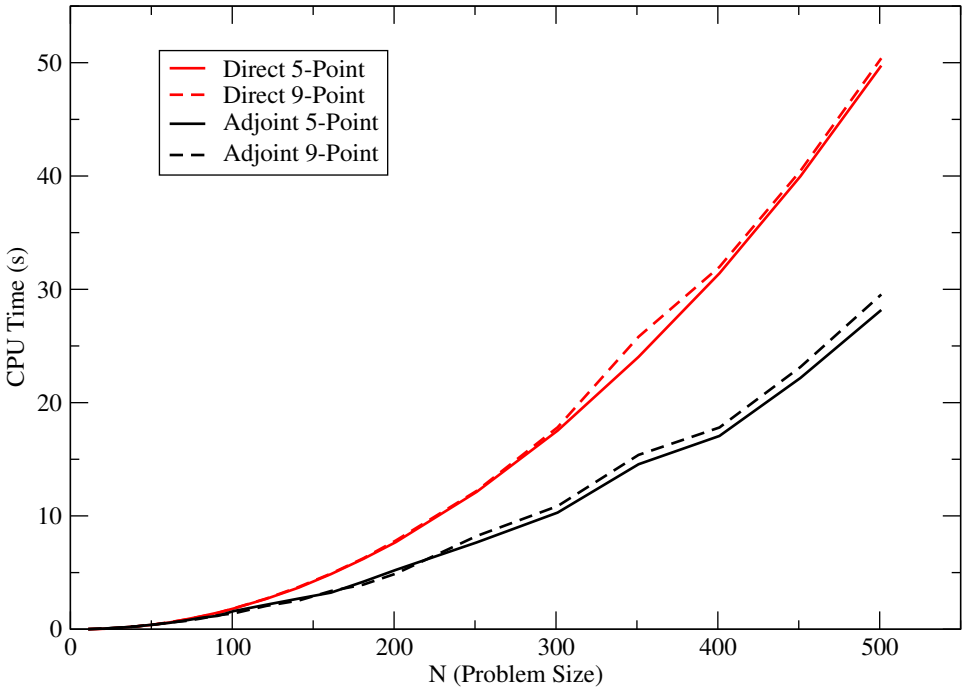

Figure 3.4: **CPU Time (s) to converge vs. Problem Size (N for an N $\times$ N square mesh).** *Both the adjoint and direct solvers are used with the five point and nine point stencils. A CPU time speedup is noted with the adjoint method due to the higher density of random walk events in regions with a large residual.*

yields a roughly unchanging number of iterations required to converge as the problem size increases. Again, if we desire a correction value for all states in the problem, then we must start a random walk in each state in the system which does not reduce the number of iterations need as the problem size grows. Conversely, as the problem size grows in the adjoint method, the additional stochastic histories that will be computed are concentrated in regions with a large residual, further reducing the stochastic error in the correction in those regions and subsequently reducing the required number of iterations to converge.

As an additional comparison, the convergence behavior of MCSA can be

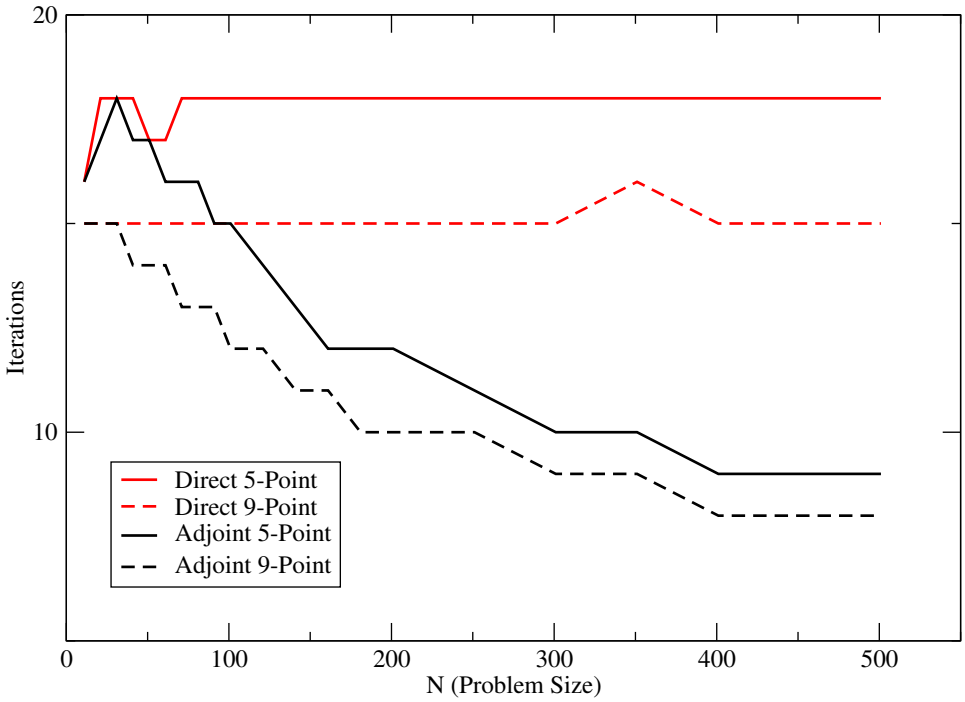

Figure 3.5: **Iterations to converge vs. Problem Size (N for an $N \times N$ square mesh).** *Both the adjoint and direct solvers are used with the five-point and nine-point stencils.*

analyzed using both the adjoint and direct solvers to detect any performance benefits. To assess the convergence properties of MCSA using each solver and stencil, the infinity norm of the residual computed in Eq. (3.49) was collected at each iteration for a fixed problem size of $N = 500$. Figure 3.6 gives the results of these computations. First, it is worthy to note on the semilog plot that we are indeed achieving the expected exponential convergence from MCSA with both Monte Carlo solvers. Second, we note that using the adjoint method with the same number of stochastic histores per MCSA iteration gives a faster rate of converge for the same reasons as above. We also note here that fewer iterations are required for convergence when the 9-point stencil is used to discretize the Laplacian operator (although at no

gain in speed as given by the results in Figure 3.4). This is due to the fact that the smaller discretization error directly corresponds to a more well defined residual source generated by the Richardson extrapolation for the Monte Carlo calculation. In addition, the better defined source is transported through a domain described more accurately by the 9-point stencil, thus yielding a more accuracte correction vector from the Monte Carlo calculation.

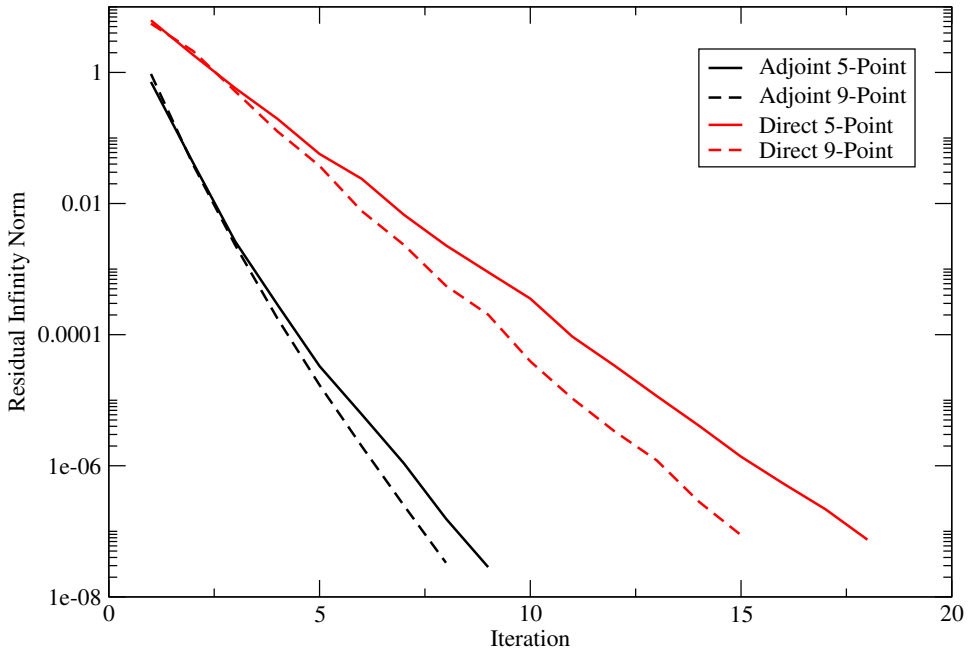

Figure 3.6: **Infinity norm of the solution residual vs. iteration number for a problem of size** $\mathsf{N} = 500$**.** *Both the adjoint and direct solvers are used with the five point and nine point stencils. A higher rate of convergence is observed for MCSA using the adjoint Monte Carlo solver as compared to the direct method when both solvers compute the same number of random walks per iteration.*

3.7 MCSA Comparison to Sequential Monte Carlo

To further motivate using Monte Carlo Synthetic Acceleration, we compare its performance to Halton's Sequential Monte Carlo method on which our previous work in this area was based. For this comparison, we use the same transient Poisson problem as described in the previous section and choose only the 5-point stencil to discretize the Laplacian operator as the previous results yielded little qualitative difference between the discretizations. Both MCSA and Halton's method are used with the adjoint Monte Carlo solver. In order to complete the same study as in the previous section, the number of histories computed by the Monte Carlo solver at each iteration had to be doubled to $2 \times \mathsf{N} \times \mathsf{N}$ in order to ensure convergence in Sequential Monte Carlo Method. Figure 3.7 gives the CPU time results for this comparison as a function of problem size while Figure 3.8 gives the number of iterations to converge as a function of problem size. In both cases, using the Monte Carlo solver as a synthetic acceleration rather than in a pure residual Monte Carlo scheme resulted in a reduction in both CPU time and iterations required to converge. The additional Richardson extrapolation between each Monte Carlo solve in the MCSA method gives a better converged residual source to use with the Monte Carlo calculation while the Sequential method requires more iterations to achieve the same level of convergence in the residual.

The benefits of using a synthetic acceleration scheme are also noted when the infinity norm of the residual computed at each iteration for both methods was collected at each iteration for a fixed problem sizes of $\mathsf{N} = 100$ and $\mathsf{N} = 500$ as shown in figures Figure 3.9 and 3.10 respectively. In both cases, the Sequential method is subject to two regimes of exponential convergence with the later regime converging the slowest while the MCSA method exhibits a single rate of exponential convergence observed to be much higher than that computed by Halton's method. Even with the doubling of

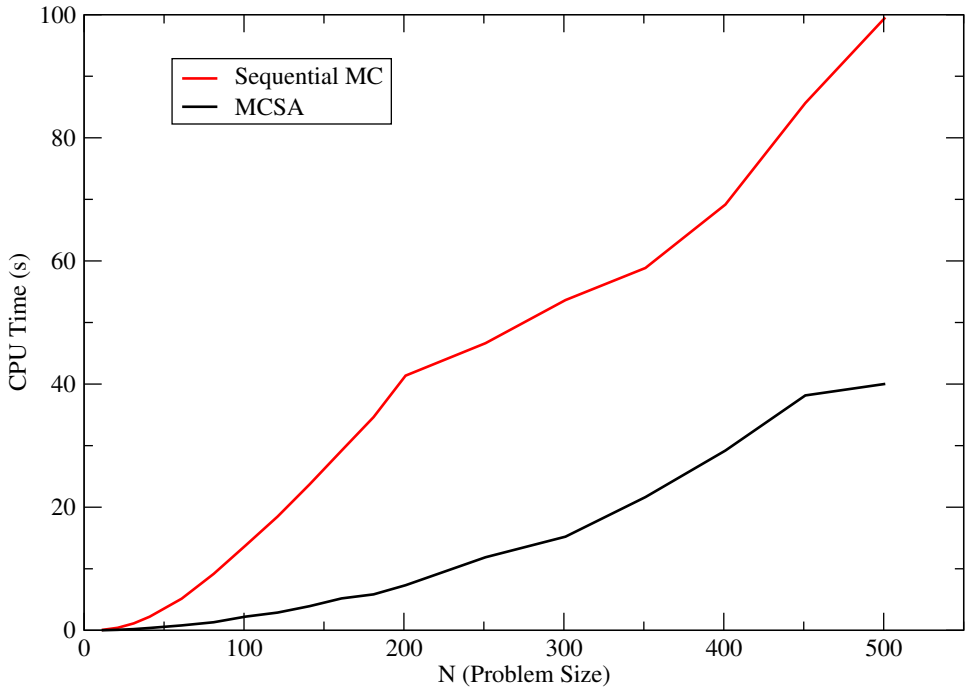

Figure 3.7: **CPU Time (s) to converge vs. Problem Size (N for an N $\times$ N square mesh).** *oth the Sequential Monte Carlo and MCSA solvers are used with the five point stencils and the adjoint Monte Carlo solver. The number of random walks was twice the number of discrete states in the system in order to ensure convergence in the Sequential Monte Carlo method.*

the number of stochastic histories computed per time step in order to ensure convergence for the Sequential method, we still see robustness issues with a non-monotonically decreasing residual observed for the $\mathsf{N} = 100$ case. In both cases the MCSA solver is observed to be robust with a monotonically decreasing residual.

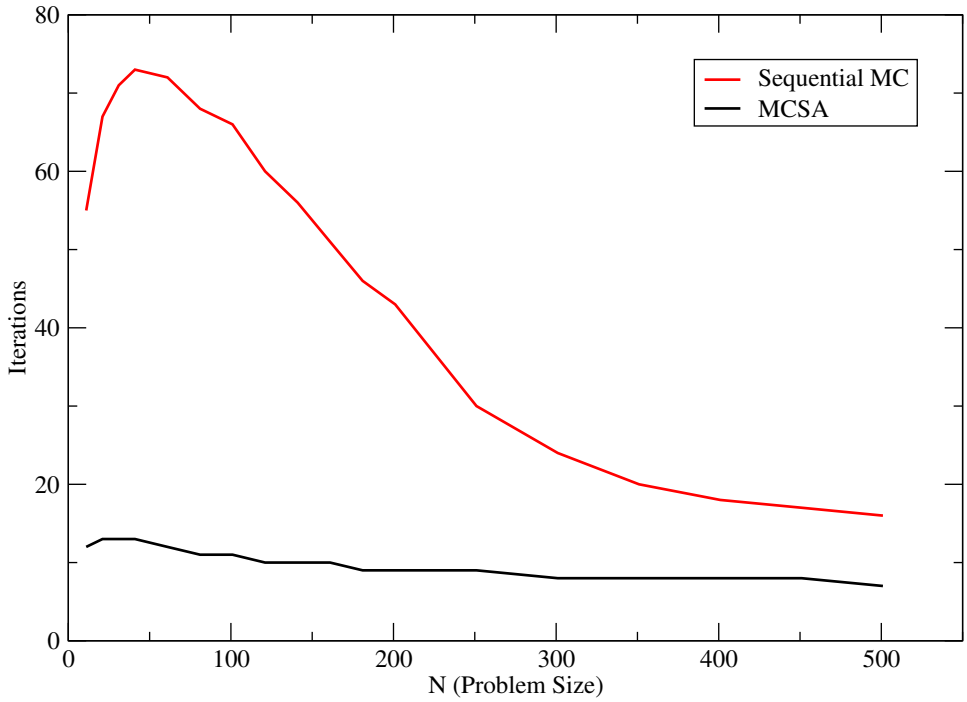

Figure 3.8: **Iterations to converge vs. Problem Size (N for an N $\times$ N square mesh).** *Both the Sequential Monte Carlo and MCSA solvers are used with the five point stencils and the adjoint Monte Carlo solver.*

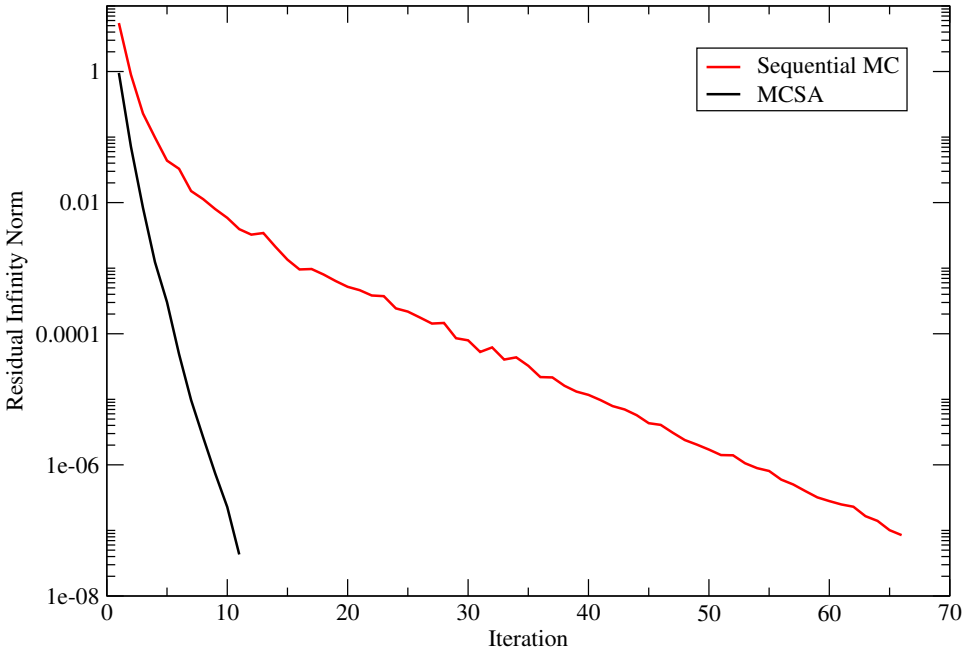

Figure 3.9: **Infinity norm of the solution residual vs. iteration number for a problem of size** $\mathsf{N} = 100$**.** *Both the Sequential Monte Carlo and MCSA solvers are used with the five point stencils and the adjoint Monte Carlo solver.*

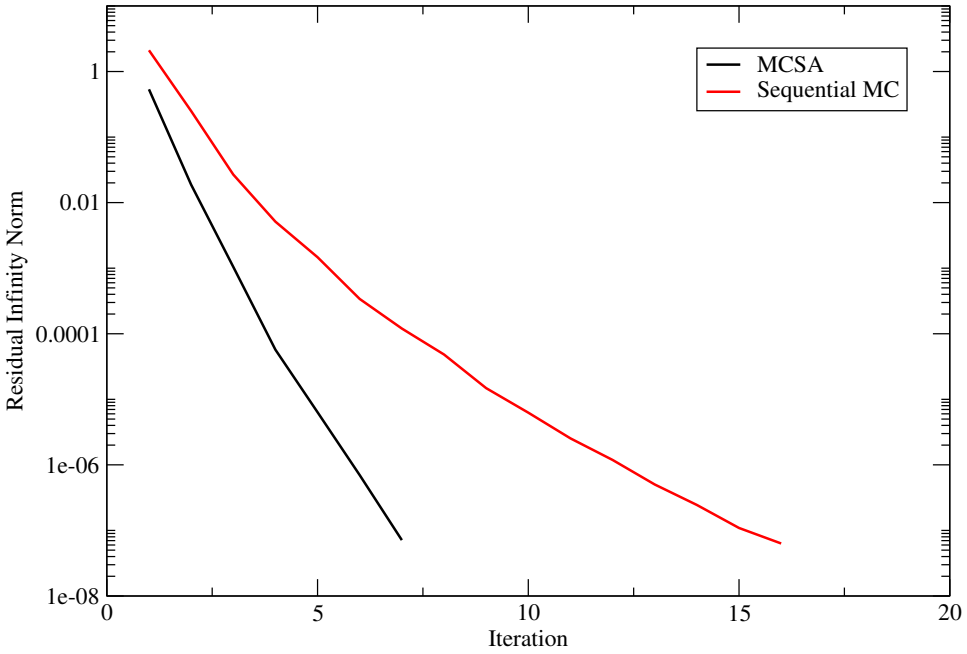

Figure 3.10: **Infinity norm of the solution residual vs. iteration number for a problem of size** $\mathsf{N} = 500$**.** *Both the Sequential Monte Carlo and MCSA solvers are used with the five point stencils and the adjoint Monte Carlo solver.*

Chapter 4

Parallel Monte Carlo Solution Methods for Linear Systems

For Monte Carlo methods, and in particular MCSA, to be viable at the production scale, scalable parallel implementations are required. In a general linear algebra context for discrete systems, this has not yet been achieved. Therefore, we will develop and implement parallel algorithms for these methods leveraging both the knowledge gained from the general parallel implementations of Krylov methods and modern parallel strategies for Monte Carlo as developed by the reactor physics community. In order to formulate a parallel MCSA algorithm, we recognize that the algorithm occurs in two stages, an outer iteration performing Richardson's iteration and applying the correction, and an inner Monte Carlo solver that is generating the correction via the adjoint method. The parallel aspects of both these components must be considered.

4.1 Domain Decomposition for Monte Carlo

As observed in the discussion on parallel Krylov methods, large-scale problems will surely have their data partitioned such that each parallel process owns a subset of the equations in the linear system. Given this convention, the adjoint Monte Carlo algorithm must perform random walks over a domain that is decomposed and must remain decomposed due to memory limitations. This naturally leads us to seek parallel algorithms that handle domain decomposition.

In the context of radiation transport, Brunner and colleagues provided a survey of algorithms for achieving this as implemented in production implicit Monte Carlo codes (Brunner et al., 2006). In their work they identify two data sets that are required to be communicated: the sharing of particles that are transported from one domain to another and therefore from one processor to another and a global communication that signals if particle transport has been completed on all processors. The algorithms presented are a fully-locking synchronous scheme, an asynchronous-send/synchronous-receive pattern, a traditional master/slave scheme, and a modified master/slave scheme the implements a binary tree pattern for the global reduction type operations needed to communicate between the master and slave processes. They observed that the modified master/slave scheme performed best in that global communications were implemented more efficiently than those required by the asynchronous scheme. Furthermore, none of these schemes handled load-imbalanced cases efficiently. Such cases will be common if the source sampled in the Monte Carlo random walk is not isotropic and not evenly distributed throughout the global domain. It was noted that efficiencies were improved by increasing the frequency by which particle data was communicated between domain-adjacent processors. However, this ultimately increases communication costs. In 2009, Brunner extended his work by using a more load-balanced approach with a fully asynchronous communication pattern (Brunner and Brantley, 2009). Although the extended implementation was more robust and allowed for scaling to larger numbers of processors, performance issues were still noted with parallel efficiency improvements needed in both the weak and strong scaling cases for unbalanced problems. These results led Brunner to conclude that a combination of domain decomposition and domain replication could be used to solve some of these issues.

Multiple-Set Overlapping-Domain Decomposition

In 2010, Wagner and colleagues developed the *multiple-set overlapping-domain* (MSOD) decomposition for parallel Monte Carlo applications for full-core light water reactor analysis (Wagner et al., 2010). In their work, an extension of Brunner's, their scheme employed the similar parallel algorithms for particle transport but a certain amount of overlap between adjacent domains was used to decrease the number of particles leaving the local domain. In addition, Wagner utilized a level of replication of the domain such that the domain was only decomposed on $\mathsf{O}(100)$ processors and if replicated $\mathsf{O}(1,000)$ times achieves simulation on $\mathsf{O}(100,000)$ processors, thus providing spatial and particle parallelism. Each collection of processors that constitutes a representation of the entire domain is referred to as a set, and within a set overlap occurs among its sub-domains. The original motivation was to decompose the domain in a way that it remained in a physical cabinet in a large distributed machine, thus reducing latency costs during communication. A multiple set scheme is also motivated by the fact that communication during particle transport only occurs within a set, limiting communications during the transport procedure to a group of $\mathsf{O}(100)$ processors, a number that was shown to have excellent parallel efficiencies in Brunner's work and therefore will scale well in this algorithm. The overlapping domains within each set also demonstrated reduced communication costs. On each processor, the source is sampled in the local domain that would exist if no overlap was used while tallies can be made over the entire overlapping domain.

To demonstrate this, consider the example adapted from Mervin's work with Wagner and others in the same area (Mervin et al., 2012) and presented in Figure 4.1. In this example, 3 particle histories are presented emanating from the blue region of interest. Starting with particle A, if no domain overlap is used then the only the blue domain exists on the starting processor. Particle A is then transported through 3 other domains before the history ends, therefore requiring three communications to occur in Brunner's

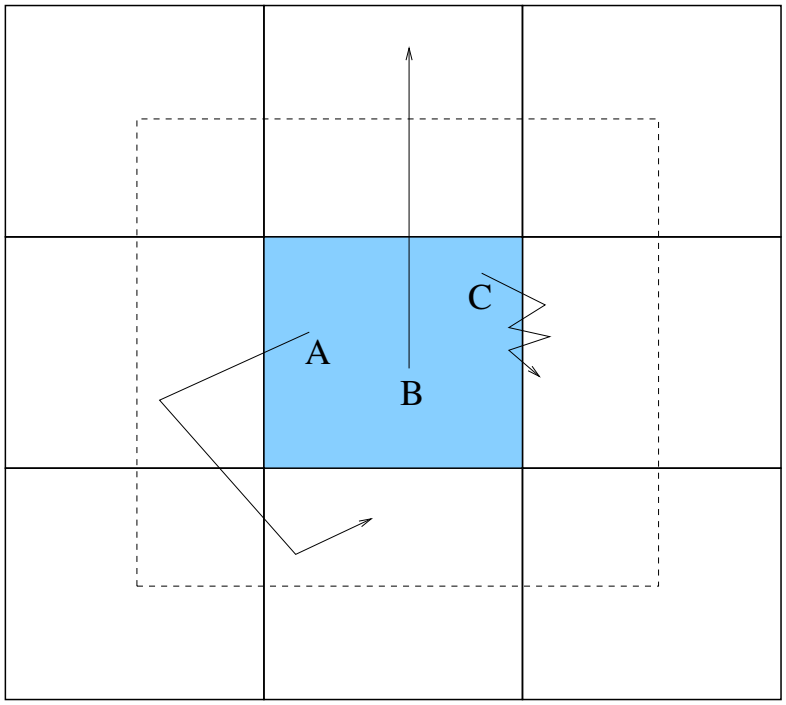

Figure 4.1: **Overlapping domain example illustrating how domain overlap can reduce communication costs.** *All particles start in the blue region of interest. The dashed line represents 0.5 domain overlap between domains.*

algorithm. If a 0.5 domain overlap is permitted as shown by the dashed line, then the starting process owns enough of the domain such that no communications must occur in order to complete the particle A transport process. Using 0.5 domain overlap also easily eliminates cases such as the represented by the path of particle C. In this case, particle C is scattering between two adjacent domains, incurring a large latency cost for a single particle. Finally, with particle B we observe that 0.5 domain overlap will still not eliminate all communications. However, if 1 domain overlap were used, the entire geometry shown in Figure 4.1 would be contained on the source processor and therefore transport of all 3 particles without communication

would occur.

Wagner and colleagues used this methodology for a 2-dimensional calculation of a pressurized water reactor core and varied the domain overlap from 0 to 3 domain overlap (a 7×7 box in the context of our example) where a domain constituted a fuel assembly. For the fully domain decomposed case, they observed that 76.12% of all source particles leave the domain. At 1.5 domain overlap, the percentage of source particles born in the center assembly leaving the processor domain dropped to 1.05% and even further for 0.02% for the 3 domain overlap. Based on these results, this overlap approach, coupled with the multiple sets paradigm that will scale for existing parallel transport algorithms, provides a scalable Monte Carlo algorithm for today's modern machines.

4.2 Load Balancing Concerns

Although domain decomposition was shown to be efficient in a perfectly load balanced situation in Siegel's work (Siegel et al., 2012a), careful consideration must be made for situations where this is not the case. Given the stochastic nature of the problem and lack of a globally homogeneous domain, parallel Monte Carlo simulations are inherently load imbalanced. Procassini and others worked to alleviate some of the load imbalances that are generated by both particle and spatial parallelism and are therefore applicable to the MSOD algorithm (Procassini et al., 2005). They chose a dynamic balancing scheme in which the number of times a particular domain was replicated was dependent on the amount of work in that domain (i.e. domains with a high particle flux and therefore more particle histories to compute require more work). In this variation, domains that require more work will be replicated more frequently at reduced particle counts in each replication. Furthermore, Procassini and colleagues noted that as the simulation progressed and particles were transported throughout the domain, the amount of replication

for each domain would vary as particle histories began to diffuse, causing some regions to have higher work loads and some to have smaller work loads than the initial conditions.

Consider the example in Figure 4.2 adapted from Procassini's work. In

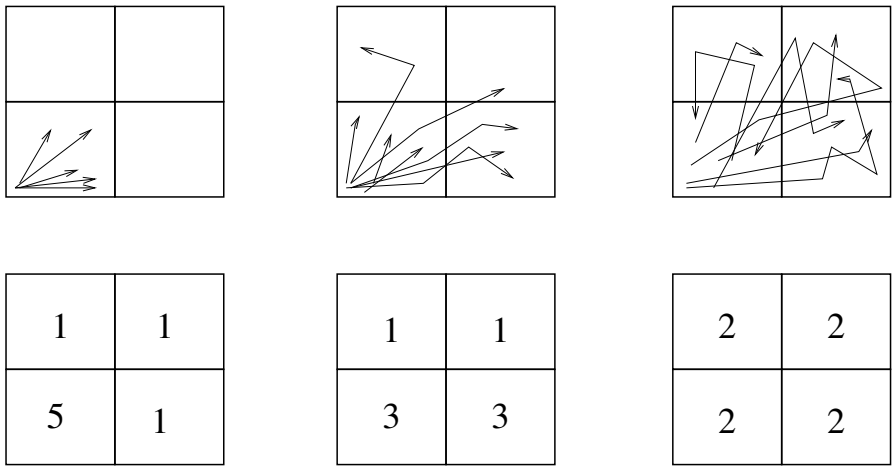

Figure 4.2: **Example illustrating how domain decomposition can create load balance issues in Monte Carlo.** *A domain is decomposed into 4 zones on 8 processors with a point source in the lower left zone. As the particles diffuse from the source in the random walk sequence as shown in the top row, their tracks populate the entire domain. As given in the bottom row, as the global percentage of particles increases in a zone, that zone's replication count is increased.*

this example, a geometry is decomposed into 4 domains on 8 processors with a point source in the bottom left domain. To begin, because the point source is concentrated in one domain, that domain is replicated 5 times such the amount of work it has to do per processor is roughly balanced with the others. As the particles begin to diffuse away from the point source, the amount of replication is adjusted to maintain load balance. Near the end of the simulation, the diffusion of particles is enough that all domains have equal replication. By doing this, load balance is improved

as each domain has approximately equal work although each domain may represent a different spatial location and have a differing number of histories to compute. Compared to Wagner's work where the fission source was distributed relatively evenly throughout the domain, fixed source problems (and especially those that have a point-like source) like those presented in Procassini's work will be more prone to changing load balance requirements.

4.3 Reproducible Domain Decomposed Results

The 2006 work of Brunner is notable in that the Monte Carlo codes used to implement and test the algorithms adhered to a strict policy of generating identical results independent of domain decomposition or domain replication as derived from the work of Gentile and colleagues (Gentile et al., 2005). In Gentile's work, a procedure is given for obtaining results reproducible to machine precision for an arbitrary number of processors and domains. Differences can arise from using a different random number sequence in each domain and performing a sequence of floating point operations on identical data in a different order, leading to variations in round-off error and ultimately a non-identical answer. They use a simple example, recreated below in Figure 4.3, that illustrates these issues. In this example, the domain is decomposed on two processors with each processor owning one of the two zones. Starting with particle A, it is born in zone 1 and is transported to zone 2 where a scattering event occurs. Concerning the first reproducibility issue, if the same sequence of random numbers is not used to compute the trajectory from the new scattering event, we cannot expect to achieve the same result if the domain were not decomposed. If the numbers are different, the scattering event in zone 2 may keep the particle there or even eject it from the domain if the sequence were different. The second issue is demonstrated by adding another particle B that remains in the domain.

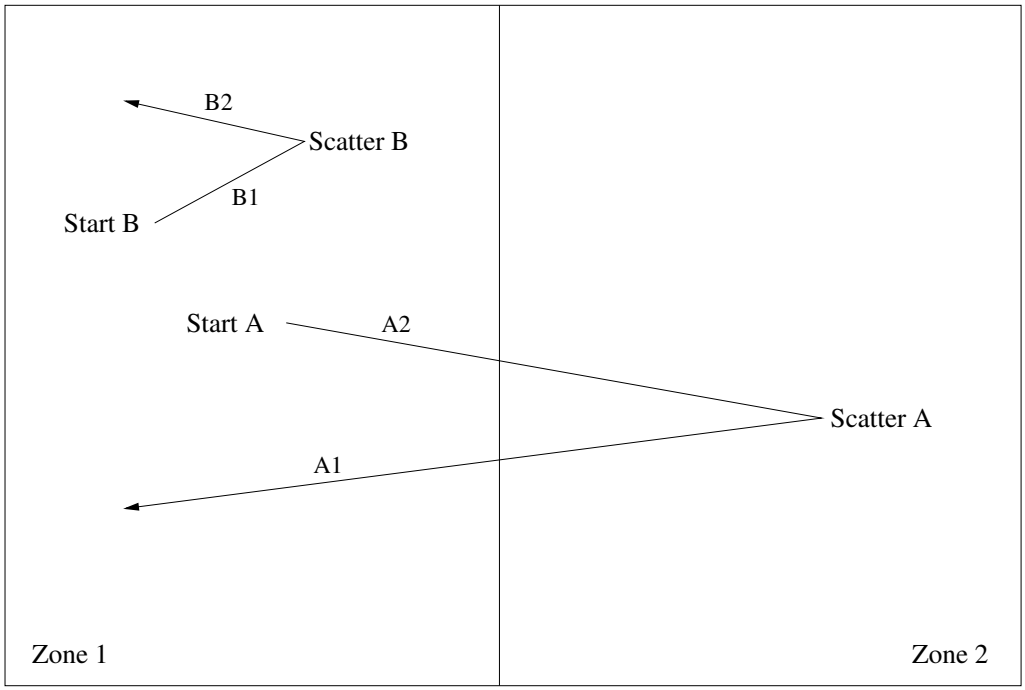

Figure 4.3: **Gentile's example illustrating how domain decomposition can create reproducibility issues in Monte Carlo.** *Both particles A and B start in zone 1 on processor 1. Particle A moves to zone 2 on processor 2 and scatters back to zone 1 while B scatters in zone 1 and remains there. A1 and A2 denote the track of particle A that is in zone 1 while B1 and B2 denote the track of particle B that is in zone 1.*

In this case, an efficient algorithm will transport particle A on processor 1 until it leaves zone 1 and then transport particle B. Particle A will not renter the domain until it has been communicated to processor 2, processor 2 performs the transport, and it is communicated back to processor 1. If we are doing a track-length tally in zone 1, then we sum the tracks lengths observed in that zone. In the single processor, single zone case particle A would be transported in its entirety and then particle B transported. This would result in a tally sum with the following order of operations:

$(((A1 + A2) + B1) + B2)$. If we were instead to use 2 processors, we would instead have the following order: $(((A1 + B1) + B2) + A2)$. In the context of floating point operations, we cannot expect these to have an identical result to machine precision as round-off approximations will differ resulting in non-commutative addition.

Procassini's solutions to these problems are elegant in that they require a minimal amount of modification to be applied to the Monte Carlo algorithm. To solve the first issue, in order to ensure each particle maintains an invariant random number sequence that determines its behavior regardless of domain decomposition, each particle is assigned a random number seed that describes its current state upon entering the domain of a new processor. These seeds are derived from the actual geometric location of the particle such that it is decomposition invariant. Non-commutative floating point operations are overcome by instead mapping floating point values to 64-bit integer values for which additions will always be commutative. Once the operations are complete, these integers are mapped back to floating point values.

4.4 Parallel Adjoint Method

We can take much of what was learned from the survey of parallel Monte Carlo methods for radiation transport and directly apply it to a parallel formulation of our stochastic linear solvers. Direct analogs can be derived from these works by noting that the primary difference between solving a linear system with Monte Carlo methods and fixed source Monte Carlo transport problems is the content of the Markov chains that are generated. The transitions represented by these chains are bound by probabilities and weights and are initiated by the sampling of a source. In the context of transport problems, those transitions represent events such as particle scattering and absorption with probabilities that are determined by physical data in the form of cross sections. For stochastic matrix inversion, those

transitions represent moving between the equations of the linear system (and therefore the physical domain which they represent) and their probabilities are defined by the coefficients of those equations. Ultimately, we tally the contributions to generate expectation values in the desired states as we progress through the chains. Therefore, parallel methods for Monte Carlo radiation transport can be abstracted and we can use those concepts that apply to matrix inversion methods as an initial means of developing a parallel Neumann-Ulam-type solver. Based on the results observed in the last decade of parallel Monte Carlo development, we can generate many practical questions that this type of work could answer.

Given a decomposed domain, per Wagner's work (Wagner et al., 2010) is clear that domain overlap significantly reduces the amount of communication required between adjacent domains as histories move to states that are not owned by the local processor. How much domain overlap is suitable for matrix inversion problems? Are we memory limited by large problems such that only so much overlap is feasible? Are there metrics related to the properties of the matrix including the eigenvalues and sparsity pattern such that we can provide guidelines for selecting the amount of overlap required? Furthermore, as Wagner and colleagues observed (Wagner et al., 2010), with marginal domain overlap for reactor problems, the percentage of histories leaving the local domain can easily be reduced to less than 1%. Evans and colleagues in their initial MCSA development typically used only 50 particle histories in order to compute a correction in an MCSA iteration (Evans et al., 2012). Per the Central Limit Theorem, that correlates to a statistical uncertainty of 14.1% in the correction, yet as compared to conventional Krylov solvers, MCSA achieved identical numerical results. If good convergence and numerically accurate solutions can be achieved with such a large uncertainty in the correction computation, then perhaps with enough domain overlap the minimal amount of histories that do transition to non-local states can be ignored and thus eliminate all communication

in the parallel Monte Carlo adjoint solver transport sequence and create an embarrassingly parallel method. Given Gropp's work on parallel Krylov methods that we discussed in § 2.4 and the empirical results of Siegel (Siegel et al., 2012a), we know that these nearest neighbor computations between adjacent domains do not scale as well as global reduction operations and therefore we are improving scaling by eliminating them from the transport sequence. It will be important to determine if the expectation value bias in the MCSA correction generated by this approximation will remain within the bounds of the already high statistical uncertainty for unbiased estimates, thus providing numerically equivalent results.

From a domain replication perspective, this may be difficult to achieve with a production scale linear solver. Typically, memory is at a premium and therefore the more distinct domains available in the decomposition, the spatially finer and/or the numerically more accurate the discretization that can be implemented. How much replication is possible for large problems? How does replication facilitate parallel performance when coupled with domain overlap? How can we measure how much domain overlap is feasible? Replicating domains may therefore run into memory limitations for exceptionally large problems such that the operator, solution vector, and source vector must be copied in their entirety multiple times. From a resiliency standpoint, such an operation will be required, and therefore its performance and memory implications on conventional problems must be analyzed.

4.5 Parallel MCSA

With a parallel adjoint Neumann-Ulam solver implementation, the parallel implementation of the MCSA method will be trivial. Recall the MCSA iteration procedure outlined in Eq (3.49). In § 2.4 we discussed parallel matrix and vector operations as utilized in conventional Krylov methods.

We utilize these here for the parallel MCSA implementation. In the first step, a parallel matrix-vector multiply is used to apply the split operator to the previous iterate's solution. A parallel vector update is then performed with the source vector to arrive at the initial iteration guess. In the next step, the residual is computed by the same operations where now the operator is applied to the solution guess with a parallel matrix-vector multiply and then a parallel vector update with the source vector is performed. Once the correction is computed with a parallel adjoint Neumann-Ulam solve, this correction is applied to the guess with a parallel vector update to get the new iteration solution. Additionally, as given by Eq (3.50), 2 parallel vector reductions will be required to check the stopping criteria: one initially to compute the infinity norm of the source vector, and another at every iteration to compute the infinity norm of the residual vector. For this implementation, all of the issues that will be potentially generated by the parallel adjoint solver implementation will manifest themselves here as the quality of the correction will be of intense study.

In addition to parallel implementation and performance, MCSA's potential for aiding advancement in non-symmetric matrix solutions leads to a natural comparison with the GMRES algorithm. As both solvers are aimed at the same class of problem, we desire a set of metrics that will allow us to quantitatively compare the two. Given that the Krylov subspace maintained by GMRES can become large, do we benefit from a memory standpoint with an MCSA scheme in that no subspace is required? Does this benefit outweigh the fact that the linear operator must be explicitly formed in order to build the transition probabilities for the random walk sequence? For non-symmetric systems, does MCSA exhibit similar convergence properties to Krylov methods? If a Krylov methods build a subspace, can those memory savings in MCSA be used to implement domain replication in the adjoint solver? Such questions can be answered by a comparative study of the two solvers that controls the system size and the iterations required to converge.

Chapter 5

An Analytic Performance Framework for Domain-Decomposed Monte Carlo

5.1 Leakage Fractions for Symmetric Systems

With Wagner's work, we observed that domain overlap implemented with a domain decomposed Monte Carlo setting reduces the amount of nearest neighbor communication that must occur during transport.

To date, parallel Neumann-Ulam methods have been limited to full domain replication with parallelism exploited through individual histories **?**. In reactor physics Monte Carlo applications, however, domain decomposition has been identified as a key principle in moving forward in high performance computing to enable higher fidelity simulations Brunner et al. (2006); Siegel et al. (2012a). To accomplish this, we recognize from the literature that stochastic histories must be transported from domain to domain as the simulation progresses and they transition to states that are not in the local domain. Because we have chosen a domain decomposition strategy in a parallel environment, this means that communication of these histories must occur between compute nodes owning neighboring pieces of the global domain. We wish to characterize this communication not only because communication is in general expensive, but also because these nearest-neighbor communication sequences, specifically, have poor algorithmic strong scaling Gropp et al. (2001).

The purpose of this study is to provide a simple, analytic theory based on the properties of the linear system that will allow for estimates of the domain decomposed behavior of the adjoint Neumann-Ulam method. When solving problems where the linear operator is symmetric, a host of analytic theories exist based on the eigenvalue spectrum of the operator that characterize their behavior in the context of deterministic linear solvers. Using past work, these theories are adapted to the domain decomposed adjoint Neumann-Ulam method using the one-speed, two-dimensional neutron diffusion equation. In this paper we describe the adjoint Neumann-Ulam Monte Carlo method followed by a presentation of the model problem. Using the linear system generated by the discretization of the model problem, we use a spectral analysis to generate analytic relations for the eigenvalues of the operator based on system parameters. Using the eigenvalue spectra, we then build relationships to characterize the transport of stochastic histories in a decomposed domain and the fraction of histories that leak from a domain and will therefore have to be communicated. Finally, we compare these analytic results to numerical experiments conducted with the model problem and draw conclusions looking towards future work.

Model Problem

For our numerical experiments, we choose the one-speed, two-dimensional neutron diffusion equation as a model problem **?**:

$$-\boldsymbol{\nabla}\cdot \mathsf{D}\boldsymbol{\nabla}\phi + \Sigma_{\mathrm{a}}\phi = \mathsf{S}\,, \tag{5.1}$$

where ϕ is the neutron flux, Σ_{a} is the absorption cross section, and S is the source of neutrons. In addition, D is the diffusion coefficient defined as:

$$\mathsf{D} = \frac{1}{3(\Sigma_{\mathrm{t}} - \bar{\mu}\Sigma_{\mathrm{s}})}\,, \tag{5.2}$$

where Σ_s is the scattering cross section, $\Sigma_t = \Sigma_a + \Sigma_s$ is the total cross section, and $\bar{\mu}$ is the cosine of the average scattering angle. For simplicity, we will take $\bar{\mu} = 0$ for our analysis giving $D = (3\Sigma_t)^{-1}$. In addition, to further simplify we will assume a homogeneous domain such that the cross sections remain constant throughout. Doing this permits us to rewrite Eq (5.1) as:

$$-D\boldsymbol{\nabla}^2\phi + \Sigma_a\phi = S\,. \tag{5.3}$$

We choose a finite difference scheme on a square Cartesian grid to discretize the problem. For the Laplacian, we choose the 9-point stencil shown in Figure 5.1 over a grid of size h LeVeque (2007):

$$\begin{aligned}\nabla_9^2\phi = \frac{1}{6h^2}[&4\phi_{i-1,j} + 4\phi_{i+1,j} + 4\phi_{i,j-1} + 4\phi_{i,j+1} + \phi_{i-1,j-1} \\ &+ \phi_{i-1,j+1} + \phi_{i+1,j-1} + \phi_{i+1,j+1} - 20\phi_{i,j}]\,.\end{aligned} \tag{5.4}$$

We then have the following linear system to solve:

$$\begin{aligned}-\frac{1}{6h^2}[&4\phi_{i-1,j} + 4\phi_{i+1,j} + 4\phi_{i,j-1} + 4\phi_{i,j+1} + \phi_{i-1,j-1} \\ &+ \phi_{i-1,j+1} + \phi_{i+1,j-1} + \phi_{i+1,j+1} - 20\phi_{i,j}] + \Sigma_a\phi_{i,j} = s_{i,j}\,,\end{aligned} \tag{5.5}$$

and in operator form:

$$\mathbf{D}\boldsymbol{\phi} = \mathbf{s}\,, \tag{5.6}$$

where $\mathbf{D}$ is the diffusion operator, $\mathbf{s}$ is the source in vector form and $\boldsymbol{\phi}$ is the vector of unknown fluxes.

To close the system, a set of boundary conditions is required. In the case of a non-reentrant current condition applied to all global boundaries of the domain, we choose the formulation of Duderstadt by assuming the flux is zero at some ghost point beyond the grid. Consider for example the

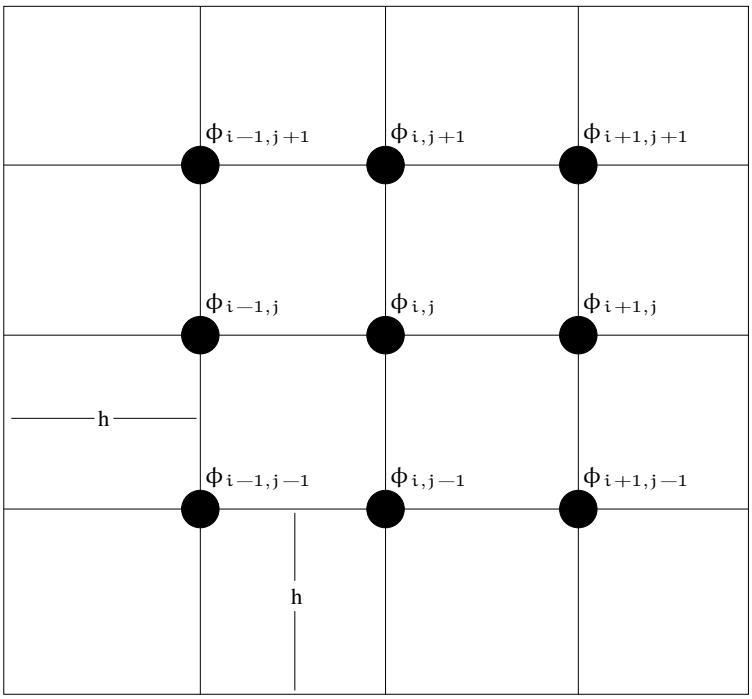

Figure 5.1: **Nine-point Laplacian stencil.**

equations on the $i = 0$ boundary of the domain:

$$-\frac{1}{6h^2}[4\phi_{-1,j} + 4\phi_{1,j} + 4\phi_{0,j-1} + 4\phi_{0,j+1} + \phi_{-1,j-1} + \phi_{-1,j+1} + \phi_{1,j-1} + \phi_{1,j+1} - 20\phi_{0,j}] + \Sigma_a\phi_{0,j} = s_{0,j}\,. \quad (5.7)$$

Here we note some terms where $i = -1$ and therefore are representative of grid points beyond the boundary of the domain. We set the flux at these points to be zero, giving a valid set of equations for the $i = 0$ boundary:

$$-\frac{1}{6h^2}[4\phi_{1,j} + 4\phi_{0,j-1} + 4\phi_{0,j+1} + \phi_{-1,j+1} + \phi_{1,j-1} + \phi_{1,j+1} - 20\phi_{0,j}] + \Sigma_a\phi_{0,j} = s_{0,j}\,. \quad (5.8)$$

We repeat this procedure for the other boundaries of the domain. For reflecting boundary conditions, the net current across a boundary is zero.

Spectral Analysis

The convergence of the Neumann series in Eq (3.31) approximated by the Monte Carlo solver is dependent on the eigenvalues of the iteration matrix. We will compute these eigenvalues by assuming eigenfunctions of the form LeVeque (2007):

$$\Phi_{p,q}(x, y) = e^{2\pi\imath px} e^{2\pi\imath qy} \,, \tag{5.9}$$

where different combinations of p and q represent the different eigenmodes of the solution. As these are valid forms of the solution, then the action of the linear operator on these eigenfunctions should give the eigenvalues of the matrix as they exist on the unit circle in the complex plane.

Iteration Matrix Spectrum

For the model problem, we first compute the eigenvalues for the diffusion operator $\mathbf{D}$ by applying the operator to the eigenfunctions and noting that $x = ih$ and $y = jh$:

$$\begin{aligned}\mathbf{D}\Phi_{p,q}(x, y) &= \lambda_{p,q}(\mathbf{D}) = \\ &- \frac{D}{6h^2}\Big[4e^{-2\pi\imath ph} + 4e^{2\pi\imath ph} + 4e^{-2\pi\imath qh} + 4e^{2\pi\imath qh} + e^{-2\pi\imath ph}e^{-2\pi\imath qh} \\ &+ e^{-2\pi\imath ph}e^{2\pi\imath qh} + e^{2\pi\imath ph}e^{-2\pi\imath qh} + e^{2\pi\imath ph}e^{2\pi\imath qh} - 20\Big] + \Sigma_a \,. \end{aligned} \tag{5.10}$$

Using Euler's formula, we can collapse the exponentials to trigonometric functions:

$$\lambda_{p,q}(\mathbf{D}) = -\frac{D}{6h^2}[8\cos(\pi ph) + 8\cos(\pi qh) + 4\cos(\pi ph)\cos(\pi qh) - 20] + \Sigma_a \,. \tag{5.11}$$

As Eq (5.1) is diagonally dominant, Jacobi preconditioning is sufficient to reduce the spectral radius of the iteration matrix below unity and therefore ensure convergence of the Neumann series. The preconditioner in this case is then $\mathbf{M} = \mathtt{diag}(\mathbf{D})$ such that we are solving the following linear system:

$$\mathbf{M}^{-1}\mathbf{D}\boldsymbol{\phi} = \mathbf{M}^{-1}\mathbf{s}\,. \tag{5.12}$$

The operator $\mathbf{M}^{-1}\mathbf{D}$ is merely the original diffusion operator with each row scaled by the diagonal component. As we have defined a homogeneous domain, the scaling factor, α, is the same for all rows in the operator and defined as the $\phi_{i,j}$ coefficient from Eq (5.5):

$$\alpha = \left[\frac{10D}{3h^2} + \Sigma_a\right]^{-1}\,. \tag{5.13}$$

Using this coefficient, we then have the following spectrum of preconditioned eigenvalues:

$$\lambda_{p,q}(\mathbf{M}^{-1}\mathbf{D}) = \alpha\lambda_{p,q}(\mathbf{D})\,. \tag{5.14}$$

The spectral radius of the iteration matrix is obtained by seeking its largest eigenvalue. As with the diffusion operator, we can use the same analysis techniques to find the eigenvalues for the iteration matrix. We use a few simplifications by noting that if the Jacobi preconditioned iteration matrix is $\mathbf{H} = \mathbf{I} - \mathbf{M}^{-1}\mathbf{D}$, the we except all terms on the diagonal of the iteration matrix to be zero such that we have the following stencil:

$$\mathbf{H}\boldsymbol{\phi} = \frac{\alpha D}{6h^2}[4\phi_{i-1,j}+4\phi_{i+1,j}+4\phi_{i,j-1}+4\phi_{i,j+1}+\phi_{i-1,j-1}+\phi_{i-1,j+1}+\phi_{i+1,j-1}+\phi_{i+1,j+1}]. \tag{5.15}$$

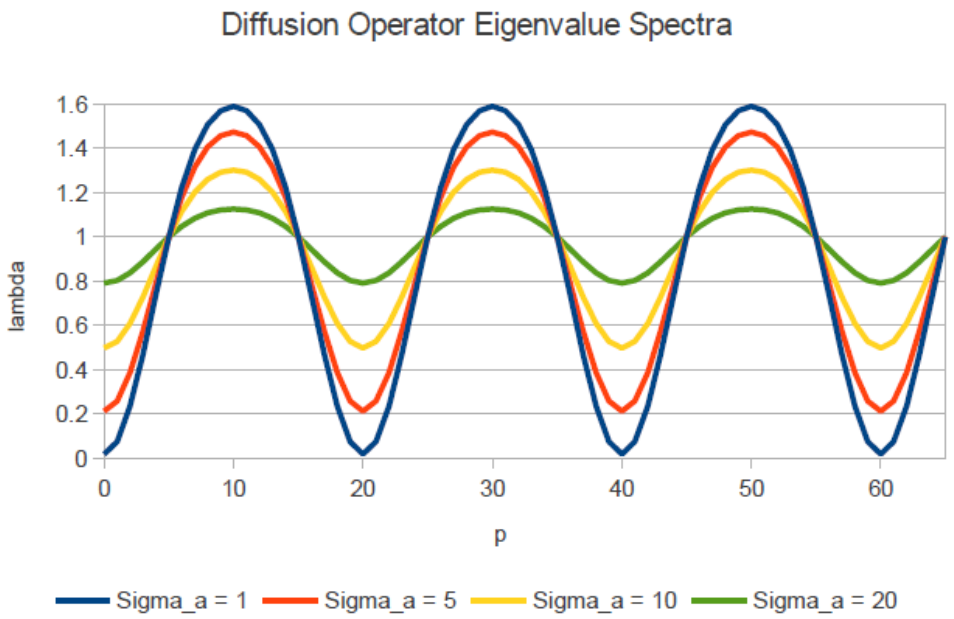

Figure 5.2: **Eigenvalue spectra for the diffusion equation.**

Inserting the eigenfunctions defined by Eq (5.9) we get:

$$\lambda_{p,q}(\mathbf{H}) = \frac{\alpha D}{6h^2}\Big[4e^{-2\pi\imath ph} + 4e^{2\pi\imath ph} + 4e^{-2\pi\imath qh} + 4e^{2\pi\imath qh} + e^{-2\pi\imath ph}e^{-2\pi\imath qh} + e^{-2\pi\imath ph}e^{2\pi\imath qq} + e^{2\pi\imath ph}e^{-2\pi\imath qh} + e^{2\pi\imath ph}e^{2\pi\imath qh}\Big], \quad (5.16)$$

which simplifies to:

$$\lambda_{p,q}(\mathbf{H}) = \frac{\alpha D}{6h^2}[8\cos(\pi ph) + 8\cos(\pi qh) + 4\cos(\pi ph)\cos(\pi qh)], \quad (5.17)$$

giving the eigenvalue spectrum for the Jacobi preconditioned iteration matrix. To find these maxium eigenvalue, Eq (5.14) is plotted as a function of p with $p = q$ in Figure 5.2 for various values of Σ_a. . We find that the maximum eigenvalue exists when $p = q = 0$, giving the following for the spectral

radius of the Jacobi preconditioned iteration matrix:

$$\rho(\mathbf{H}) = \frac{10\alpha \mathsf{D}}{3\mathsf{h}^2} \,. \tag{5.18}$$

Neumann Series Convergence

The adjoint Monte Carlo method is effectively an approximation to a stationary method. Stationary methods for linear systems arise from splitting the operator in Eq (2.1) and iterating:

$$\mathbf{x}^{\mathsf{k}+1} = \mathbf{H}\mathbf{x}^{\mathsf{k}} + \mathbf{c} \,, \tag{5.19}$$

with $\mathsf{k} \in \mathbb{Z}^+$ defined as the *iteration index*. Defining $\mathbf{e}^{\mathsf{k}} = \mathbf{u}^{\mathsf{k}} - \mathbf{u}$ as the solution error at the k^{th} iterate, the error after k iterations is then:

$$\mathbf{e}^{\mathsf{k}} = \mathbf{H}^{\mathsf{k}}\mathbf{e}^0 \,. \tag{5.20}$$

By assuming $\mathbf{H}$ is diagonalizable LeVeque (2007), we then have:

$$\|\mathbf{e}^{\mathsf{k}}\|_2 \leqslant \rho(\mathbf{H})^{\mathsf{k}} \|\mathbf{e}^0\|_2 \,. \tag{5.21}$$

In the adjoint Neumann-Ulam method, k iterations, equivalent to k applications of the iteration matrix, are approximated by a random walk of average length k to yield the summation in Eq (3.32) Dimov et al. (1998); Danilov et al. (2000). This random walk length, or the number of transitions before the termination of a history (either by the weight cutoff, absorption, or exiting the global domain) is therefore approximately the number of stationary iterations required to converge to the specified tolerance. In the case of the adjoint Neumann-Ulam method, no such tolerance exists, however, we have specified a weight cutoff, W_{c}, that determines when low-weight histories will be prematurely terminated as their contributions are deemed minute. After k iterations, a stationary method is terminated as

the error has reached some fraction, ϵ, of the initial error:

$$\|\mathbf{e}^k\|_2 = \epsilon\|\mathbf{e}^0\|_2 \,. \tag{5.22}$$

Per Eq (7.10), we see that this fraction is equivalent to $\epsilon = \rho(\mathbf{H})^k$. For the adjoint Neumann-Ulam method, if we take this fraction to be the weight cutoff, a measure of how accurately the contributions of a particular history to the solution are tallied, we then have the following relationship for k:

$$k = \frac{\log(W_c)}{\log(\rho(\mathbf{H}))} \,. \tag{5.23}$$

This then gives us a means to estimate the length of the random walks that will be generated from a particular linear operator based on the eigenvalues of its iteration matrix (independent of the linear operator splitting chosen) and based on the weight cutoff parameter used in the Neumann-Ulam method.

Domain Leakage Approximations

In a domain decomposed situation, not all histories will remain within the domain they started in and must instead be communicated. This communication, expected to be expensive, was analyzed by Siegel and colleagues for idealized, load balanced situations for full nuclear reactor core Monte Carlo simulations Siegel et al. (2012a). To quantify the number of particles that leak out of the local domain they define a leakage fraction, Λ, as:

$$\Lambda = \frac{\text{average \# of particles leaving local domain}}{\text{total of \# of particles starting in local domain}} \,. \tag{5.24}$$

For their studies, Siegel and colleagues assumed that the value of Λ was dependent on the total cross section of the system via the Wigner rational approximation. Outlined more thoroughly by Hwang's chapter in ?, we will use both the Wigner rational approximation and the mean chord

approximation as a means to estimate the leakage fraction.

In the case of domain decomposed linear operator equations, we can use diffusion theory to estimate the optical thickness of a domain in the decomposition and the corresponding leakage fraction in terms of properties of the linear operator and the discretization. To begin we must first calculate the mean distance a Monte Carlo history will move in the grid by computing the mean squared distance of its movement along the chord of length l defined across the domain. After a single transition a history will have moved a mean squared distance of:

$$\langle \bar{r}_1^2 \rangle = (n_s h)^2 \,, \tag{5.25}$$

where h is the size of the discrete grid elements along the chord and n_s is the number of grid elements a history will move on average every transition. For our diffusion model problem, n_s would equate to the expected number of states in the i (or j as the problem is symmetric) direction that a history will move in a single transition and is dependent on the stencil used for the discretization. After k transitions in the random walk, the history will have moved a mean squared distance of:

$$\langle \bar{r}_k^2 \rangle = k(n_s h)^2 \,. \tag{5.26}$$

If our chord is of length l and there are n_i grid elements (or states to which a history may transition) along that chord, then $h = l/n_i$ giving:

$$\langle \bar{r}_k^2 \rangle = k\left(\frac{n_s l}{n_i}\right)^2 \,. \tag{5.27}$$

From diffusion theory, we expect the average number of interactions along the chord to be:

$$\tau = \frac{l}{2d\sqrt{\langle \bar{r}_k^2 \rangle}} \,, \tag{5.28}$$

where $\mathtt{d}$ is the dimensionality of the problem and $\sqrt{\langle \bar{\mathtt{r}}_{\mathtt{k}}^2 \rangle}$ is effectively the mean free path of the Monte Carlo history in the domain. We can readily interpret τ to be the *effective optical thickness* of a domain of length $\mathtt{l}$. Inserting Eq (5.27) we arrive at:

$$\tau = \frac{\mathtt{n_i}}{2\mathtt{d}\mathtt{n_s}\sqrt{\mathtt{k}}}\,, \tag{5.29}$$

which if expanded with Eq (5.23) gives us the final relation for the effective optical thickness:

$$\tau = \frac{\mathtt{n_i}}{2\mathtt{d}\mathtt{n_s}}\sqrt{\frac{\log(\rho(\mathbf{H}))}{\log(W_c)}}\,. \tag{5.30}$$

For optically thin domains, we expect that most histories will be communicated, while optically thick domains will leak the fraction of histories that did not interact within. Using the optical thickness defined in Eq (5.30), we can then complete the leakage approximations by defining the bounds of $\tau \to 0, \Lambda \to 1$ and $\tau \to \infty, \Lambda \to \tau^{-1}$. With these bounds we can then define the leakage fraction out of a domain for the adjoint Neumann-Ulam method using the Wigner rational approximation:

$$\Lambda = \frac{1}{1+\tau}\,, \tag{5.31}$$

and using the mean-chord approximation:

$$\Lambda = \frac{1-e^{-\tau}}{\tau}\,. \tag{5.32}$$

Here, the leakage fraction is explicitly bound to the eigenvalues of the iteration matrix, the size of the domain, the content of the discretization stencil, and the weight cutoff selected to terminate low weight histories.

Numerical Experiments

To test the relationships developed by the spectral analysis, we form two simple numerical experiments using the diffusion model problem: one to measure the length of the random walks as a function of the iteration matrix eigenvalues, and one to measure the domain leakage fraction as a function of the iteration matrix eigenvalues and the discretization properties. Before doing this, we verify our computation of the spectral radius of the iteration matrix by numerically computing the largest eigenvalue of the diffusion operator using an iterative eigenvalue solver. For this verification, a 100×100 square grid with $\mathtt{h} = 0.01$, $\mathtt{h} = 0.1$, and $\mathtt{h} = 1.0$ and the absorption cross varied from 0 to 100 while the scattering cross section was fixed at unity. Figure 5.3 gives the measured spectral radius of the iteration matrix and the computed spectral radius for the preconditioned diffusion operator using Eq (5.18) as function of the absorption to scattering ratio ($\Sigma_\mathtt{a}/\Sigma_\mathtt{s}$). Excellent agreement was observed between the analytic and numerical results with all data points computed within the tolerance of the iterative eigenvalue solver.

Random Walk Length

With the spectral data in hand, we can go about setting up an experiment to measure the length of the random walks generated by the adjoint Neumann-Ulam solver. To do this, we again use a 100×100 square grid with $\mathtt{h} = 0.1$ and the absorption cross varied from 0 to 100 while the scattering cross section was fixed at unity. Three weight cutoff values of 1×10^{-2}, 1×10^{-4}, and 1×10^{-8} were used with 10,000 histories generated by a point source of strength 1 in the center of the domain. For each of the histories, the number of transitions made was tallied to provide an effective value of $\mathtt{k}$ for each history. This value was then averaged over all histories to get a measured value of $\mathtt{k}$ for the particular operator. On the left, Figure 5.4

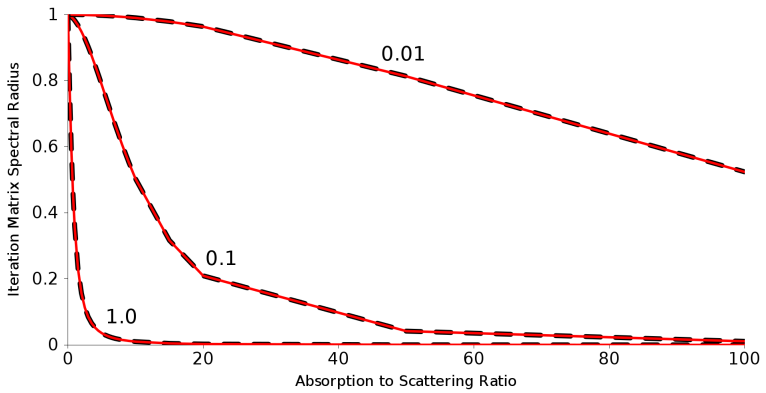

Figure 5.3: **Measured and analytic preconditioned diffusion operator spectral radius as a function of the absorption cross section to scattering cross section ratio.** *Values of* $\mathsf{h} = 0.01$, $\mathsf{h} = 0.1$, *and* $\mathsf{h} = 1.0$ *were used. The red data was computed numerically by an eigensolver while the black dashed data was generated by Eq (5.18).*

presents these measurements as well as the analytic result computed by Eq (5.23) as a function of the iteration matrix spectral radius, $\rho(\mathbf{H})$. On the right, Figure 5.4 gives the relative error between the predicted and observed results. We note good qualitative agreement between the measured and analytic results. However, we observe a larger relative error for both long and short random walks.

Domain Leakage

Finally, we seek to measure the leakage from a domain in a domain decomposed Monte Carlo calculation and assess the quality of our analytic relation for the optical thickness of domain and the associated leakage approximations. For this experiment, a square grid with $\mathsf{h} = 0.1$ was decomposed into 9 square domains, 3 in each cardinal direction with measurements occurring in the central domain without boundary grid points. For the cross sections, the absorption cross section was varied from 1 to 100 while the scattering

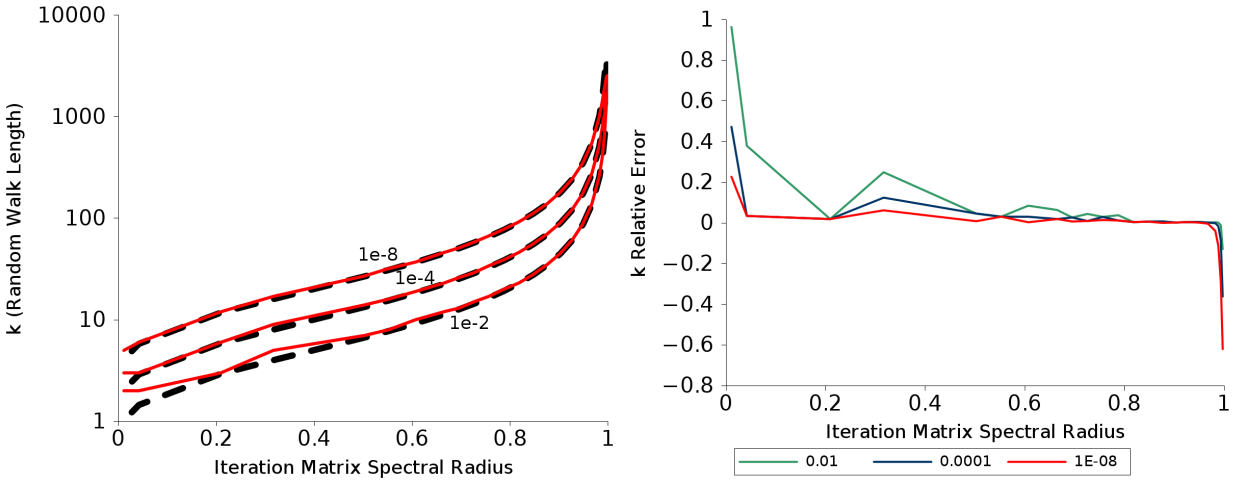

Figure 5.4: **Measured and analytic random walk length as a function of the iteration matrix spectral radius.** *The weight cutoff was varied with* 1×10^{-2}, 1×10^{-4}, *and* 1×10^{-8}. *In the left plot, the red data was computed numerically by an adjoint Neumann-Ulam implementation while the black dashed data was generated by Eq (5.23). In the right plot, the relative error between the predicted and measured results is presented for each weight cutoff.*

cross section was set to zero to create a purely absorbing environment with weight cutoff of 1×10^{-4}. The optical thickness of these domains will vary as a function of the absorption cross section if the other parameters are fixed. To compute the optical thickness, along with the spectral radius as given by Eq (5.18), we also need the parameters $\mathfrak{n}_\mathfrak{i}$ and $\mathfrak{n}_\mathfrak{s}$ which respectively describe the typical domain length and the average number of states moved along that typical length per history transition. For our grid above, the domains are varied in size with 50×50, 100×100, and 200×200 cells giving $\mathfrak{n}_\mathfrak{i} = 50$, $\mathfrak{n}_\mathfrak{i} = 100$, and $\mathfrak{n}_\mathfrak{i} = 200$ grid points or states along the typical length of the domain respectively. Looking at the Laplacian stencil in Eq (5.4), we see that all history transitions will only move a single state in either the $\mathfrak{i}$ or $\mathfrak{j}$ directions due to the symmetry of the problem. Furthermore, if we choose

the $\mathtt{i}$ direction, not all states we will transition to will move the history in that direction. Therefore, we look to the definition of the iteration matrix in Eq (5.15) and the definition of the adjoint probability matrix in Eq (3.36) to estimate the $\mathtt{n}_\mathtt{s}$ parameter. For a particular transition starting at state $(\mathtt{i},\mathtt{j})$, 6 of the 8 possible new states in the stencil move the history in $\mathtt{i}$ direction with relative coefficients of 4 for moving in the $(\pm\mathtt{i},0)$ direction and of 1 for moving in the $(\pm\mathtt{i},\pm\mathtt{j})$. These coefficients dictate the frequency those states are visited relative to the others. For those 6 states we can visit along the typical length, their sum is 12 out of the total 20 for the coefficients for all possible states with their ratio giving $\mathtt{n}_\mathtt{s} = \frac{3}{5}$.

To compute the leakage fraction numerically, 3×10^5 histories were sampled from a uniform source of strength unity over the global domain. At the start of a stage of histories, the number of histories starting in the center domain was computed and as the stage progressed, the number of histories that exited that domain was tallied with the ratio of the two numbers providing a numerical measure for the leakage fraction. Figure 5.5 gives the domain leakage measurements for the domain in the center of the global grid as well as the analytic result computed by Eqs (5.31) and (5.32) as a function of the iteration matrix spectral radius. Again, we note good qualitative agreement between the measured and analytic quantities but we begin to see the limits of the leakage approximations. To compare the quality of the two approximations, the absolute error between the computed leakage fraction and that generated by the Wigner rational and mean chord approximations is plotted in Figure 5.6 for all domain sizes tested. From these error results, the mean chord approximation is shown to have a lower error for ill-conditioned systems as compared to the Wigner approximation while the Wigner approximation produces less error for more well-conditioned systems. We also note that for the optically thick domains, the error is likely corresponded to that observed in Figure 5.4 for the $\mathtt{k}$ parameter while the large relative error in $\mathtt{k}$ for optically thin domains does not affect the

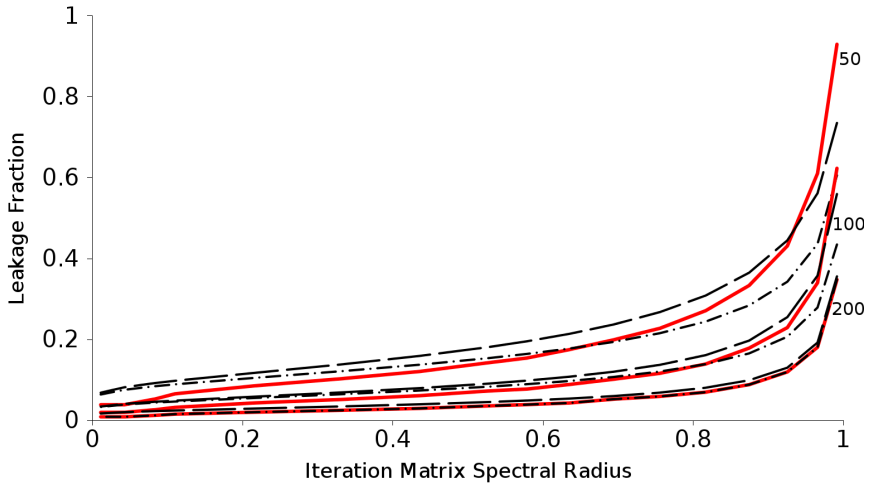

Figure 5.5: **Measured and analytic domain leakage as a function of the iteration matrix spectral radius.** *To test the behavior with respect to domain size,* $\mathfrak{n}_\mathfrak{i} = 50$, $\mathfrak{n}_\mathfrak{i} = 100$,*and* $\mathfrak{n}_\mathfrak{i} = 200$ *were used. The red data was computed numerically by a domain-decomposed adjoint Neumann-Ulam implementation, the black dashed data was generated by Eq (5.32) using the mean-chord approximation, and the dashed-dotted black data was generated by Eq (5.31) using the Wigner rational approximation.*

approximation significantly. In general, the mean chord approximation is a better choice to estimate the leakage fraction in a domain from the adjoint Neumann-Ulam method and except for a single data point with $\mathfrak{n}_\mathfrak{i} = 50$, the mean chord approximation yielded leakage fractions within 0.05 of the measured results. As the domain becomes more optically thick (with both increasing $\mathfrak{n}_\mathfrak{i}$ and decreasing $\rho(\mathbf{H})$), the approximations are more accurate.

5.2 Communication Costs for Symmetric Systems

Use Seigel's work to get communication costs.

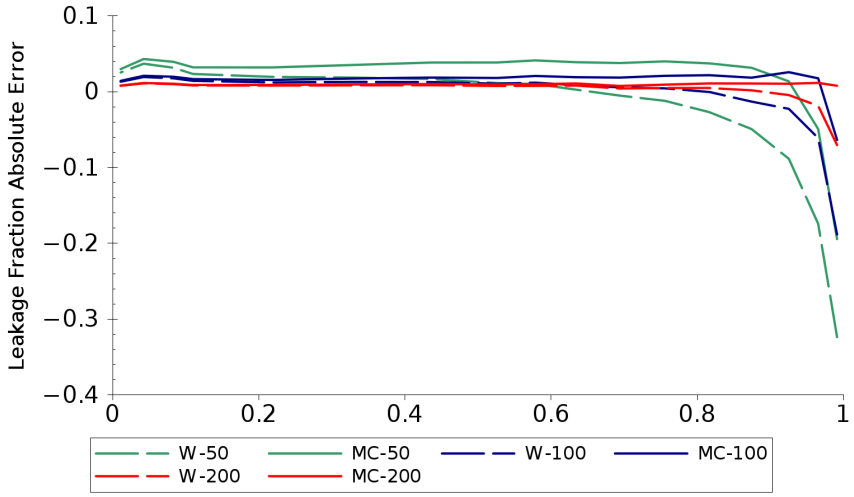

Figure 5.6: **Measured and analytic domain leakage absolute error as a function of the iteration matrix spectral radius.** *To test the behavior with respect to domain size,* $n_i = 50$ *(green),* $n_i = 100$ *(blue), and* $n_i = 200$ *(red) were used. The dashed lines represent the error using the Wigner rational approximation while the solid lines represent the error using the mean-chord approximation.*

5.3 Leakage Fractions for Asymmetric Systems

Extend the above results to asymmetric systems.

5.4 Communication Costs for Asymmetric Systems

Use Seigel's work to get communication costs.

Chapter 6

The Simplified P_N Equations

The neutron transport problem is complicated. Solutions cover a large phase space and the problems of interest are often geometrically complex, very large, or both, requiring tremendous computational resources to generate an adequate solution. Modern deterministic methods for large scale problems are commonly variants on the discrete ordinates (S_N) method Evans et al. (2010). For full reactor core neutronics simulations, the S_N method requires potentially trillions of unknown angular flux moments to be computed to achieve good accuracy for the repsonses of interest. Other forms of the transport problem, including the P_N method, take on a simpler form than the more common S_N methods but lack in accuracy when compared while still requiring considerable computational resources for solutions in multiple dimensions.

In the 1960's, Gelbard developed an ad-hoc multidimensional extension of the simple single dimension planar P_N equations that created a system of coupled, diffusion-like equations known as the simplified P_N (SP_N) equations. Up until around the 1990's, the SP_N methods was either widely unknown, widely unused, or combination of both even though numerical studies showed promising results with better solutions than diffusion theory and a significant reduction in computational time over more accurate methods such as discrete ordinates. Why did this happen? A significant problem, pointed out by Larsen, was that little rigor had been applied to the formulation of the SP_N equations since their derivation through primarily heuristic arguments. Instead, studies at that time focused on simply comparing the results of the method to other contemporary transport solution strategies. In addition, many problems of interest from the literature at the time were either solved using nodal-type methods for reactor-sized problems or S_N-type methods for

benchmark problems with intricate material configurations and potentially large flux gradients over small spatial domains.

So why reconsider the SP_N equations? Starting in the 1990's and primarily due to Larsen and his colleagues, the SP_N equations have been given a more rigorous treatment with both variational and asymptotic derivations performed as a means of verification. In addition, these equations have been more rigorously studied as solution methods to MOX fuel problems and have been shown to provide accurate solutions. With this mathematical literature to provide a solid numerical footing for the method, we look at its application to today's challenge problems in full reactor core transport. The reduction in numerical complexity of current full core deterministic solution methods using the S_N approximation could mean significant savings in both compute time and memory required. In addition, the characteristics of the solution to the transport problem for a steady state reactor core permit diffusion theory to be used; a staple of the nuclear industry since its inception. Therefore, if diffusion theory is applicable, then finer grained solutions that capture more of the physics contained in the transport equation should be possible with the SP_N method. In doing so, we also expect from the literature to obtain computed responses on the order of accuracy we would expect from an appropriately discretized S_N method at a fraction of the cost.

To further motivate moving in this direction, recent developments in the Exnihilo neutronics package at Oak Ridge National Laboratory have permitted generation of the SP_N system of equations for detailed full core reactor models. By fully forming these equations and formulating them as a linear algebra problem, we now have access to all of the modern advancements in computational linear algebra including Krylov solvers for asymmetric systems and preconditioning methods such as algebraic multigrid. This leads us to then explore the applicability of our work in discrete Monte Carlo methods for linear systems as a possible solution method for the SP_N equations. If formulated correctly, we hypothesize

that signficant improvement in usage of computational resources may be observed compared to modern solution techniques such as those suggested. In addition, solving the $\mathsf{SP_N}$ equations in this way also breaks away from the $\mathsf{S_N}$ forms of parallelism where spatial parallelism is achieved by an efficient parallel sweep, angular efficiency achieved by pipelining, and energy parallelism achieved by decoupling the groups. With the $\mathsf{SP_N}$ equations as a full matrix system, we now can parallelize the problem as prescribed by the linear solver, which may be significantly more scalable than current $\mathsf{S_N}$ transport practices.

In this document we derive the multigroup $\mathsf{SP_N}$ equations from the Boltzmann transport equation. We then perform a spectral analysis on the resulting system of equations to determine its potential performance with both modern Krylov methods and Monte Carlo methods for asymmetric linear systems. Following this, we devise a Monte Carlo synthetic acceleration method as a proposed solution scheme.

In this chapter, we derive the $\mathsf{SP_N}$ equations, closely following the work of Evans. We begin by stating the general time-independent neutron transport equation followed by a derivation of the $\mathsf{P_N}$ equations in planar geometry for multiple energy groups. From these equations, we then apply a set of approximations to yield the multi-dimensional, multi-group $\mathsf{SP_N}$ equations for fixed source problems.

6.1 The Neutron Transport Equation

As a starting point we define the time-independent neutron transport equation Lewis (1993):

$$\hat{\Omega}\cdot\vec{\nabla}\psi(\vec{r},\hat{\Omega},\mathsf{E})+\sigma(\vec{r},\mathsf{E})\psi(\vec{r},\hat{\Omega},\mathsf{E})= \iint\sigma_s(\vec{r},\mathsf{E}'\rightarrow\mathsf{E},\hat{\Omega}'\rightarrow\hat{\Omega})\psi(\vec{r},\hat{\Omega}',\mathsf{E}')\mathrm{d}\Omega'\mathrm{d}\mathsf{E}'+q(\vec{r},\hat{\Omega},\mathsf{E})\,, \quad (6.1)$$

with the variables defined as:

- $\vec{r}$ - neutron spatial position
- $\hat{\Omega}$ - neutron streaming direction with radial component μ and azimuthal component ω
- $\hat{\Omega}' \cdot \hat{\Omega} = \mu_0$ is the angle of scattering
- E - neutron energy
- $\psi(\vec{r}, \hat{\Omega}, E)$ - angular flux
- $\sigma(\vec{r}, E)$ - total interaction cross section
- $\sigma_s(\vec{r}, E' \rightarrow E, \hat{\Omega}')$ - probability of scattering from direction $\hat{\Omega}'$ into an angular domain $d\hat{\Omega}'$ about the direction $\hat{\Omega}$ and from energy E' to an energy domain dE' about energy E
- $q(\vec{r}, \hat{\Omega}, E)$ - external source of neutrons.

For this work, it is sufficient to formulate Eq (6.1) in 1-dimensonal Cartesian geometry:

$$\mu \frac{\partial}{\partial x}\psi(x, \mu, E) + \sigma(x, E)\psi(x, \mu, E) = \int\int \sigma_s(x, E') \rightarrow E, \hat{\Omega}' \rightarrow \hat{\Omega})\psi(x, \hat{\Omega}', E')d\Omega' dE' + \frac{q(x, E)}{4\pi}, \quad (6.2)$$

where the angular component of the solution is no longer dependent on the azimuthal direction of travel and an isotropic source of neutrons is assumed.

6.2 Derivation of the P_N Equations

Next, we derive the P_N equations, a simplified form of the general transport equation where Legendre polynomials are used to expand the angular flux

and scattering cross section variables as a means of capturing the angular structure of the solution. Before deriving this form of the transport equation, we briefly discuss a few properties of Legendre polynomials that we will find useful in the derivation.

Legendre Polynomials

The Legendre polynomials are an orthogonal set of functions that are solutions to Legendre's differential equation. They have the following form Lewis (1993):

$$P_l(\mu) = \frac{1}{2^l l!}\frac{d^l}{d\mu^l}(\mu^2 - 1)^l \,. \tag{6.3}$$

These functions have several useful properties including orthogonality:

$$\int_{-1}^{1} P_l(\mu)P_{l'}(\mu)d\mu = \frac{1}{2l+1}\delta_{ll'} \,, \tag{6.4}$$

a recurrence relation:

$$\mu P_l(\mu) = \frac{1}{2l+1}[(l+1)P_{l+1}(\mu) + lP_{l-1}(\mu)] \,, \tag{6.5}$$

and an addition theorem:

$$P_l(\hat{\Omega}\cdot\hat{\Omega}') = \frac{1}{2n+1}\sum_{m=-l}^{l} Y_{lm}(\hat{\Omega})Y^*_{lm}(\hat{\Omega}') \,, \tag{6.6}$$

where the functions $Y_{lm}(\hat{\Omega})$ are the spherical harmonics. We can form the addition theorem in this way because the spherical harmonics are in fact just harmonic multiples of the Legendre polynomials:

$$Y_{lm}(\hat{\Omega}) = \sqrt{\frac{(2l+1)(l-m)!}{(l+m)!}}P_l^m(\mu)e^{i\omega m} \,, \tag{6.7}$$

where ω is the azimuthal component of the streaming direction. We can reduce Eq (6.6) for the planar geometry we are studying by ignoring the azimuthal components of the addition theorem. As shown in Eq (6.7), the azimuthal dependence is given by the harmonic component, $e^{i\omega m}$, and therefore we choose to ignore all terms in Eq. (6.6) where $m \neq 0$. This gives:

$$P_l(\hat{\Omega} \cdot \hat{\Omega}') = \frac{1}{2n+1} Y_{l0}(\hat{\Omega}) Y^*_{l0}(\hat{\Omega}') \,. \tag{6.8}$$

Per Eq (6.7) we have:

$$Y_{l0}(\hat{\Omega}) = \sqrt{2l+1} P^0_l(\mu) \,, \tag{6.9}$$

where $P^0_l(\mu) = P_l(\mu)$ is the 0^{th} associated Legendre function. Finally, we can reduce the addition theorem from Eq (6.8) with Eq (6.9) to a simple product for planar geometry:

$$P_l(\hat{\Omega} \cdot \hat{\Omega}') = P_l(\mu) P_l(\mu') \,. \tag{6.10}$$

Planar P_N Equations

With the Legendre polynomial properties defined above, we can proceed by deriving the P_N equations for planar geometry. For these equations, we will start by assuming a monoenergtic field of neutrons such that we are solving the following reduced form of the transport equation:

$$\mu \frac{\partial}{\partial x} \psi(x, \mu) + \sigma(x) \psi(x, \mu) = \int d\Omega' \sigma_s(x, \hat{\Omega}' \to \hat{\Omega}) \psi(\vec{r}, \hat{\Omega}') + \frac{q(x)}{4\pi} \,. \tag{6.11}$$

The P_N equations introduce the approximation that the angular dependence of the scattering cross section, σ_s, and the angular flux ψ, can be discretized

by expanding them in Legendre polynomials as follows:

$$\psi(x,\mu) = \sum_{n=0}^{\infty}(2n+1)P_n(\mu)\phi_n(x)\,, \tag{6.12}$$

$$\sigma_{sm}(x) = \sum_{m=0}^{\infty}(2m+1)P_m(\mu)\sigma_s(x)\,, \tag{6.13}$$

where we have supressed the 2π generated by integrating away the azimuthal angular component and $\phi_n(x)$ in Eq (6.12) is referred to as the n^{th} Legendre moment of the neutron flux and is given by:

$$\phi_n(x) = \int_{-1}^{1} P_n(\mu)\psi(x,\mu)d\mu\,. \tag{6.14}$$

We first insert the expansions given by Eq (6.12) and (6.13) into the planar transport equation given by Eq (6.11):

$$\frac{\partial}{\partial x}\Big[\sum_{n=0}^{\infty}(2n+1)\phi_n\mu P_n(\mu)\Big] + \sigma\sum_{n=0}^{\infty}(2n+1)\phi_n P_n(\mu) = \int_{-1}^{1}\sum_{m=0}^{\infty}(2m+1)\sigma_{sm}P_m(\mu_0)\sum_{n=0}^{\infty}(2n+1)\phi_n P_n(\mu')d\mu' + q\,, \tag{6.15}$$

where the dependence on the spatial variable, x, has been supressed. To arrive at the P_N equations we multiply Eq (6.15) by $P_m(\mu)$ and integrate over the angular domain $\int_{-1}^{1} d\mu$. We will look at each term in Eq (6.15) individually.

Streaming Term We first apply the multiplication and integration as prescribed above:

$$\frac{\partial}{\partial x}\left[\sum_{n=0}^{\infty}(2n+1)\mu\phi_n P_n(\mu)\right] \rightarrow \int_{-1}^{1}\frac{\partial}{\partial x}\left[\sum_{n=0}^{\infty}(2n+1)\phi_n \mu P_n(\mu)P_m(\mu)\right]d\mu\,. \tag{6.16}$$

The $\mu P_n(\mu)$ term can be eliminated via the recurrence relation given by Eq (6.5):

$$\int_{-1}^{1}\frac{\partial}{\partial x}\left[\sum_{n=0}^{\infty}(2n+1)\frac{\phi_n}{2n+1}[(n+1)P_{n+1}(\mu)+nP_{n-1}(\mu)]P_m(\mu)\right]d\mu, \tag{6.17}$$

which expands to:

$$\sum_{n=0}^{\infty}\frac{\partial}{\partial x}\phi_n\left[(n+1)\int_{-1}^{1}P_{n+1}(\mu)P_m(\mu)d\mu+n\int_{-1}^{1}P_{n-1}(\mu)P_m(\mu)d\mu\right]. \tag{6.18}$$

This reveals the orthogonality relation given by Eq (6.4) that when inserted into Eq (6.17):

$$\sum_{n=0}^{\infty}\frac{\partial}{\partial x}\phi_n\left[(n+1)\frac{1}{2n+1}\delta_{n,n+1}+n\frac{1}{2n+1}\delta_{n,n-1}\right]. \tag{6.19}$$

We can then distribute the Legendre moment to arrive at the final form of the streaming term:

$$\sum_{n=0}^{\infty}\frac{\partial}{\partial x}\frac{1}{2n+1}\Big[(n+1)\phi_{n+1}+n\phi_{n-1}\Big]. \tag{6.20}$$

Collision Term To reduce the collision term, the orthogonality relation is again applied after the integration:

$$\sigma\sum_{n=0}^{\infty}(2n+1)\phi_n P_n(\mu) \rightarrow \int_{-1}^{1}\sigma\sum_{n=0}^{\infty}(2n+1)\phi_n P_n(\mu)P_m(\mu)d\mu\,, \tag{6.21}$$

$$\sigma \sum_{n=0}^{\infty} (2n+1)\phi_n \frac{1}{2n+1} \,, \tag{6.22}$$

giving for the final collision term:

$$\sum_{n=0}^{\infty} \sigma\phi_n \,. \tag{6.23}$$

Scattering Term For the scattering term:

$$\int_{-1}^{1} \sum_{m=0}^{\infty} (2m+1)\sigma_{sm} P_m(\mu_0) \sum_{n=0}^{\infty} (2n+1)\phi_n P_n(\mu')d\mu' \rightarrow \int_{-1}^{1}\int_{-1}^{1} \sum_{m=0}^{\infty} (2m+1)\sigma_{sm} P_m(\mu)P_m(\mu_0) \sum_{n=0}^{\infty} (2n+1)\phi_n P_n(\mu')d\mu' d\mu \,. \tag{6.24}$$

The addition thereom from Eq (6.10) is applied to give:

$$\int_{-1}^{1}\int_{-1}^{1} \sum_{m=0}^{\infty} (2m+1)\sigma_{sm} P_m(\mu)P_m(\mu)P_m(\mu') \sum_{n=0}^{\infty} (2n+1)\phi_n P_n(\mu')d\mu' d\mu \,, \tag{6.25}$$

which can be rearranged as:

$$\sum_{m=0}^{\infty}\sum_{n=0}^{\infty} (2m+1)\sigma_{sm}(2n+1)\phi_n \int_{-1}^{1} P_m(\mu')P_n(\mu')d\mu' \int_{-1}^{1} P_m(\mu)P_m(\mu)d\mu \,. \tag{6.26}$$

Again we can apply orthogonality to eliminate the Legendre polynomials:

$$\sum_{m=0}^{\infty}\sum_{n=0}^{\infty} (2m+1)\sigma_{sm}(2n+1)\phi_n \frac{1}{2n+1}\delta_{nm}\frac{1}{2m+1}\delta_{mm} \,, \tag{6.27}$$

which is reduced to:

$$\sum_{n=0}^{\infty} \sigma_{sn}\phi_n \,, \tag{6.28}$$

with the dependence on the index m eliminated.

Source Term The last term we are concerned with in Eq (6.15) is the source term:

$$q \to \int_{-1}^{1} q P_n(\mu) d\mu \,. \tag{6.29}$$

We can leverage orthogonality by multiplying by $P_0(\mu) = 1$:

$$\int_{-1}^{1} q P_0 P_n(\mu) d\mu = \frac{q}{2 * 0 + 1} \delta_{n0} \,, \tag{6.30}$$

giving a final source term of:

$$q \delta_{n0} \,. \tag{6.31}$$

Now that we have expanded all angular dependent terms in Eq (6.15) and reduced them appropriately, we can combine them to generate the P_N equations:

$$\sum_{n=0}^{\infty} \frac{\partial}{\partial x} \frac{1}{2n+1} \Big[(n+1)\phi_{n+1} + n\phi_{n-1} \Big] + \sum_{n=0}^{\infty} \sigma \phi_n = \sum_{n=0}^{\infty} \sigma_{sn} \phi_n + q\delta_{n0} \,. \tag{6.32}$$

More formally, the P_N equations are written as:

$$\frac{1}{2n+1} \frac{\partial}{\partial x} \Big[(n+1)\phi_{n+1} + n\phi_{n-1} \Big] + \Sigma_n \phi_n = q\delta_{n0} \,, \tag{6.33}$$

where $\Sigma_n = \sigma - \sigma_{sn}$ and the summations are truncated at some level of approximation N such that $n = 0, 1, \ldots, N$. This yields a set of $N + 1$ equations for $N + 2$ flux moments. We therefore require an additional equation to close the system. In accordance with the series truncation as an approximation we choose the last moment in the expansion to be zero:

$$\phi_{N+1} = 0 \,. \tag{6.34}$$

As an example, we will construct the P5 equations from Eq (6.33) and the closure given by Eq (6.34):

$$\frac{\partial}{\partial x}\phi_1 + \Sigma_0\phi_0 = q\,, \tag{6.35a}$$

$$\frac{1}{3}\frac{\partial}{\partial x}\Big[2\phi_2 + \phi_0\Big] + \Sigma_1\phi_1 = 0\,, \tag{6.35b}$$

$$\frac{1}{5}\frac{\partial}{\partial x}\Big[3\phi_3 + 2\phi_1\Big] + \Sigma_2\phi_2 = 0\,, \tag{6.35c}$$

$$\frac{1}{7}\frac{\partial}{\partial x}\Big[4\phi_4 + 3\phi_2\Big] + \Sigma_3\phi_3 = 0\,, \tag{6.35d}$$

$$\frac{1}{9}\frac{\partial}{\partial x}\Big[5\phi_5 + 4\phi_3\Big] + \Sigma_4\phi_4 = 0\,, \tag{6.35e}$$

$$\frac{1}{11}\frac{\partial}{\partial x}5\phi_4 + \Sigma_5\phi_5 = 0\,. \tag{6.35f}$$

This gives us a set of 6 coupled equations for the six Legendre moments requested defined over the entire spatial domain for a single energy group. In practice, only odd-numbered P_N orders are generally used Lewis (1993). This is due to the fact that using odd N yields an even number of $N+1$ equations which can be split evenly on the left and right boundaries of the problem to facilitate the description of boundary conditions. We will choose this convention when deriving the boundary conditions.

Boundary Conditions for the P_N Equations

Per the analysis in Lewis (1993), two types of boundary conditions will be discussed: reflecting and Marshak. Marshak boundary conditions can be used to specify both vacuum conditions and isotropic source conditions on the boundary.

Reflecting Boundary Conditions In this case, the incoming flux should be equivalent to the outgoing flux at the boundary point x_b:

$$\psi(x_b, \mu) = \psi(x_b, -\mu) \,. \tag{6.36}$$

Given the legendre expansion for the flux defined in Eq (6.12) and the Legendre polynomial property that $P_n(\mu) = (-1)^n P_n(-\mu)$, the condition specified by Eq (6.36) can be satisfied if

$$\phi_n = 0, \ \forall \text{ odd } n \,, \tag{6.37}$$

as all even n yield $P_n(\mu) = P_n(-\mu)$ and therefore an equivalent reflecting condition for the flux moments.

Marshak Boundary Conditions The Marshak conditions come directly from the Legendre moments of the flux:

$$\int_{\mu_b} P_i(\mu)\psi(\mu)d\mu = \int_{\mu_b} P_i(\mu)\psi_b(\mu)d\mu \qquad \text{for } i = 1, 3, ..., N \,, \tag{6.38}$$

where $\psi_b(\mu)$ is the prescribed angular flux on the boundary of interest and μ_b the angular domain defined by the boundary. To discretize this condition, we again insert the angular flux expansions from Eq (6.12) for the fluxes defined in the domain:

$$\int_{\mu_b} P_i(\mu) \sum_{n=0}^{N} (2n+1)\phi_n P_n(\mu)d\mu = \int_{\mu_b} P_i(\mu)\psi_b(\mu)d\mu \,. \tag{6.39}$$

The boundary flux, $\phi_b(\mu)$ is assumed to known and therefore Eq (6.39) defines a set of $(N+1)/2$ equations to be solved on each boundary in the planar case, closing the system in the spatial domain.

As an example of applying the Marshak conditions, consider the P_3 case with an isotropic boundary source ϕ_b on the left side of the domain. In this

case, the angular domain over which the boundary flux is defined will be $\mu_b \in [0,1]$, giving the bounds of integration. We first expand the summation for $i = 1$:

$$\int_0^1 \mu \left[\phi_0 + 3\phi_1\mu + \frac{5}{2}\phi_2(3\mu^2-1) + \frac{7}{2}\phi_3(5\mu^3-3\mu) \right] d\mu = \int_0^1 \mu\phi_b \, d\mu \,, \quad (6.40)$$

and then $i = 3$:

$$\int_0^1 \frac{1}{2}(5\mu^3-3\mu) \left[\phi_0 + 3\phi_1\mu + \frac{5}{2}\phi_2(3\mu^2-1) + \frac{7}{2}\phi_3(5\mu^3-3\mu) \right] d\mu = \int_0^1 \frac{1}{2}(5\mu^3-3\mu)\phi_b \, d\mu. \quad (6.41)$$

Expanding the polynomials in μ and carrying out the simple integration then gives 2 equations for the left hand boundary:

$$\phi_0 + 2\phi_1 + \frac{5}{4}\phi_2 = \phi_b \,, \quad (6.42)$$

$$\phi_0 - 5\phi_2 - 8\phi_3 = \phi_b \,. \quad (6.43)$$

The right hand side boundary condition will yield 2 complementary equations if Marshak conditions are used or 2 non-zero moments to be solved for if reflected conditions are used. The formulation above also holds for vacuum conditions where $\phi_b = 0$.

6.3 Derivation of the SP_N Equations

The P_N equations give $N + 1$ coupled first-order equations capturing the spatial and angular-dependence of the solution. In multiple dimensions, the equation set becomes large and coupled not only through angular moments but also through the spatial variables. As a simpler alternative to multidimensional P_N solutions, Gelbard recognized in 1960 that the planar P_N equations could be simplified and applied an ad-hoc method to extend

them to multiple dimensions, yielding the SP_N equations. These equations are not only fewer in number, but also take on a diffusion-like form while maintaining the angular character of the flux, making them amenable to solutions with modern diffusion methods.

First, the P_N equations can be simplified to $(N+1)/2$ second-order equations by solving for the n^{th} Legendre flux moment in the odd-order equations:

$$\phi_n = \frac{1}{\Sigma_n}\left[q\delta_{no} - \frac{\partial}{\partial x}\Big(\frac{n}{2n+1}\phi_{n-1} + \frac{n+1}{2n+1}\phi_{n+1}\Big)\right], \tag{6.44}$$

for $n = 1, 3, \cdots, N$ and $\delta_{no} = 0\ \forall n \neq 0$. We can insert the odd moments into Eq (6.33) to get a reduced group of equations for the even moments:

$$\begin{aligned} -\frac{\partial}{\partial x}\Bigg[&\frac{n}{2n+1}\frac{1}{\Sigma_{n-1}}\frac{\partial}{\partial x}\Big(\frac{n-1}{2n-1}\phi_{n-2} + \frac{n}{2n-1}\phi_n\Big) \\ &+ \frac{n+1}{2n+1}\frac{1}{\Sigma_{n+1}}\frac{\partial}{\partial x}\Big(\frac{n+1}{2n+3}\phi_n + \frac{n+2}{2n+3}\phi_{n+2}\Big)\Bigg] \\ &+ \Sigma_n\phi_n = q\delta_{n0} \qquad n = 0, 2, 4, \cdots, N\,. \end{aligned} \tag{6.45}$$

Immediately, we note the diffusion-like nature of Eq (6.45) as compared to the original P_N equations. To extend these equations to multiple dimensions, gelbard simple replaced the x-plane spatial derivatives in the reduced set of equations with general multidimensional gradient operators:

$$\begin{aligned} -\nabla\cdot\Bigg[&\frac{n}{2n+1}\frac{1}{\Sigma_{n-1}}\nabla\Big(\frac{n-1}{2n-1}\phi_{n-2} + \frac{n}{2n-1}\phi_n\Big) \\ &+ \frac{n+1}{2n+1}\frac{1}{\Sigma_{n+1}}\nabla\Big(\frac{n+1}{2n+3}\phi_n + \frac{n+2}{2n+3}\phi_{n+2}\Big)\Bigg] \\ &+ \Sigma_n\phi_n = q\delta_{n0} \qquad n = 0, 2, 4, \cdots, N\,, \end{aligned} \tag{6.46}$$

yielding a multidimensional set of $(\mathsf{N}+1)/1$ angular coupled equations known as the $\mathsf{SP_N}$. Again, we provide closure to this set of equations with $\phi_{\mathsf{N}+1} = 0$. As a concrete example, we will consider the $\mathsf{SP_7}$ equations:

$$-\nabla \cdot \frac{1}{3\Sigma_1}\nabla(\phi_0 + 2\phi_2) + \Sigma_0\phi_0 = \mathsf{q} \tag{6.47a}$$

$$-\nabla \cdot \left[\frac{2}{15\Sigma_1}\nabla(\phi_0 + 2\phi_2) + \frac{3}{35\Sigma_3}\nabla(3\phi_2 + 4\phi_4)\right] + \Sigma_2\phi_2 = 0 \tag{6.47b}$$

$$-\nabla \cdot \left[\frac{4}{63\Sigma_3}\nabla(3\phi_2 + 4\phi_4) + \frac{5}{99\Sigma_5}\nabla(5\phi_4 + 6\phi_6)\right] + \Sigma_4\phi_4 = 0 \tag{6.47c}$$

$$-\nabla \cdot \left[\frac{6}{143\Sigma_5}\nabla(5\phi_4 + 6\phi_6) + \frac{7}{195\Sigma_7}\nabla(7\phi_6)\right] + \Sigma_6\phi_6 = 0\,. \tag{6.47d}$$

To further modify these equations, we can use a change of variables to create a new group of equations such that the gradients are operating on a single vector:

$$u_1 = \phi_0 + 2\phi_2 \tag{6.48a}$$

$$u_2 = 3\phi_2 + 4\phi_4 \tag{6.48b}$$

$$u_3 = 5\phi_4 + 6\phi_6 \tag{6.48c}$$

$$u_4 = 7\phi_6\,, \tag{6.48d}$$

or equivalently:

$$\phi_0 = u_1 - \frac{2}{3}u_2 + \frac{8}{15}u_3 - \frac{16}{35}u_4 \tag{6.49a}$$

$$\phi_2 = \frac{1}{3}u_2 - \frac{4}{15}u_3 + \frac{8}{35}u_4 \tag{6.49b}$$

$$\phi_4 = \frac{1}{5}u_3 - \frac{6}{35}u_4 \tag{6.49c}$$

$$\phi_6 = \frac{1}{7}u_4\,. \tag{6.49d}$$

When substituted into Eq (6.47), these terms give:

$$-\nabla\cdot\frac{1}{3\Sigma_1}\nabla u_1+\Sigma_0\left[u_1-\frac{2}{3}u_2+\frac{8}{15}u_3-\frac{16}{35}u_4\right]=-q \tag{6.50a}$$

$$-\nabla\cdot\left[\frac{2}{15\Sigma_1}\nabla u_1+\frac{3}{35\Sigma_3}\nabla u_2\right]+\Sigma_2\left[\frac{1}{3}u_2-\frac{4}{15}u_3+\frac{8}{35}u_4\right]=0 \tag{6.50b}$$

$$-\nabla\cdot\left[\frac{4}{63\Sigma_3}\nabla u_2+\frac{5}{99\Sigma_5}\nabla u_3\right]+\Sigma_4\left[\frac{1}{5}u_3-\frac{6}{35}u_4\right]=0 \tag{6.50c}$$

$$-\nabla\cdot\left[\frac{6}{143\Sigma_5}\nabla u_3+\frac{7}{195\Sigma_7}\nabla u_4\right]+\Sigma_6\left[\frac{1}{7}u_4\right]=0\,. \tag{6.50d}$$

If we rearrange the Eq (6.50 such that only one divergence operation is present in each equation, we can formulate this as a matrix system of 4 equations in the case of the SP_7 approximation:

$$-\nabla\cdot D_n\nabla u_n+\sum_{m=1}^{4}A_{nm}u_m=q_n\qquad n=1,2,3,4\,, \tag{6.51}$$

with $\mathbf{u}$ the vector of solution variables:

$$\mathbf{u}=(u_1\;\;u_2\;\;u_3\;\;u_4)^T\,, \tag{6.52}$$

$\mathbf{D}$ the vector of effective diffusion coefficients:

$$\mathbf{D}=\left(\frac{1}{3\Sigma_1}\;\;\frac{1}{7\Sigma_3}\;\;\frac{1}{11\Sigma_5}\;\;\frac{1}{15\Sigma_7}\right)^T\,, \tag{6.53}$$

$\mathbf{q}$ the vector of source terms where the 0^{th} moment source has now been distributed through the system:

$$\mathbf{q}=(q\;\;-\frac{2}{3}q\;\;\frac{8}{15}q\;\;-\frac{16}{35}q)^T\,, \tag{6.54}$$

and $\mathbf{A}$ a matrix of angular scattering terms:

$$\mathbf{A} = \begin{bmatrix} (\Sigma_0) & (-\frac{2}{3}\Sigma_0) & (\frac{8}{15}\Sigma_0) & (-\frac{16}{35}\Sigma_0) \\ (-\frac{2}{3}\Sigma_0) & (\frac{4}{15}\Sigma_0 + \frac{1}{3}\Sigma_2) & (-\frac{16}{45}\Sigma_0 - \frac{4}{9}\Sigma_2) & (\frac{32}{105}\Sigma_0 + \frac{8}{21}\Sigma_2) \\ (\frac{8}{15}\Sigma_0) & (-\frac{16}{45}\Sigma_0 - \frac{4}{9}\Sigma_2) & (\frac{64}{225}\Sigma_0 + \frac{16}{45}\Sigma_2 + \frac{9}{25}\Sigma_4) & (-\frac{128}{525}\Sigma_0 - \frac{32}{105}\Sigma_2 - \frac{54}{175}\Sigma_4) \\ (-\frac{16}{35}\Sigma_0) & (\frac{32}{105}\Sigma_0 + \frac{8}{21}\Sigma_2) & (-\frac{128}{525}\Sigma_0 - \frac{32}{105}\Sigma_2 - \frac{54}{175}\Sigma_4) & (\frac{256}{1225}\Sigma_0 + \frac{64}{245}\Sigma_2 + \frac{324}{1225}\Sigma_4 + \frac{13}{49}\Sigma_6) \end{bmatrix}. \tag{6.55}$$

Note that the term $\sum_{m=1}^{4} A_{nm}u_m$ in Eq (6.51) couples the moments in each equation while the diffusive term in each equation is only for a single 'psuedo-moment' u_n. This completes the derivation of the SP_7 equations for a single energy group. As noted by Evans, lower order SP_N approximations can be generated by setting higher order even moments in this system to zero (e.g. $\phi_6 = \phi_4 = 0$ yields the SP_3 equations).

Boundary Conditions for the SP_N Equations

We approach the formulation of the boundary conditions in much the same way as we did for the P_N equations with both reflecting and Marshak conditions possible. To begin, we perform the expansion in Eq (6.39) for the left side of the planar system, this time for $N = 7$ to correspond to our SP_7 system. For $i = 1$:

$$\int_0^1 \mu \left[\phi_0 + 3\phi_1\mu + \frac{5}{2}\phi_2(3\mu^2 - 1) + \frac{7}{2}\phi_3(5\mu^3 - 3\mu) + \frac{1}{8}(63\mu^5 - 70\mu^3 + 15\mu) \right] d\mu = \int_0^1 \mu\phi_b \, d\mu \,, \tag{6.56}$$

for $\mathtt{i} = 3$,

$$\int_0^1 \frac{1}{2}(5\mu^3 - 3\mu)\left[\phi_0 + 3\phi_1\mu + \frac{5}{2}\phi_2(3\mu^2 - 1) + \frac{7}{2}\phi_3(5\mu^3 - 3\mu) + \frac{1}{8}(63\mu^5 - 70\mu^3 + 15\mu)\right] \mathrm{d}\mu = \int_0^1 \frac{1}{2}(5\mu^3 - 3\mu)\phi_\mathtt{b}\,\mathrm{d}\mu\,, \quad (6.57)$$

for $\mathtt{i} = 5$:

$$\int_0^1 \frac{1}{8}(63\mu^5 - 70\mu^3 + 15\mu)\left[\phi_0 + 3\phi_1\mu + \frac{5}{2}\phi_2(3\mu^2 - 1) + \frac{7}{2}\phi_3(5\mu^3 - 3\mu) + \frac{1}{8}(63\mu^5 - 70\mu^3 + 15\mu)\right] \mathrm{d}\mu = \int_0^1 \frac{1}{8}(63\mu^5 - 70\mu^3 + 15\mu)\phi_\mathtt{b}\,\mathrm{d}\mu\,, \quad (6.58)$$

and for $\mathtt{i} = 7$:

$$\int_0^1 \frac{1}{16}(429\mu^7 - 693\mu^5 + 315\mu^3 + 35\mu)\left[\phi_0 + 3\phi_1\mu + \frac{5}{2}\phi_2(3\mu^2 - 1) + \frac{7}{2}\phi_3(5\mu^3 - 3\mu) + \frac{1}{8}(63\mu^5 - 70\mu^3 + 15\mu) + \frac{1}{16}(429\mu^7 - 693\mu^5 + 315\mu^3 + 35\mu)\right] \mathrm{d}\mu = \int_0^1 \frac{1}{16}(429\mu^7 - 693\mu^5 + 315\mu^3 + 35\mu)\phi_\mathtt{b}\,\mathrm{d}\mu\,. \quad (6.59)$$

Carrying out the simple integrations yields the following system of equations:

$$\frac{1}{2}\phi_0 + \phi_1 + \frac{5}{8}\phi_2 - \frac{3}{16}\phi_4 + \frac{13}{128}\phi_6 = \frac{1}{2}\phi_\mathtt{b} \quad (6.60a)$$

$$-\frac{1}{8}\phi_0 + \frac{5}{8}\phi_2 + \phi_3 + \frac{81}{128}\phi_4 - \frac{13}{64}\phi_6 = -\frac{1}{8}\phi_\mathtt{b} \quad (6.60b)$$

$$\frac{1}{16}\phi_0 - \frac{25}{128}\phi_2 + \frac{81}{128}\phi_4 + \phi_5 + \frac{325}{512}\phi_6 = \frac{1}{16}\phi_\mathtt{b} \quad (6.60c)$$

$$-\frac{5}{128}\phi_0 + \frac{7}{64}\phi_2 - \frac{105}{512}\phi_4 + \frac{325}{512}\phi_6 + \phi_7 = -\frac{5}{128}\phi_\mathtt{b}\,, \quad (6.60d)$$

where ϕ_b is again an isotropic source prescribed on the planar boundary. For the odd moment in each boundary equation, we insert Eq (6.44) to remove them, leaving only the even moments and a set of differential equations:

$$\frac{1}{2}\phi_0 + \frac{1}{3\Sigma_1}\frac{\partial}{\partial x}(\phi_0 + 2\phi_2) + \frac{5}{8}\phi_2 - \frac{3}{16}\phi_4 + \frac{13}{128}\phi_6 = \frac{1}{2}\phi_b \tag{6.61a}$$

$$-\frac{1}{8}\phi_0 + \frac{5}{8}\phi_2 + \frac{1}{7\Sigma_3}\frac{\partial}{\partial x}(3\phi_2 + 4\phi_4) + \frac{81}{128}\phi_4 - \frac{13}{64}\phi_6 = -\frac{1}{8}\phi_b \tag{6.61b}$$

$$\frac{1}{16}\phi_0 - \frac{25}{128}\phi_2 + \frac{81}{128}\phi_4 + \frac{1}{11\Sigma_5}\frac{\partial}{\partial x}(5\phi_4 + 6\phi_6) + \frac{325}{512}\phi_6 = \frac{1}{16}\phi_b \tag{6.61c}$$

$$-\frac{5}{128}\phi_0 + \frac{7}{64}\phi_2 - \frac{105}{512}\phi_4 + \frac{325}{512}\phi_6 + \frac{1}{15\Sigma_7}\frac{\partial}{\partial x}(7\phi_6) = -\frac{5}{128}\phi_b\,. \tag{6.61d}$$

We can again make the substitution of variables given by Eqs (6.48) and (6.49) for consitency with the equations defined on the domain. In addition, we apply the $\mathsf{SP_N}$ approximation to the derivatives by assuming they are instead multidimensional gradients on the boundary such that $\frac{\partial}{\partial x} \to \hat{\mathbf{n}} \cdot \nabla$. Doing this gives:

$$\begin{aligned}\frac{1}{2}\Big(u_1 - \frac{2}{3}u_2 + \frac{8}{15}u_3 - \frac{16}{35}u_4\Big) + \frac{1}{3\Sigma_1}\hat{\mathbf{n}}\cdot\nabla\Big(\Big(u_1 - \frac{2}{3}u_2 + \frac{8}{15}u_3 - \frac{16}{35}u_4\Big) + \\ 2\Big(\frac{1}{3}u_2 - \frac{4}{15}u_3 + \frac{8}{35}u_4\Big)\Big) + \frac{5}{8}\Big(\frac{1}{3}u_2 - \frac{4}{15}u_3 + \frac{8}{35}u_4\Big) - \\ \frac{3}{16}\Big(\frac{1}{5}u_3 - \frac{6}{35}u_4\Big) + \frac{13}{128}\Big(\frac{1}{7}u_4\Big) = \frac{1}{2}\phi_b\,,\end{aligned} \tag{6.62}$$

$$\begin{aligned}-\frac{1}{8}\Big(u_1 - \frac{2}{3}u_2 + \frac{8}{15}u_3 - \frac{16}{35}u_4\Big) + \frac{5}{8}\Big(\frac{1}{3}u_2 - \frac{4}{15}u_3 + \frac{8}{35}u_4\Big) + \\ \frac{1}{7\Sigma_3}\hat{\mathbf{n}}\cdot\nabla\Big(3\Big(\frac{1}{3}u_2 - \frac{4}{15}u_3 + \frac{8}{35}u_4\Big) + 4\Big(\frac{1}{5}u_3 - \frac{6}{35}u_4\Big)\Big) + \frac{81}{128}\Big(\frac{1}{5}u_3 - \\ \frac{6}{35}u_4\Big) - \frac{13}{64}\Big(\frac{1}{7}u_4\Big) = -\frac{1}{8}\phi_b\,,\end{aligned} \tag{6.63}$$

$$\frac{1}{16}\Big(u_1-\frac{2}{3}u_2+\frac{8}{15}u_3-\frac{16}{35}u_4\Big)-\frac{25}{128}\Big(\frac{1}{3}u_2-\frac{4}{15}u_3+\frac{8}{35}u_4\Big)+\frac{81}{128}\Big(\frac{1}{5}u_3-\frac{6}{35}u_4\Big)+\frac{1}{11\Sigma_5}\hat{\mathbf{n}}\cdot\nabla\Big(5\Big(\frac{1}{5}u_3-\frac{6}{35}u_4\Big)+6\Big(\frac{1}{7}u_4\Big)\Big)+\frac{325}{512}\Big(\frac{1}{7}u_4\Big)=\frac{1}{16}\phi_b\,, \quad (6.64)$$

$$-\frac{5}{128}\Big(u_1-\frac{2}{3}u_2+\frac{8}{15}u_3-\frac{16}{35}u_4\Big)+\frac{7}{64}\Big(\frac{1}{3}u_2-\frac{4}{15}u_3+\frac{8}{35}u_4\Big)-\frac{105}{512}\Big(\frac{1}{5}u_3-\frac{6}{35}u_4\Big)+\frac{325}{512}\Big(\frac{1}{7}u_4\Big)+\frac{1}{15\Sigma_7}\hat{\mathbf{n}}\cdot\nabla\Big(7\Big(\frac{1}{7}u_4\Big)\Big)=-\frac{5}{128}\phi_b\,. \quad (6.65)$$

By rearranging the system such that we have a single gradient operator in each equation, we again have a matrix system:

$$\mathbf{n}\cdot D_n\nabla u_n+\sum_{m=1}^{4}B_{nm}u_m=s_n \qquad n=1,2,3,4\,, \quad (6.66)$$

where $\mathbf{D}$ and $\mathbf{u}$ are defined as before and:

$$\mathbf{s}=\Big(\frac{1}{2}\phi_b\ -\frac{1}{8}\phi_b\ \frac{1}{16}\phi_b\ -\frac{5}{128}\phi_b\Big)^T\,, \quad (6.67)$$

is the source vector on the boundary and

$$\mathbf{B}=\begin{bmatrix}\frac{1}{2} & -\frac{1}{8} & \frac{1}{16} & -\frac{5}{128}\\ -\frac{1}{8} & \frac{7}{24} & -\frac{41}{384} & \frac{1}{16}\\ \frac{1}{16} & -\frac{41}{384} & \frac{407}{1920} & -\frac{233}{2560}\\ -\frac{5}{128} & \frac{1}{16} & -\frac{233}{2560} & \frac{3023}{17920}\end{bmatrix}\,, \quad (6.68)$$

is a dense matrix of coefficients. Again, as pointed out by Evans, the SP_1 approximation reduces this boundary condition to the standard Marshak diffusion boundary condition. For reflecting boundary conditions, we use the same procedure as the P_N equations where the odd-moments are zero such that Eq (6.36) is true. From setting Eq (6.44) to zero for odd ϕ_n and again substituting Eq (6.48) we immediately find that:

$$\nabla \mathbf{u} = 0 \tag{6.69}$$

for reflecting SP_N boundaries, providing enough equations to close the system.

6.4 Derivation of the Multigroup SP_N Equations

Up to this point, we have formulated the P_N and subsequently the SP_N equations for a single neutron energy. To expand these equations for multiple energies, we start by stating the multigroup neutron transport equation for a single dimension in planar geometry:

$$\mu \frac{\partial}{\partial x} \psi^g(x,\mu) + \sigma^g(x)\psi^g(x,\mu) = \sum_{g'=0}^{G} \int \sigma_s^{gg'}(x, \hat{\Omega}' \rightarrow \hat{\Omega}) \psi^{g'}(x, \hat{\Omega}') d\Omega' + \frac{q^g(x)}{4\pi}, \tag{6.70}$$

where g denotes the group index of 0 to G groups, $G = N_g - 1$, and the integration of the scattering emission term of energy has been replaced by a discrete summation. For scattering, $\sigma_s^{gg'}$ provides the probability of scattering at a particular angle from group g to g'. The result is an equation nearly identical in form to Eq (6.2) where now instead of forming the P_N and SP_N equations for a single energy group, we form them for each of the

energy groups with group coupling occuring through the scattering term. The multigroup P_N equations are then:

$$\frac{1}{2n+1}\frac{\partial}{\partial x}\Big[(n+1)\phi^g_{n+1}+n\phi^g_{n-1}\Big]+\sum_{g'}(\sigma^g\delta_{gg'}-\sigma^{gg'}_{sn})\phi^g_n=q\delta_{n0}\,, \quad (6.71)$$

for $n=0,1,\ldots,N$ where the flux and scattering moments are defined in a group. We observe that a $N_g\times N_g$ scattering matrix is formed:

$$\text{"}_n=\sum_{g'}(\sigma^g\delta_{gg'}-\sigma^{gg'}_{sn})\,, \quad (6.72)$$

and when expanded gives:

$$\text{"}_n=\begin{bmatrix}(\sigma^0-\sigma^{00}_{sn}) & -\sigma^{01}_{sn} & \cdots & -\sigma^{0G}_{sn}\\ -\sigma^{10}_{sn} & (\sigma^1-\sigma^{11}_{sn}) & \cdots & -\sigma^{1G}_{sn}\\ \vdots & \vdots & \ddots & \vdots\\ -\sigma^{G0}_{sn} & -\sigma^{G1}_{sn} & \cdots & (\sigma^G-\sigma^{GG}_{sn})\end{bmatrix}. \quad (6.73)$$

It is also useful to combine the group flux moments and sources into a single vector for more compact notation:

$$\mathbf{fl}_n=(\phi^0_n\ \phi^1_n\ \cdots\phi^G_n)^T\,, \quad (6.74)$$

$$\mathbf{q}=(q^0\ q^1\ \cdots q^G)^T\,. \quad (6.75)$$

Next, we apply the SP_N approximation to Eq (6.71) in identical fashion to the monoenergetic case. This gives:

$$-\nabla\cdot\left[\frac{n}{2n+1}\Sigma_{s,n-1}^{-1}\nabla\left(\frac{n-1}{2n-1}\phi_{n-2}+\frac{n}{2n-1}\phi_n\right)\right.$$
$$\left.+\frac{n+1}{2n+1}\Sigma_{s,n+1}^{-1}\nabla\left(\frac{n+1}{2n+3}\phi_n+\frac{n+2}{2n+3}\phi_{n+2}\right)\right]$$
$$+\Sigma_{t,n}\phi_n=q\delta_{n0}\qquad n=0,2,4,\cdots,N\,. \quad (6.76)$$

This adds more complexity than the monoenergetic formulation in that all unknowns in this group of equations are now vector quantities and scattering relationships are contained in matrices rather than a scalar quantity. Because of this, the same sequence of variable changes and algebra can be used to build a set of matrix equations, this time in a block formulation:

$$-\nabla\cdot\mathbb{D}_n\nabla\mathbb{U}_n+\sum_{m=1}^{4}\mathbb{A}_{nm}\mathbb{U}_m=\mathbb{Q}_n\,, \quad (6.77)$$

where the definition of all quantities are the same with internal scalar values replaced by the group-vector values. In addition, $\mathbb{A}$ is now a block matrix of $N_g\times N_g$ submatrices generated from the moment scattering matrices:

$$\mathbf{A}=\begin{bmatrix}
(\Sigma_{s,0}) & (-\frac{2}{3}\Sigma_{s,0}) & (\frac{8}{15}\Sigma_{s,0}) & (-\frac{16}{35}\Sigma_{s,0})\\
(-\frac{2}{3}\Sigma_{s,0}) & (\frac{4}{15}\Sigma_{s,0}+\frac{1}{3}\Sigma_{s,2}) & (-\frac{16}{45}\Sigma_{s,0}-\frac{4}{9}\Sigma_{s,2}) & (\frac{32}{105}\Sigma_{s,0}+\frac{8}{21}\Sigma_{s,2})\\
(\frac{8}{15}\Sigma_{s,0}) & (-\frac{16}{45}\Sigma_{s,0}-\frac{4}{9}\Sigma_{s,2}) & (\frac{64}{225}\Sigma_{s,0}+\frac{16}{45}\Sigma_{s,2}+\frac{9}{25}\Sigma_{s,4}) & (-\frac{128}{525}\Sigma_{s,0}-\frac{32}{105}\Sigma_{s,2}-\frac{54}{175}\Sigma_{s,4})\\
(-\frac{16}{35}\Sigma_{s,0}) & (\frac{32}{105}\Sigma_{s,0}+\frac{8}{21}\Sigma_{s,2}) & (-\frac{128}{525}\Sigma_{s,0}-\frac{32}{105}\Sigma_{s,2}-\frac{54}{175}\Sigma_{s,4}) & (\frac{256}{1225}\Sigma_{s,0}+\frac{64}{245}\Sigma_{s,2}+\frac{324}{1225}\Sigma_{s,4}+\frac{13}{49}\Sigma_{s,6})
\end{bmatrix}. \quad (6.78)$$

Analogously, for Marshak conditions on the boundaries we have:

$$\hat{\mathbf{n}} \cdot \mathbb{D}_n \nabla \mathbb{U}_n + \sum_{m=1}^{4} \mathbb{B}_{nm} \mathbb{U}_m = \mathbb{S}_n \, , \tag{6.79}$$

with $\mathbb{S}_n$ the vector of group-wise boundary source term on each boundary for each psuedo-moment and $\mathbb{B}_{nm}$ is an $\mathsf{N_g} \times \mathsf{N_g}$ diagonal matrix with the value B_{nm} on the diagonal. For reflecting conditions, again we have $\nabla \mathbb{U}_n = 0$ for all pseudo-moments.

6.5 A Note on Spatial Discretization and Matrix Symmetry

To this point, the formulation of the multigroup $\mathsf{SP_N}$ equations presented have discretized the transport equation in angle and energy but have yet to consider the spatial component of phase space. We don't explicitly consider it in this document but instead we will briefly comment on possible means of discretization. Of primary interest here is the discretization of the diffusive term in Eq (6.77) and the convective term on the boundaries in Eq (6.79). Many popular choices for spatial discretization are available here and include finite difference and finite element formulations. In the Denovo package at ORNL, Evans has implemented a finite volume scheme for these equations. Although arbitrary grids could be handled effectively through a finite element scheme, the rectilinear grid used in Denovo is easily discretized through the finite volume method in a conservative form. This conservative form is ideal for the diffusion-like equations in the domain given by Eq (6.77) and the effective boundary current conditions given by Eq (6.79) as the neutron current is balanced from cell-to-cell, continuity of the flux is preserved across cell/material boundaries, and boundary conditions are naturally represented through cell-face currents. Furthermore, this spatial discretization is a

natural extension of the balance principles used to arrive at the general transport equation. The result of this finite volume discretization is one that is symmetric for all equations in the domain with respect to the spatial components of the solution.

Given the symmetry of the spatial discretization equations in the domain given by monoenergetic Eq (6.51) form a symmetric linear operator acting on the pseudo-moment vector to give:

$$\mathbf{Lu} = \mathbf{Q}\,, \tag{6.80}$$

where $\mathbf{L} = -\nabla \cdot \mathbf{D}\nabla + \mathbf{A}$. Moving to the multigroup formulation in Eq (6.77) we have:

$$\mathbb{L}\mathbb{U} = \mathbb{Q}\,, \tag{6.81}$$

where $\mathbb{L} = -\nabla \cdot \mathbb{D}\nabla + \mathbb{A}$. Whether or not the resulting matrix is symmetric is determined by the group scattering matrices, $\sigma_{sn}^{gg'}$, for each of the moments. In general, the cross sections in these matrices do not form a symmetric matrix and therefore the resulting linear operator in Eq (6.81) will always be asymmetric for multigroup problems. Solutions to this linear system will then require techniques specifically formulated for asymmetric systems.

Chapter 7

Monte Carlo Solution Methods for the Simplified P_N Equations

In this chapter we apply a preconditioned MCSA method as a solution scheme for the SP_N equations.

7.1 Spectral Analysis of the SP_N Equations

Now that we have an understanding of the linear system generated by the SP_N approximation to the neutron transport equation and the various parameters in the system that may be adjusted, we can consider various means of solution. As the solution is asymmetric, modern iterative solvers should be considered for this task. The performance of Krylov subspace methods are bound to various properties of the eigenvalue spectrum of the linear operator while methods based on stationary iterations have performance limits imposed by the spectral radius of the sytem. In this section we will review the important spectral properties to study for common iterative methods for asymmetric systems. Based on these properties, we will then perform a parameter-based spectral analysis for the linear operator generated by the multigroup SP_N equations. Preconditioning strategies for these methods are not considered. Krylov subspace method restarts and truncation will also not be considered.

Stationary Methods for Linear Systems

Stationary methods for linear systems arise from splitting the operator in Eq (6.81) LeVeque (2007):

$$\mathbb{L} = \mathbf{M} - \mathbf{N}\,, \tag{7.1}$$

where the choice of $\mathbf{M}$ and $\mathbf{N}$ will be dictated by the particular method chosen. Using this split definition of the operator we can then write:

$$\mathbf{M}\mathbb{U} - \mathbf{N}\mathbb{U} = \mathbb{Q}\,. \tag{7.2}$$

By rearranging, we can generate a form more useful for analysis:

$$\mathbb{U} = \mathbf{H}\mathbb{U} + \mathbf{c}\,, \tag{7.3}$$

where $\mathbf{H} = \mathbf{M}^{-1}\mathbf{N}$ is defined as the *iteration matrix* and $\mathbf{c} = \mathbf{M}^{-1}\mathbb{Q}$. With the solution vector on both the left and right hand sides, an iterative method can then be formed:

$$\mathbb{U}^{\mathsf{k}+1} = \mathbf{H}\mathbb{U}^{\mathsf{k}} + \mathbf{c}\,, \tag{7.4}$$

with $\mathsf{k} \in \mathbf{Z}^+$ defined as the *iteration index*. Defining $\mathbf{e}^{\mathsf{k}} = \mathbf{u}^{\mathsf{k}} - \mathbf{u}$ as the solution error at the k^{th} iterate, we can subtract Eq (7.3) from Eq (7.4):

$$\mathbf{e}^{\mathsf{k}+1} = \mathbf{H}\mathbf{e}^{\mathsf{k}}\,. \tag{7.5}$$

Our error after k iterations is then:

$$\mathbf{e}^{\mathsf{k}} = \mathbf{H}^{\mathsf{k}}\mathbf{e}^{0}\,. \tag{7.6}$$

In other words, successive application of the iteration matrix is the mechanism driving down the error in a stationary method. By assuming $\mathbf{H}$ is

diagonalizable Saad (2003), we then have:

$$\mathbf{e}^k = \mathbf{R}\boldsymbol{\Lambda}^k\mathbf{R}^{-1}\mathbf{e}^0 \,, \tag{7.7}$$

where $\boldsymbol{\Lambda}$ contains the Eigenvalues of $\mathbf{H}$ on its diagonal and the columns of $\mathbf{R}$ contain the Eigenvectors of $\mathbf{H}$. Computing the 2-norm of the above form then gives:

$$||\mathbf{e}^k||_2 \leqslant ||\boldsymbol{\Lambda}^k||_2 \, ||\mathbf{R}||_2 \, ||\mathbf{R}^{-1}||_2 \, ||\mathbf{e}^0||_2 \,, \tag{7.8}$$

which gives:

$$||\mathbf{e}^k||_2 \leqslant \rho(\mathbf{H})^k \kappa(\mathbf{R}) ||\mathbf{e}^0||_2 \,. \tag{7.9}$$

For iteration matrices where the Eigenvectors are orthogonal, $\kappa(\mathbf{R}) = 1$ and the error bound reduces to:

$$||\mathbf{e}^k||_2 \leqslant \rho(\mathbf{H})^k ||\mathbf{e}^0||_2 \,. \tag{7.10}$$

We can now restrict $\mathbf{H}$ by asserting that $\rho(\mathbf{H}) < 1$ for a stationary method to converge such that k applications of the iteration matrix will not cause the error to grow in Eq (7.10). In addition, the performance of the stationary method is dictated by $\rho(\mathbf{H})$ such that performance of the method decreases as it approaches to unity.

Krylov Subspace Methods for Linear Systems

The performance of different Krylov subspace solvers can depend on different properties of the linear system. As a means to study these differences, we use a 1992 paper by Nachtigal and colleagues Nachtigal et al. (1992) that performs and in-depth analysis of three Krylov subspace methods that are still used today in modern physics applications: conjugate gradient iteration for the normal equations (CGN), generalized minimum residual iteration (GMRES), and a biconjugate gradient-based method (CGS). For our work, we will consider only their analysis of GMRES as it currently leveraged in

Denovo for $\mathsf{SP_N}$ solutions and as it also applies to CGS for most matrices.

For GMRES, at each iteration we are extracting a correction for the solution from the Krylov subspace:

$$\mathbb{U}^{\mathsf{k}} \in \mathbb{U}^0 + \langle \mathbf{r_0}, \mathbb{L}\mathbf{r_0}, \cdots, \mathbb{L}^{\mathsf{k}-1}\mathbf{r_0} \rangle \,, \tag{7.11}$$

where the extraction is constrained by ensuring orthogonality of the new residual with the Krylov space:

$$\mathbf{r}^{\mathsf{k}} \perp \langle \mathbb{L}\mathbf{r_0}, \mathbb{L}^2\mathbf{r_0}, \cdots, \mathbb{L}^{\mathsf{k}}\mathbf{r_0} \rangle \,, \tag{7.12}$$

with the residual at the k^{th} iteration defined as:

$$\mathbf{r}^{\mathsf{k}} = \mathbb{Q} - \mathbb{L}\mathbb{U}^{\mathsf{k}} \,. \tag{7.13}$$

From Nachtigal et al. (1992), we then have the following error at each iteration:

$$\mathbf{e}^{\mathsf{k}} = \mathsf{p}_{\mathsf{k}}(\mathbb{L})\mathbf{e}^0 \,, \tag{7.14}$$

where $\mathsf{p}_{\mathsf{k}}(\mathbb{L})$ is an arbitrary k^{th} degree polynomial and $\mathsf{p}_{\mathsf{k}}(0) = 1$. This is a very similar form for the iteration error as observed for stationary methods in Eq (7.10) where now as these p_{k} polynomials are constructed as the iterations progress, a rapid decrease in $\|\mathsf{p}_{\mathsf{k}}(\mathbb{L})\|$ means a rapid rate of convergence. For matrices $\mathbb{L}$ that are approximately normal (which was exactly the assumption we made to arrive at Eq (7.10)), then we can write the polynomial norm as:

$$\|\mathsf{p}_{\mathsf{k}}(\mathbb{L})\| = \sup_{z \in \Lambda(\mathbb{L})} |\mathsf{p}_{\mathsf{k}}(z)| \,, \tag{7.15}$$

where $\Lambda(\mathbb{L})$ is the eigenvalue spectrum of the normal matrix $\mathbb{L}$. So if we could obtain the polynomials, the largest eigenvalue of $\mathbb{L}$ could be used to calculate convergence rates. Next we consider a choice of polynomials

to use for the convergence rate approximation. They should of course be orthogonal to reflect the orthogonal projection mechanism by which the residual is reduced. In Nachtigal's work, Chebyshev polynomials were used and defined on the interval of Eigenvalues, $[\lambda_{min}, \lambda_{max}]$, and then normalized via the constraint $p_k(0) = 1$. Thus the rate of convergence for these polynomials is an approximation to the rate of convergence of the method.

We can check the validity of the normal approximation by computing the condition number of $\mathbb{L}$:

$$\kappa(\mathbb{L}) = ||\mathbb{L}||\ ||\mathbb{L}^{-1}|| \tag{7.16}$$

The closer $\kappa(\mathbb{L})$ is to one, the more normal the matrix and the better the above approximation. The same check can also be performed to verify the assumption used to generate Eq (7.10) where $\kappa(\mathbf{H})$ can be computed. For our analysis, we will compute κ_2 where the matrix norms are induced by the 2-norm of a vector such that:

$$||\mathbb{L}||_2 = \sqrt{\rho(\mathbb{L}^T\mathbb{L})}\,. \tag{7.17}$$

Organization of the Spectral Analysis

For the spectral analysis we will perform a numerical parameter study for the multigroup $\mathsf{SP_N}$ equations. Based on the above information for iterative methods, several key quantities should be computed for the $\mathsf{SP_N}$ system:

- Eigenvalue spectrum for the linear operator $\mathbb{L}$
- Largest eigenvalue for the linear operator $\mathbb{L}$
- Smallest eigenvalue for the linear operator $\mathbb{L}$
- Condition number for the linear operator $\mathbb{L}$

- For each stationary method:
  - Eigenvalue spectrum for the iteration matrix $\mathbf{H}$
  - Largest eigenvalue for the iteration matrix $\mathbf{H}$
  - Smallest eigenvalue for the iteration matrix $\mathbf{H}$
  - Condition number for the iteration matrix $\mathbf{H}$
- For GMRES:
  - Chebyshev polynomial norm using eigenvalues of $\mathbb{L}$ for a fixed number of iterations determined by stationary method convergence

In addition, the following parameters may be varied in the SP_N system in Denovo:

- SP_N (angular flux expansion) order
- P_N (scattering cross section expansion) order
- Number of energy groups N_g
- Total cross sections σ^g
- Scattering cross section matrix $\sigma_{sn}^{gg'}$
- Boundary conditions (Marshak or reflecting)
- Finite volume mesh size (Δ in all directions)
- Number of mesh elements
- Source of neutrons (Uniform or Point)

We will restrict the problem description in Denovo to one similar to Brantley and Larsen's $\mathsf{SP_N}$ work where the spectral radius was computed for convergence analysis of several proposed solution methods. From this definition we choose a single material problem with a uniform source of unity in all energy groups. For the boundary conditions, we choose reflecting conditions on all six sides of the cubic domain for an effectively homogenous infinite medium problem which we will mesh with a $5 \times 5 \times 5$ grid with $\Delta = 0.1$. We are then left to vary the angular and energy components of the system in our parameter studies: the $\mathsf{SP_N}$ order, the number of energy groups, and their cross sections of order $\mathsf{P_N}$. In Brantley and Larsen's work, a single energy group was used and therefore we may not use their cross sections in our multigroup computations. For our work, we will always choose a total cross section of unity for all groups and all flux moments. For the scattering matrix, two classes will be chosen: one with upscatter and one without. For the downscatter only case, all groups may scatter within the group and to all groups of lower energy (yielding a lower triangular scattering matrix) with a cross section of 0.5. For the upscatter case, all groups may scatter within the group and to all groups of lower energy given a cross section of 0.5 and for upscatter, all groups may scatter up to two groups higher in energy with a cross section of 0.25. All cross section matrices will be equivalent for each scattering moment. For these cross sections, the $\mathsf{P_N}$ order will be varied with $\mathsf{N} = 0, 1, 3$. Both 1 and 10 energy groups will be used with the 10 energy group case using the scattering matrices specified above. For the angular flux, the $\mathsf{SP_N}$ order will be varied with $\mathsf{N} = 1, 3, 5, 7$. This gives a total of 36 linear system variations for the spectral analysis.

Spectral Analysis Results

Preconditioning Strategy

7.2 Fuel Assembly Scaling Results for the SP_N Equations

7.3 Full Core Scaling Results for the SP_N Equations

Chapter 8

Monte Carlo Solution Methods for Nonlinear Systems

Nonlinear equation sets are a common occurrence in multiphysics problems. Systems of partial differential equations such as those that describe fluid flow or more general transport processes when discretized by conventional methods yield discrete sets of stiff equations with nonlinearities present in the variables. Traditionally, such systems have been solved by linearizing them in a form where the nonlinearities in the variables are eliminated and more traditional linear methods can be used for solutions. Often characterized as segregated methods where physics operators are split and their action on the system approximated in steps, such methods lack consistency and accuracy in resolving the nonlinear component of the solution. In the last 30 years, fully consistent nonlinear methods based on Newton's method have become more popular and many advances have been made in the computational physics field to employ these methods.

In the context of solving standalone linear systems, Monte Carlo methods do not provide significant merit over Krylov methods due to the fact that the linear operator must be explicitly formed. For many applications, such a requirement is prohibitive and perhaps not even feasible to implement. Therefore, a Monte Carlo solver is best suited for situations in which not only are Krylov methods applicable, but also in which the operator is readily, if not naturally, formed. Modern nonlinear methods meet both of these requirements with Newton methods used in conjunction with Krylov methods for a robust, fully implicit solution strategy. Furthermore, modern techniques exist that permit the automatic construction of the linear operator generated within a Newton method based on the nonlinear residual

evaluations, providing all of the components necessary for a Monte Carlo solver to provide value. We therefore devise a new nonlinear method based on the MCSA algorithm and Newton's method and discuss its potential benefits.

8.1 Preliminaries

We formulate the *nonlinear problem* as follows (Knoll and Keyes, 2004):

$$\mathbf{F}(\mathbf{u}) = \mathbf{0}\,, \tag{8.1}$$

where $\mathbf{u} \in \mathbb{R}^{\mathsf{n}}$ is the solution vector and $\mathbf{F} : \mathbb{R}^{\mathsf{N}} \to \mathbb{R}^{\mathsf{N}}$ is the function of nonlinear residuals. We write the nonlinear system in this form so that when an exact solution for $\mathbf{u}$ is achieved, all residuals evaluate to zero. *Newton's method* is a root finding algorithm and therefore we can use it to solve Eq (8.1) if we interpret the exact solution $\mathbf{u}$ to be the roots of $\mathbf{F}(\mathbf{u})$. Newton's method is also an iterative scheme, and we can generate this procedure by building the Taylor expansion of the $\mathsf{k}+1$ iterate of the nonlinear residuals about the previous k iterate:

$$\mathbf{F}(\mathbf{u}^{\mathsf{k}+1}) = \mathbf{F}(\mathbf{u}^{\mathsf{k}}) + \mathbf{F}'(\mathbf{u}^{\mathsf{k}})(\mathbf{u}^{\mathsf{k}+1} - \mathbf{u}^{\mathsf{k}}) + \frac{\mathbf{F}''(\mathbf{u}^{\mathsf{k}})}{2}(\mathbf{u}^{\mathsf{k}+1} - \mathbf{u}^{\mathsf{k}})^2 + \cdots\,. \tag{8.2}$$

If we ignore the nonlinear terms in the expansion and assert that at the $\mathsf{k}+1$ iterate $\mathbf{u}^{\mathsf{k}+1}$ is the exact solution such that $\mathbf{F}(\mathbf{u}^{\mathsf{k}+1}) = \mathbf{0}$, then we are left with the following equality:

$$-\mathbf{F}(\mathbf{u}^{\mathsf{k}}) = \mathbf{F}'(\mathbf{u}^{\mathsf{k}})(\mathbf{u}^{\mathsf{k}+1} - \mathbf{u}^{\mathsf{k}})\,. \tag{8.3}$$

We note two things of importance in Eq (8.3). The first is that $\mathbf{F}'(\mathbf{u}^{\mathsf{k}})$ is in fact the *Jacobian*, $\mathbf{J}(\mathbf{u})$, of the set of nonlinear residuals and is defined

element-wise as:

$$J_{ij} = \frac{\partial F_i(\mathbf{u})}{\partial u_j} \,. \tag{8.4}$$

Second, we note that $(\mathbf{u}^{k+1} - \mathbf{u}^k)$ is simply the solution update from the k iterate to the $k+1$ iterate. We will define this update as the *Newton correction* at the k iterate, $\delta\mathbf{u}^k$. To finish, we can then rearrange Eq (8.3) to define the Newton iteration scheme for nonlinear problems:

$$\mathbf{J}(\mathbf{u})\delta\mathbf{u}^k = -\mathbf{F}(\mathbf{u}^k) \tag{8.5a}$$

$$\mathbf{u}^{k+1} = \mathbf{u}^k + \delta\mathbf{u}^k \,. \tag{8.5b}$$

There are then three distinct steps to perform: evaluation of the nonlinear residuals using the solution at the k iterate, the solution of a linear system to compute the Newton correction where the Jacobian matrix of the nonlinear equation set is the linear operator, and the application of the correction to the previous iterate's solution to arrive at the next iterate's solution. In the asymptotic limit, the iterations of Newton's method will converge the nonlinear residual quadratically (Kelley, 1995). Convergence criteria is set for stopping the iteration sequence based on the nonlinear residual. Commonly, the following criteria is used:

$$||\mathbf{F}(\mathbf{u}^k)|| < \epsilon||\mathbf{F}(\mathbf{u}^0)|| \,, \tag{8.6}$$

where ϵ is a user defined tolerance parameter. Newton's method is *consistent* in that all components of the nonlinear functions that describe the physics we are modeling are updated simultaneously in the iteration sequence with respect to one another. This is in comparison to *inconsistent* strategies, such as a pressure correction strategy for solving the Navier-Stokes equations (Pletcher et al., 1997), where the components of $\mathbf{u}$ are updated in a staggered fashion depending on the particular equations that they are associated with.

8.2 Inexact Newton Methods

Inexact Newton methods arise when the Jacobian operator is not exactly inverted, resulting in an inexact Newton correction as initially described by Dembo and others (Dembo et al., 1982). For common sparse nonlinear systems, which in turn yield a sparse Jacobian matrix, this situation occurs when conventional iterative methods are applied. In their definition, Dembo formulated inexact methods such that they are independent of the linear method used to solve for the Newton correction and therefore are amenable to use with any linear solver. Furthermore, they bind the convergence of the outer nonlinear iteration to the inner linear iteration such that:

$$||\mathbf{J}(\mathbf{u}^{\mathsf{k}})\delta\mathbf{u}^{\mathsf{k}} + \mathbf{F}(\mathbf{u}^{\mathsf{k}})|| \leqslant \eta^{\mathsf{k}}||\mathbf{F}(\mathbf{u}^{\mathsf{k}})|| \,, \tag{8.7}$$

where $\eta^{\mathsf{k}} \in [0, 1)$ is defined as the *forcing term* at the k iterate. Eq (8.7) then states that the residual generated by the linear solver is bound by the nonlinear residual and how tightly it is bound is defined by the forcing term. This is useful in that we can vary how tightly coupled the convergence of the linear iterations used to generate the Newton correction is to the nonlinear iteration by relaxing or tightening the convergence properties on the linear iterative method. As a result, strategies for determining the forcing term can vary depending on the problem type and can greatly affect the convergence of the method or even prohibit convergence (Eisenstat and Walker, 1996). In addition, *globalization methods* may be used to modify the Newton correction in a more desire able direction such that convergence properties can be improved when the initial guess for $\mathbf{u}$ is poor (Pawlowski et al., 2006).

Newton-Krylov Methods

A form of inexact Newton methods, *Newton-Krylov methods* are nonlinear iterative methods that leverage a Krylov subspace method as the linear solver for generating the Newton correction (Kelley, 1995). As we investigated in Chapter 2, Krylov methods are robust and enjoy efficient parallel implementations on modern architectures. Furthermore, their lack of explicit dependence on the operator make them easier to implement than other methods. Additionally, although many iterations can become memory intensive due to the need to store the Krylov subspace for the orthogonalization procedure, at each nonlinear iteration this cost is reset as the Jacobian matrix will change due to its dependence on the solution vector. This means that for every nonlinear iteration, a completely new linear system is formed for generating the Newton correction and we can modify the Krylov solver parameters accordingly to accommodate this. In most nonlinear problems, the Jacobian operator is generally non-symmetric and therefore either Krylov methods with long recurrence relations that can handle non-symmetric systems must be considered or the Newton correction system must be preconditioned such that the operator is symmetric and short recurrence relation methods can be potentially be used.

With many Krylov methods available, which to use with the Newton method is dependent on many factors including convergence rates and memory usage. Several studies have been performed to investigate this (McHugh and Knoll, 1993; Knoll and McHugh, 1995). In their numerical studies in 1995, Knoll and McHugh used the set of highly nonlinear and stiff convection-diffusion-reaction equations to solve a set of tokamak plasma problems with the goal of measuring solver performance with Newton's method. They note several trade offs in using Krylov methods with the Newton solver. The first is that the optimization condition that results from the constraints (e.g. the minimization of the GMRES residual over the Krylov space) can be relaxed by restricting the size of the subspace such that

only a fixed number of subspace vectors may be maintained, thus reducing memory requirements. We can also relax the optimization condition by instead restarting the recurrence relation with a new set of vectors once a certain number of vectors have been generated. The optimization condition is maintained over that particular set of vectors, however, Knoll and McHugh note that this ultimately slows the convergence rate as compared to keeping all vectors as the new set of vectors is not necessarily orthogonal to the previous set, and therefore not optimal over the entire iteration procedure. The orthogonality condition can be relaxed by using a recurrence relation that does not generate a strictly orthonormal basis for the Krylov subspace such as the Lanzcos biorthogonalization procedure, resulting in memory savings due to the shorter Lanzcos recurrence relation.

As a comparison, Knoll and McHugh chose an Arnoldi-based GMRES with a fixed vector basis approximately the size of the number of iterations required to converge as the long recurrence relation solver and conjugate gradients squared (CGS), bi-orthogonalized conjugate gradient stabilized (Bi-CGSTAB), and transpose-free quasiminimal residual (TFQMR) methods as Lanzcos-based short recurrence relation solvers. All solvers were used to compute the right-preconditioned Newton correction system. For standard implementations of Newton's method where the Jacobian operator was explicitly formed using difference equations, all methods exhibited roughly equivalent iteration count performance for both the inner linear iterations and the outer nonlinear iterations in terms of iterations required to converge. Bi-CGSTAB typically performed the best for implementations where the Jacobian was explicitly formed and GMRES performing best for matrix-free implementations. However, upon investigating the convergence of the inner iterations, it was observed that the GMRES solver was significantly more robust, always generating a monotonically decreasing residual as compared to the Lanzcos-based methods which had the tendency to oscillate. Based on these results, in all of their future work Knoll and McHugh tended to

use GMRES as the Krylov solver (Knoll and Keyes, 2004).

Jacobian-Free Approximation

In most cases, the Jacobian is difficult to form from the difference equations and costly to evaluate for large equation sets. For simple nonlinear cases such as the Navier-Stokes equations, the derivatives can be computed and coded, but due to the complexity of those derivatives and the resulting difference equations this task can be tedious, error prone, and must be repeated for every equation set. Furthermore, in their 1995 work, Knoll and McHugh also noted that a dominating part of their computation time was the evaluation of the difference equations for building the Jacobian (Knoll and McHugh, 1995). By recognizing that Krylov methods only need the action of the operator on the vector instead of the operator itself, the Jacobian can instead be approximated through various numerical methods including a difference-based Jacobian-free formulation.

Jacobian-Free methods, and in particular *Jacobian-Free Newton-Krylov* (JFNK) methods (Knoll and Keyes, 2004), rely on forming the action of the Jacobian on a vector as required by the Krylov solver through a forward difference scheme. In this case, the action of the Jacobian on some vector $\mathbf{v}$ is given as:

$$\mathbf{J}(\mathbf{u})\mathbf{v} = \frac{\mathbf{F}(\mathbf{u} + \epsilon\mathbf{v}) - \mathbf{F}(\mathbf{u})}{\epsilon}\,, \tag{8.8}$$

where ϵ is a small number typically on the order of machine precision. Kelley (Kelley, 1995) points out a potential downfall of this formulation in that if the discretization error in $\mathbf{F}(\mathbf{u})$ is on the order of the perturbation parameter ϵ, then the finite difference error from Eq (8.8) pollutes the solution. In addition, Knoll and McHugh noted that for preconditioning purposes, part of the Jacobian must still explicitly be formed periodically and that linear solver robustness issues were magnified by the matrix-free approach due to the first-order approximation. This formation frequency coupled with

the numerous evaluations of the Jacobian approximation create a situation where after so many nonlinear iterations, it becomes cheaper to instead fully form the Jacobian. For simple equation sets, this may only take 5-10 Newton iterations to reach this point while over 30 may be required for larger equations sets and therefore larger Jacobians.

Automatic Differentiation for Jacobian Generation

If it is acceptable to store the actual Jacobian matrix, other methods are available to construct it without requiring hand-coding and evaluating derivatives, thus eliminating the associated issues. In addition, if any additional equations are added to the system or a higher order functional approximation is desired, it would be useful to avoid regenerating and coding these derivatives. Becoming more prominent in the 1990's, *automatic differentiation* is a mechanism by which the derivatives of a function can be generated automatically by evaluating it. Automatic differentiation is built on the concept that all functions discretely represented in a computer are ultimately represented by elementary mathematical operations. If the chain rule is applied to those elementary operations, then the derivatives of those functions can be computed to the order of accuracy of their original discretization in a completely automated way (Averick et al., 1994).

The work of Bartlett and others (Bartlett et al., 2006) extended initial Fortran-based work in the area of automatic differentiation implementations to leverage the parametric type and operator overloading features of C++ (Stroustrup, 1997). They formulate the differentiation problem from an element viewpoint by assuming that a global Jacobian can be assembled from local element function evaluations of $e_k : \mathbb{R}^{n_k} \to \mathbb{R}^{m_k}$, similar to the finite element assembly procedure as:

$$\mathbf{J}(\mathbf{u}) = \sum_{i=1}^{N} \mathbf{Q}_i^T \mathbf{J}_k \mathbf{P}_i \,, \tag{8.9}$$

where $\mathbf{J}_{k_i} = \partial e_{k_i} / \partial P_i u$ is the k^{th} element function Jacobian, $\mathbf{Q} \in \mathbb{R}^{n_{k_i} \times N}$ is a projector onto the element domain and $\mathbf{P} \in \mathbb{R}^{m_{k_i} \times N}$ a projector onto the element range for $\mathbf{F}(\mathbf{u}) \in \mathbb{R}^{N \times N}$. The Jacobian matrix for each element will therefore have entirely local data in a dense structure, eliminating the need for parallel communication and sparse techniques during differentiation. Only when all local differentials are computed does communication of the Jacobian occur through gather/scatter operations in order to properly assembly it. Also of benefit is the fact that element-level computations generally consist of a smaller number of degrees of freedom, thus reducing memory requirements during evaluation as compared to a global formulation of the problem. Such a formulation is not limited to finite element formulations and is amenable to any scheme where the system is globally sparse with degrees of freedom coupled to local domains including finite volume representations. The templating capabilities of C++ were leveraged with the element-based evaluation and assembly scheme as in Eq (8.9) by templating element function evaluation code on the evaluation type. If these functions are instantiated with standard floating point types then the residual is returned. If they are instead instantiated with the operator-overloaded automatic differentiation types, both the residual and Jacobian are returned.

Of interest to Bartlett, Averick, and the many others that have researched automatic differentiation are measures of its performance relative to hand-coded derivatives and capturing the Jacobian matrix from matrix-free approximations. Given their element-based function evaluation scheme, Bartlett's work varied the number of degrees of freedom per element and compared both the floating point operation count and CPU time for both the templated automatic differentiation method and hand-coded derivatives for Jacobian evaluations. Although they observed a 50% increase in floating point operations in the templated method over the hand-coded method, run times were observed to be over 3 times faster for the templated method. They hypothesize that this is due to the fact that the element-based for-

mulation of the templated method is causing better utilization of cache and therefore faster data access. Furthermore, they observed linear scaling behavior for automatic differentiation as the number of degrees of freedom per element were increased up to a few hundred. Based on these results, this type of automatic differentiation formulation was deemed acceptable for use in large-scale, production physics codes.

8.3 The FANM Method

In production physics codes based on nonlinear equations sets, Newton-Krylov methods are the primary means of generating a fully consistent solution scheme (Evans et al., 2006, 2007; Gaston et al., 2009; Godoy and Liu, 2012). Typically, for large scale simulations these problems are memory limited due to the subspaces generated by robust Krylov methods. Often, a matrix-free approach is chosen to relax memory requirements over directly generating the Jacobian matrix and facilitate the implementation. However, as we observed in previous sections, these matrix-free methods suffer from poorly scaled problems and the first order error introduced by the Jacobian approximation. In addition, it was observed that the savings induced by the matrix-free approach is eventually amortized over a number of nonlinear iterations where it becomes more efficient computationally to instead form the Jacobian.

In Chapter 3, we focused our efforts on developing and improving Monte Carlo methods for inverting linear systems. These methods, when used to accelerate a stationary method in MCSA, enjoy a robust implementation and exponential convergence rates. Further, the only storage required is that of the full linear system including the linear operator so that we may generate transition probabilities for the random walk sequence. Although this requires more storage to represent the linear system than that of a Krylov method where the operator is not required, we do not incur any

additional storage costs once the iteration sequence begins. In the context of nonlinear problems, the Jacobian matrix that we are required to generate for the Monte Carlo solvers may be generated at will from the nonlinear functions in the Newton system using automatic differentiation. Not only do we then have a simple and automated way to generate the Jacobian, but we also enjoy a Jacobian of numerical precision equivalent to that of our function evaluations. We therefore propose the *Forward-Automated Newton-MCSA* (FANM) method that utilizes all of the above components. We hypothesize that such a method will be competitive with Newton-Krylov methods not only from a convergence and timing perspective, but also relax scaling requirements of matrix-free methods and memory costs of both matrix-free and fully formed Jacobian methods to allow the application developer to solve problems of finer discretization and higher-order functional representations while maintaining a robust and efficient parallel implementation.

Jacobian Storage vs. Subspace Storage and Restarts

To gauge the memory benefits of a FANM method over a Krylov-based scheme, we must look at the storage requirements of the Jacobian matrix as compared to the Krylov subspace vectors for sparse linear problems. Saad's text provides us relations for both of these cases (Saad, 2003). Beginning with the Jacobian storage, for sparse problems production linear algebra library implementations utilize *compressed row storage* to efficiently store the non-zero components of a sparse matrix while still allowing for all standard parallel matrix computations to be performed. Per § 2.4, recall that efficient parallel matrix-vector multiplications rely on processors knowing which other processors contain their neighboring matrix and vector elements. Typically this information is represented by a graph which must be stored along with the matrix elements themselves. To store the elements, consider the

following sparse matrix:

$$\mathbf{A} = \begin{bmatrix} 2 & 0 & 8 & 0 & 0 & 0 \\ 4 & 5 & 0 & 1 & 0 & 0 \\ 0 & 2 & 1 & 0 & 1 & 0 \\ 0 & 0 & 3 & 7 & 0 & 2 \\ 0 & 0 & 0 & 4 & 9 & 0 \\ 0 & 0 & 0 & 0 & 9 & 1 \end{bmatrix}.$$

The compressed form of $\mathbf{A}$ would then be:

$\mathbf{A}$ *values* :	2	8	4	5	1	2	1	1	3	7	2	4	9	9	1
column :	1	3	1	2	4	2	3	5	3	4	6	4	5	5	6
row start :	1	3	6	9	12	14	16								

where the first row contains the non-zero values of the matrix $\mathbf{A}$ starts at, the second row contains the column index of those values, and the third row contains the index of the A value and column index rows that each matrix row starts at ending with the start of the next row. For this simple example, we actually break even by storing 36 elements in the full matrix and 36 pieces of data in the compressed format. However, for large, sparse matrices there is a significant storage savings using the compressed format.

In his discussion on orthogonalization schemes for Krylov subspaces, Saad provides us with space and time complexities for these operations. To find a solution vector $\mathbf{x} \in \mathbb{R}^{\mathsf{N}\times\mathsf{N}}$ with $\mathfrak{m}$ Krylov iterations (and therefore $\mathfrak{m}+1$ subspace vectors) the storage requirement is then $(\mathfrak{m}+1)\mathsf{N}$ for most common orthogonalization techniques. Using our simple example above (even though we did not see any gains in storage over the full matrix representation), if it takes 10 GMRES iterations using Arnoldi orthogonalization to converge to a solution, then a total of 66 pieces of data are required to be stored instead of 36 for the explicitly formed matrix case (we do not consider graph storage here for comparison as both methods will require the graph for

parallel operations). For larger sparse matrices, this disparity in memory requirements will be even greater, especially for ill-conditioned systems that require many GMRES iterations to converge.

Parallel FANM Implementation

Like the parallelization of the MCSA method described in § **??**, a parallel FANM method relies on a basic set of parallel matrix-vector operations as well as the global residual and Jacobian assembly procedure described in § 8.2. Consider the Newton iteration scheme in Eq (8.5). We must first assemble the linear system in parallel through the element-wise function evaluations to generate both the global Jacobian operator and the global residual vector on the right hand side. Per Bartlett's work, efficient and automated parallel mechanisms are available to do this through a sequence of scatter/gather operations. With these tools available for residual and Jacobian generation, the remainder of the parallel procedure is simple, with the linear Newton correction system solved using the parallel MCSA method as previously described and the Newton correction applied to the previous iterate's solution through a parallel vector update operation.

As Newton methods are formulated independent of the inner linear solver generating the Newton corrections, the actual performance of the nonlinear iterations using MCSA is expected to be similar to that of traditional Newton-Krylov methods. Furthermore, we expect to achieve numerically identical answers with a Newton-MCSA method as other Newton methods and we should indeed verify this. The parallel performance of such a method will inherently be bound to the parallel Monte Carlo implementation of the linear solver as the parallel operations at the nonlinear iteration level are identical to those that you would perform with a Newton-Krylov method. Matrix-free formulations will have different parallel performance than these methods, and therefore we should compare FANM performance to JFNK-based schemes. More important than performance in this situation is

the reduced memory pressure that a FANM implementation provides, as discussed in § 8.3, because a FANM method will not generate a subspace in the linear solver and compressed storage for sparse matrices are utilized, we expect significant memory savings over Newton-Krylov methods. We must measure the memory utilization of both of these methods in order to quantify their differences and provide additional analysis of the FANM method's merits, or lack thereof.

Chapter 9

Monte Carlo Solution Methods for the Navier-Stokes Equations

FANM Verification

To verify the FANM method for nonlinear problems, we choose benchmark solutions for the 2-dimensional, steady, incompressible Navier-Stokes equations on a rectilinear grid in much the same way as Shadid and Pawlowski's work on Newton-Krylov methods for the solution of these equations (Shadid et al., 1997; Pawlowski et al., 2006). We define these equations as follows:

$$\rho\mathbf{u}\cdot\nabla\mathbf{u} - \nabla\cdot\mathbf{T} - \rho\mathbf{g} = \mathbf{0} \tag{9.1a}$$

$$\nabla\cdot\mathbf{u} = 0 \tag{9.1b}$$

$$\rho C_p\mathbf{u}\cdot\nabla T + \nabla\cdot\mathbf{q} = 0\,, \tag{9.1c}$$

where ρ is the fluid density, $\mathbf{u}$ is the fluid velocity, $\mathbf{g}$ gravity, C_p the specific heat capacity at constant pressure of the fluid and T the temperature of the fluid. Eq (9.1a) provides momentum transport, Eq (9.1b) provides the mass balance, and Eq (9.1c) provides energy transport with viscous dissipation effects neglected. In addition, we close the system with the following equations:

$$\mathbf{T} = -P\mathbf{I} + \mu[\nabla\mathbf{u} + \nabla\mathbf{u}^T] \tag{9.2a}$$

$$\mathbf{q} = -k\nabla T\,, \tag{9.2b}$$

where $\mathbf{T}$ is the stress tensor, P is the hydrodynamic pressure, μ is the dynamic viscosity of the fluid, $\mathbf{q}$ is the heat flux in the fluid, and k is the

thermal conductivity of the fluid. This set of strongly coupled equations possesses both the nonlinearities and asymmetries that we are seeking for qualification of the FANM method. Further, physical parameters within these equations can be tuned to enhance the nonlinearities. We will then apply these equations to the following three standard benchmark problems.

Thermal Convection Cavity Problem

In 1983 a benchmark solution for the natural convection of air in a square cavity was published (De Vahl Davis, 1983) as shown in Figure 9.1 for the solution of the energy, mass, and momentum equations. In this problem, a rectilinear grid is applied to the unit square. No heat flow is allowed out of the top and bottom of the square with a zero Neumann condition specified. Buoyancy driven flow is generated by the temperature gradient from the cold and hot Dirichlet conditions on the left and right boundaries of the box. By adjusting the Rayleigh number of the fluid (and therefore adjusting the ratio of convective to conductive heat transfer), we can adjust the influence of the nonlinear convection term in Eq (9.1a). In Shadid's work, Rayleigh numbers of up to 1×10^6 were used for this benchmark on a 100×100 square mesh grid.

Lid Driven Cavity Problem

As an extension of the convection problem, the second benchmark problem given by Ghia (Ghia et al., 1982) adds a driver for the flow to introduce higher Reynolds numbers into the system, providing more inertial force to overcome the viscous forces in the fluid. The setup for this problem is equally simple, containing only the Dirichlet conditions as given in Figure 9.2 and is only applied to the mass and momentum equations on the unit square. The top boundary condition will provide a driver for the flow and its variation will in turn vary the Reynolds number of the fluid. An increased velocity will generate more inertial forces in the fluid, which will overcome the viscous

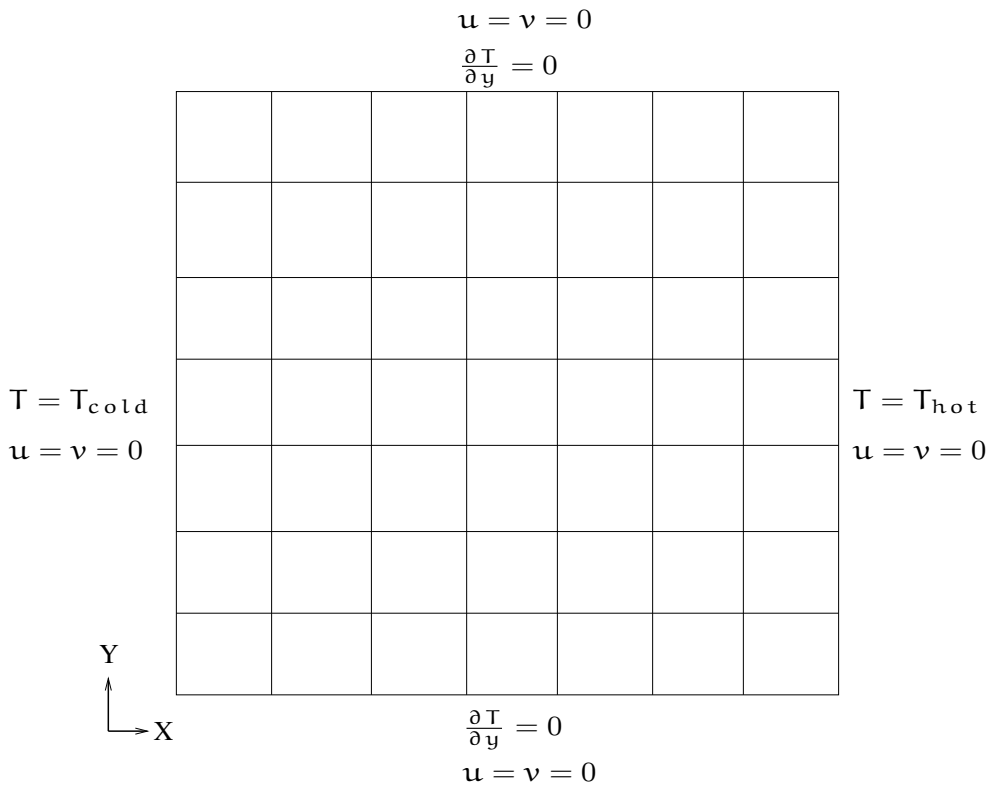

Figure 9.1: **Problem setup for the natural convection cavity benchmark.** *Dirichlet conditions are set for the temperature on the left and right while Neumann conditions are set on the top and bottom of the Cartesian grid. The temperature gradients will cause buoyancy-driven flow. Zero velocity Dirichlet conditions are set on each boundary. No thermal source was present.*

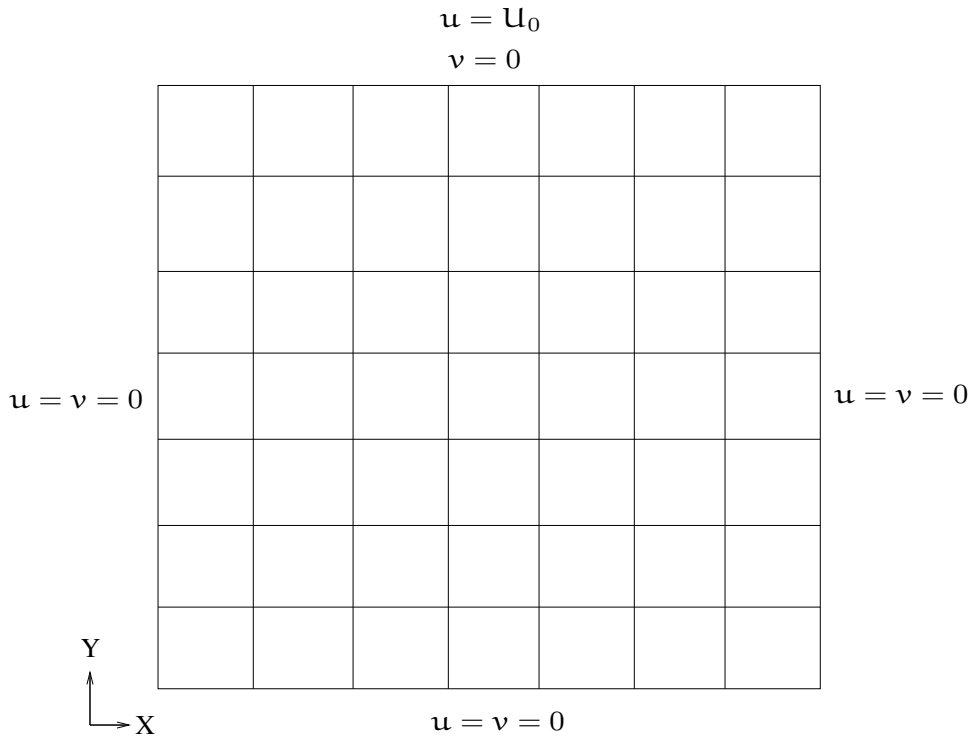

Figure 9.2: **Problem setup for the lid driven cavity benchmark.** *Dirichlet conditions of zero are set for the velocity on the left and right and bottom while the Dirichlet condition set on the top provides a driving force on the fluid.*

forces and again increase the influence of the nonlinear terms in Eq (9.1a). Shadid also used a 100×100 grid for this benchmark problem with Reynolds numbers up to 1×10^4.

Backward-Facing Step Problem

The third benchmark was generated by Gartling in 1990 and consists of both flow over a backward step and an outflow boundary condition (Gartling, 1990). Using the mass and momentum equations while neglecting the energy equation, this problem utilizes a longer domain with a 1/30 aspect ratio

with the boundary conditions as shown in Figure 9.3. In this problem, the

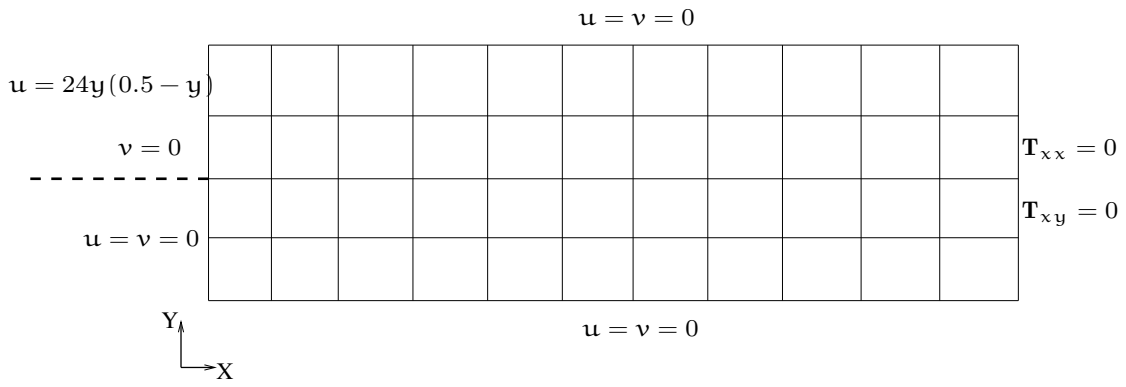

Figure 9.3: **Problem setup for the backward facing step benchmark.** *Zero velocity boundary conditions are applied at the top and bottom of the domain while the outflow boundary condition on the right boundary is represented by zero stress tensor components in the direction of the flow. For the inlet conditions, the left boundary is split such that the top half has a fully formed parabolic flow profile and the bottom half has a zero velocity condition, simulating flow over a step.*

inflow condition is specified by a fully-formed parabolic flow profile over a zero velocity boundary representing a step. The flow over this step will generate a recirculating backflow under the inlet flow towards the step. As in the lid driven cavity problem, the nonlinear behavior of this benchmark and the difficulty in obtaining a solution is dictated by the Reynolds number of the fluid. In Shadid's work, a 20×400 non-square rectilinear grid was used to discretize the domain with Reynolds number up to 5×10^2.

Chapter 10

Conclusions and Analysis

Put conclusions here.

references

Averick, Brett M., Jorge J. More, Christian H. Bischof, Alan Carle, and Andreas Griewank. 1994. Computing large sparse jacobian matrices using automatic differentiation. *SIAM Journal on Scientific Computing* 15(2): 285–294.

Baker, C. G., U. L. Hetmaniuk, R. B. Lehoucq, and H. K. Thornquist. 2009. Anasazi software for the numerical solution of large-scale eigenvalue problems. *ACM Trans. Math. Softw.* 36(3):1–23.

Bartlett, Roscoe A., David M. Gay, and Eric T. Phipps. 2006. Automatic differentiation of c++ codes for large-scale scientific computing. In *Computational science - ICCS 2006*, vol. 3994, 525–532. Berlin, Heidelberg: Springer Berlin Heidelberg.

Brunner, Thomas A., and Patrick S. Brantley. 2009. An efficient, robust, domain-decomposition algorithm for particle monte carlo. *Journal of Computational Physics* 228(10):3882–3890.

Brunner, Thomas A., Todd J. Urbatsch, Thomas M. Evans, and Nicholas A. Gentile. 2006. Comparison of four parallel algorithms for domain decomposed implicit monte carlo. *Journal of Computational Physics* 212(2): 527–539.

Cai, Xiao-Chuan, and David E. Keyes. 2002. Nonlinearly preconditioned inexact newton algorithms. *SIAM Journal on Scientific Computing* 24(1): 183–200.

Danilov, D.L., S.M. Ermakov, and J.H. Halton. 2000. Asymptotic complexity of monte carlo methods for solving linear systems. *Journal of Statistical Planning and Inference* 85(1-2):5–18.

De Vahl Davis, G. 1983. Natural convection of air in a square cavity: A bench mark numerical solution. *International Journal for Numerical Methods in Fluids* 3(3):249–264.

Dembo, Ron S., Stanley C. Eisenstat, and Trond Steihaug. 1982. Inexact newton methods. *SIAM Journal on Numerical Analysis* 19(2):400–408.

Devine, K., E. Boman, R. Heaphy, B. Hendrickson, and C. Vaughan. 2002. Zoltan data management services for parallel dynamic applications. *Computing in Science Engineering* 4(2):90 –96.

Dimov, I.T., T.T. Dimov, and T.V. Gurov. 1998. A new iterative monte carlo approach for inverse matrix problem. *Journal of Computational and Applied Mathematics* 92(1):15–35.

Eisenstat, Stanley C., and Homer F. Walker. 1996. Choosing the forcing terms in an inexact newton method. *SIAM Journal on Scientific Computing* 17(1):16–32.

Evans, Katherine J., D.A. Knoll, and Michael Pernice. 2006. Development of a 2-d algorithm to simulate convection and phase transition efficiently. *Journal of Computational Physics* 219(1):404–417.

———. 2007. Enhanced algorithm efficiency for phase change convection using a multigrid preconditioner with a SIMPLE smoother. *Journal of Computational Physics* 223(1):121–126.

Evans, Thomas, and Scott Mosher. 2009. A monte carlo synthetic acceleration method for the non-linear, time-dependent diffusion equation. *American Nuclear Society - International Conference on Mathematics, Computational Methods and Reactor Physics 2009*.

Evans, Thomas, Scott Mosher, and Stuart Slattery. 2012. A monte carlo synthetic-acceleration method for solving the thermal radiation diffusion equation. *Journal of Computational Physics* Submitted.

Evans, Thomas, Alissa Stafford, Rachel Slaybaugh, and Kevin Clarno. 2010. Denovo: A new three-dimensional parallel discrete ordinates code in SCALE. *Nuclear Technology* 171(2):171–200.

Evans, Thomas, Todd Urbatsch, H Lichtenstein, and Morel. 2003. A residual monte carlo method for discrete thermal radiative diffusion. *Journal of Computational Physics* 189(2):539–556.

Forsythe, George E., and Richard A. Leibler. 1950. Matrix inversion by a monte carlo method. *Mathematical Tables and Other Aids to Computation* 4(31):127–129. ArticleType: research-article / Full publication date: Jul., 1950 / Copyright 1950 American Mathematical Society.

Gartling, David K. 1990. A test problem for outflow boundary conditions - flow over a backward-facing step. *International Journal for Numerical Methods in Fluids* 11(7):953 – 967.

Gaston, D, G Hansen, S Kadioglu, D A Knoll, C Newman, H Park, C Permann, and W Taitano. 2009. Parallel multiphysics algorithms and software for computational nuclear engineering. *Journal of Physics: Conference Series* 180:012012.

Gentile, N.A., Malvin Kalos, and Thomas A. Brunner. 2005. Obtaining identical results on varying numbers of processors in domain decomposed particle monte carlo simulations. In *Computational methods in transport*, vol. 48, 423–433. Berlin/Heidelberg: Springer-Verlag.

Ghia, U, K.N Ghia, and C.T Shin. 1982. High-re solutions for incompressible flow using the navier-stokes equations and a multigrid method. *Journal of Computational Physics* 48(3):387–411.

Godoy, William F., and Xu Liu. 2012. Parallel jacobian-free newton krylov solution of the discrete ordinates method with flux limiters for 3D radiative transfer. *Journal of Computational Physics* 231(11):4257–4278.

Gropp, W., and B. Smith. 1993. Scalable, extensible, and portable numerical libraries. In *Scalable parallel libraries conference, 1993., proceedings of the*, 87 –93.

Gropp, William D, Dinesh K Kaushik, David E Keyes, and Barry F Smith. 2001. High-performance parallel implicit CFD. *Parallel computing in aerospace* 27(4):337–362.

Halton, J. H. 1962. Sequential monte carlo. *Mathematical Proceedings of the Cambridge Philosophical Society* 58(01):57–78.

———. 1994. Sequential monte carlo techniques for the the solution of linear systems. *Journal of Scientific Computing* 9:213–257.

Halton, John H. 1970. A retrospective and prospective survey of the monte carlo method. *SIAM Review* 12(1):1–63.

———. 2006. Sequential monte carlo techniques for solving non-linear systems. *Monte Carlo Methods & Applications* 12(2):113–141.

Hammersley, John Michael, and David Christopher Handscomb. 1964. *Monte carlo methods*. Methuen.

Heroux, Michael A., Roscoe A. Bartlett, Vicki E. Howle, Robert J. Hoekstra, Jonathan J. Hu, Tamara G. Kolda, Richard B. Lehoucq, Kevin R. Long, Roger P. Pawlowski, Eric T. Phipps, Andrew G. Salinger, Heidi K. Thornquist, Ray S. Tuminaro, James M. Willenbring, Alan Williams, and Kendall S. Stanley. 2005. An overview of the trilinos project. *ACM Trans. Math. Softw.* 31(3):397–423.

Ji, Hao, and Yaohang Li. 2012. Reusing random walks in monte carlo methods for linear systems. *Procedia Computer Science* 9(0):383–392.

Kelley, C. T. 1995. *Iterative methods for linear and nonlinear equations*. 1st ed. Society for Industrial and Applied Mathematics.

Keyes, D. E. 1999. *How scalable is domain decomposition in practice?*

Keyes, David E., Dinesh K. Kaushik, and Barry F. Smith. 1997. Prospects for CFD on petaflops systems. Tech. Rep.

Knoll, D.A., and D.E. Keyes. 2004. Jacobian-free newton-krylov methods: a survey of approaches and applications. *Journal of Computational Physics* 193(2):357–397.

Knoll, D.A., and P.R. McHugh. 1995. Newton-krylov methods applied to a system of convection-diffusion-reaction equations. *Computer Physics Communications* 88(2-3):141–160.

Kogge, Peter M., and Timothy J. Dysart. 2011. Using the TOP500 to trace and project technology and architecture trends. In *Proceedings of 2011 international conference for high performance computing, networking, storage and analysis*, 28:1–28:11. SC '11, New York, NY, USA: ACM.

LeVeque, Randall. 2007. *Finite difference methods for ordinary and partial differential equations: Steady-state and time-dependent problems*. SIAM, Society for Industrial and Applied Mathematics.

LeVeque, Randall J. 2002. *Finite volume methods for hyperbolic problems*. 1st ed. Cambridge University Press.

Lewis, E. E. 1993. *Computational methods of neutron transport*. Wiley-Interscience.

Li, Yaohang, and Michael Mascagni. 2003. Analysis of large-scale grid-based monte carlo applications. *The International Journal of High Performance Computing Applications* 17(4):369–382.

McHugh, P. R., and D. A. Knoll. 1992. *Fully implicit solutions of the benchmark backward facing step problem using finite element discretization and inexact newton's method*.

McHugh, Paul R., and Dana A. Knoll. 1993. Inexact newton's method solutions to the incompressible navier-stokes and energy equations using standard and matrix-free implementations. In *AIAA 11th computational fluid dynamics conference*, vol. -1, 385–393.

———. 1994. Fully coupled finite volume solutions of the incompressible NavierâŁ“Stokes and energy equations using an inexact newton method. *International Journal for Numerical Methods in Fluids* 19(5):439–455.

Mervin, Brenden, S.W. Mosher, Thomas Evans, John Wagner, and GI Maldonado. 2012. Variance estimation in domain decomposed monte carlo eigenvalue calculations. *PHYSOR 2012 - Advances in Reactor Physics*.

Musser, David R., and Alexander A. Stepanov. 1994. Algorithm-oriented generic libraries. *Software: Practice and Experience* 24(7):623–642.

Nachtigal, Noel M., Satish C. Reddy, and Lloyd N. Trefethen. 1992. How fast are nonsymmetric matrix iterations? *SIAM Journal on Matrix Analysis and Applications* 13(3):778–795.

Notz, P.K., and Pawlowski. 2010. Graph-based software design for managing complexity and enabling concurrency in multiphysics PDE software. *ACM Trans. Math. Softw.* 40:1–24.

Pawlowski, John N. Shadid, Thomas Smith, Eric Cyr, and Paula Weber. 2012. Drekar CFD - a turbulent fluid-flow and conjugate heat transfer code: Theory manual (Version 1.0). Technical Report, Sandia National Laboratories.

Pawlowski, Roger P., John N. Shadid, Joseph P. Simonis, and Homer F. Walker. 2006. Globalization techniques for newton-krylov methods and applications to the fully coupled solution of the navier-stokes equations. *SIAM Review* 48(4):700–721.

Pernice, Michael, and Homer F. Walker. 1998. NITSOL: a newton iterative solver for nonlinear systems. *SIAM Journal on Scientific Computing* 19(1): 302–318.

Pletcher, Richard H., John C. Tannehill, and Dale Anderson. 1997. *Computational fluid mechanics and heat transfer, second edition.* 2nd ed. Taylor & Francis.

Procassini, Richard, M.H. O'Brien, and J Taylor. 2005. Dynamic load balancing of parallel monte carlo transport calculations. *Monte Carlo 2005.*

Rief, H. 1999. Touching on a zero-variance scheme in solving linear equations by random walk processes. *Monte Carlo Methods & Applications* 5(2):135.

Romano, P., B. Forget, and F. Brown. 2010. Towards scalable parallelism in monte carlo particle transport codes using remote memory access. In *Joint international conference on supercomputing in nuclear applications and monte carlo 2010 (SNA+ MC2010)*, 17–21.

Saad, Youcef. 1993. A flexible inner-outer preconditioned GMRES algorithm. *SIAM Journal on Scientific Computing* 14(2):9.

Saad, Youcef, and Martin H. Schultz. 1986. GMRES: a generalized minimal residual algorithm for solving nonsymmetric linear systems. *SIAM Journal on Scientific and Statistical Computing* 7(3):856–869.

Saad, Yousef. 2003. *Iterative methods for sparse linear systems.* SIAM.

Sabelfeld, K., and N. Mozartova. 2009. Sparsified randomization algorithms for large systems of linear equations and a new version of the random walk on boundary method. *Monte Carlo Methods & Applications* 15(3):257–284.

Shadid, John N., and Ray S. Tuminaro. 1994. A comparison of preconditioned nonsymmetric krylov methods on a large-scale MIMD machine. *SIAM Journal on Scientific Computing* 15(2):440–459.

Shadid, John N., Ray S. Tuminaro, and Homer F. Walker. 1997. An inexact newton method for fully coupled solution of the navier-stokes equations with heat and mass transport. *Journal of Computational Physics* 137(1): 155–185.

Siegel, A., K. Smith, P. Fischer, and V. Mahadevan. 2012a. Analysis of communication costs for domain decomposed monte carlo methods in nuclear reactor analysis. *Journal of Computational Physics* 231(8): 3119–3125.

Siegel, A.R., K. Smith, P.K. Romano, B. Forget, and K. Felker. 2012b. The effect of load imbalances on the performance of monte carlo algorithms in LWR analysis. *Journal of Computational Physics* (0).

Sosonkina, M., D.C.S. Allison, and L.T. Watson. 1998. Scalable parallel implementations of the GMRES algorithm via householder reflections. In *1998 international conference on parallel processing, 1998. proceedings*, 396 –404.

Spanier, Jerome, and Ely M. Gelbard. 1969. *Monte carlo principles and neutron transport problems*. New York: Dover Publications.

Srinivasan, A. 2010. Monte carlo linear solvers with non-diagonal splitting. *Mathematics and Computers in Simulation* 80(6):1133–1143.

Stroustrup, Bjarne. 1997. *The c++ programming language*. 3rd ed. Addison-Wesley Professional.

Trefethen, Lloyd N., and David Bau III. 1997. *Numerical linear algebra*. SIAM: Society for Industrial and Applied Mathematics.

Tuminaro, Ray S., John N. Shadid, and Scott A. Hutchinson. 1998. Parallel sparse matrix vector multiply software for matrices with data locality. *Concurrency: Practice and Experience* 10(3):229–247.

U.S. Department of Energy. 2011. CASL - a project summary. CASL-U-2011-0025-000, Consortium for Advanced Simulation of LWRs.

———. 2012. Resilient extreme-scale solvers. Tech. Rep. LAB 12-742, ASCR.

Wagner, JC, Scott Mosher, Thomas Evans, Doug Peplow, and John Turner. 2010. Hybrid and parallel domain-decomposition methods development to enable monte carlo for reactor analyses. *Joint International Conference on Supercomputing in Nuclear Applications and Monte Carlo*.

Wasow, W.R. 1952. A note on the inversion of matrices by random walks. *Mathematical Tables and Other Aids to Computation* 6(38):78–81.

Zienkiewicz, O. C., R. L. Taylor, and J. Z. Zhu. 2005. *The finite element method: Its basis and fundamentals, sixth edition*. 6th ed. Butterworth-Heinemann.